

Life Cycle Behaviour of Concrete Bridges

Laboratory test and probabilistic evaluation

Markus Bergström

Luleå University of Technology
Department of Civil and Environmental Engineering
Division of Structural Engineering

2006:59 | ISSN: 1402-1757 | ISRN: LTU-LIC -- 06/59 -- SE

Licentiate Thesis 2006:59

Life Cycle Behaviour of Concrete Bridges

Laboratory test and probabilistic evaluation

Markus Bergström

Division of Structural Engineering
Department of Civil and Environmental Engineering
Luleå University of Technology
SE-971 87 Luleå
Sweden
<http://www.cee.ltu.se/>
<http://construction.project.ltu.se/>

Preface

This licentiate thesis presents findings from an on going research project at the Division of Structural Engineering, the Department of Civil and Environmental Engineering at Luleå University of Technology (LTU) within the research group “Innovative materials and structures”. The work started in June 2004 and the first part of the project is finalized in October 2006 and compiled into this report.

The financial support for the work with the thesis has been provided by the *Development Fund of Swedish Construction Industry (SBUF)*. The project has been carried out in collaboration between Luleå University of Technology and Norut Teknologi AS in Norway in terms of project definition, choice of deterioration process and FE-analysis. Tech. Dr. Roy Antonsen, M. Sc. Bård Arntsen and M. Sc. Björn Sand are acknowledged for their participation and contribution in the project and kind hospitality during my visits at Norut Teknologi in Narvik, Norway.


The work done by Tech. Dr. Claes Fahleson, Mr. Hans-Olov Johansson, Mr. Thomas Forsberg and M. Sc Georg Danielsson at Testlab, Luleå University of Technology is greatly appreciated in the discussion, preparation and execution of the laboratory experiments. Tech. Dr. Claes Fahleson is also thanked for the help with the probabilistic approach in the thesis.

I would also like to thank my supervisor, Prof. Björn Täljsten, who has shown solid interest in my project by investing both time and effort in the planning phase as well as in the execution part. His knowledge and driving force is always a source of inspiration. My co-supervisor, Tech. Dr. Anders Carolin, is acknowledged for the kind help, his knowledge in the area of research in general and structural engineering in particular. His ability of looking at things critically has brought progress in the right direction in this project.

Mom and dad, I would like to thank you very much for always supporting and being there for me.

I am very grateful to my fiancé, Sofi, how has helped me in the work with the thesis, both by letting me know her opinion but also by making our time together special and by offering things that make also a rainy Monday morning feel just fine.

Luleå, November 2006



Markus Bergström

Summary

The structural life for a concrete structure located in an environment where corrosion is promoted by humidity or chlorides from sea or de-icing salt could in general be described in the following manner. The structure is manufactured and is at that point considered to be intact. Corrosion is assumed to attack the steel reinforcement, and at a certain corrosion level the structure has to be repaired. The cover concrete is removed and the corroded steel reinforcement is cleaned from corrosion products. A repair system consisting of primer and repair mortar is used to refill the cavity left after the removed concrete. The structure is now considered repaired in the sense that the degradation rate is decreased and the signs of corrosion are taken away. The corrosion attack and repair procedure could affect the load carrying capacity of the repaired beam in terms of decreased steel content and changed interface conditions between the steel and repair mortar. Strengthening could be applied to fulfil a possible lack of load carrying capacity.

The life cycle described above has been simulated in a laboratory environment. The test program and the results provided from the monitoring of beam specimens are presented in the thesis. A probabilistic approach is employed to calculate the change in probability of failure for the different stages of the life cycle. First, all relevant parameters were considered as stochastic and given appropriate statistical properties. With this information the probability of failure is estimated for the corroded, repaired and strengthened beams compared to the intact beam.

It was found that the accelerated corrosion setup provided a steel mass content loss of 12 % in the corroded region, corresponding to an average decrease in steel bar diameter by 6 %. This corrosion damage was obtained after 75 days of accelerated corrosion at a corrosion current density of 0,10 mA/cm². Both evenly distributed corrosion as well as pitting corrosion attack was observed. The concrete beam stiffness was recorded to 2980 kNm² before the corrosion process and decreased by 15 % to 2530 kNm² after corrosion of tensile steel reinforcement. This is verified both by measuring global stiffness, using displacement gauges, and local stiffness, using strain sensors. The result indicates that there is a strong relation between the deterioration process and the change in curvature and stiffness, suggesting that this is a method to measure the status of the structure. The status could for instance be defined by a performance factor, which equals 1 for the intact structure and then decrease to represent the relation between the stiffness of the deteriorated and the intact structure. If the structure is strengthened, the performance factor could be larger than 1.

The ductility of the corroded steel reinforcing bars decreased by 55 % due to corrosion compared to the undamaged steel reinforcing bars. The ultimate strain for the corroded bars was recorded to 10 %, while the ultimate strain for the undamaged bars was 22 %. This reduction is caused by pitting corrosion, which produces local stress concentrations along the bar. The failure occurs when the ultimate strain capacity is exceeded in one cross section, leading to an early failure of the steel bar specimen. The global extension of the steel specimen remains small as the failure strain acts on a small region of the total length. For the structural element this will lead to a failure at a particular corrosion level, since the local pits will dramatically decrease the load carrying capacity in one section. A failure of a structural member which is attacked by pitting corrosion could be unnoticed in terms of visual evidence, since the elongation of the steel reinforcement is kept at a moderate level at failure because of the local damages that pitting creates. The strain at yielding is recorded to 0,39 % for the intact steel bar and 0,43 % for the corroded.

Failure was defined as yielding of steel reinforcement for unstrengthened beams, and as debonding of CFRP plate for the strengthened beam. The load carrying capacity for the intact beam was 79,8 kN. The load carrying capacity was decreased by 15 % after corrosion of steel reinforcement to 69 kN. For the beam where the cover concrete was removed the load carrying capacity was decreased another 18 % down to 60 kN in comparison to the intact beam. Yielding of steel reinforcement for the repaired beam occurred at 64,8 kN, and debonding of CFRP plate for the repaired & strengthened beam occurred at 82,7 kN. These results show that a 12 % reduction of steel content in the cross section occurred during the corrosion phase, at the same time as the stiffness was reduced by 15 %. An analytical model indicates that the 12 % reduction of steel content should decrease the stiffness by 9 %. The remaining stiffness decrease may be coupled to creep. Another important fact is that the particular strengthening design upgraded the repaired & strengthened beam to reach a load carrying capacity which exceeds the intact beam.

The life cycle behaviour for the concrete beams used in the study shows the same general results in comparison to an FE-analysis. It should be mentioned that the FE-analysis performed has not been done on the tested beams in this study. An analysis of these will however be conducted at a later stage.

The probabilistic approach of the studied life cycle shows that the probability of failure increased two times for the corroded beam compared to the intact beam, and further up to seven times for the repaired beam. The increase in probability of failure for the corroded beam is related to steel mass loss. The repaired beam has an even higher probability of failure than the corroded beam since the effective height is reduced during removal of cover concrete of the loaded beam. By strengthening the repaired beam by bonding a CFRP plate, the probability of failure is decreased beyond the intact beam for the particular strengthening operation performed in the study.

Key words: Concrete, degradation, deterioration, rehabilitation, corrosion, strengthening, carbon fibre, CFRP

Sammanfattning

Livscykeln för en konstruktion som är belägen i en miljö där risken för korrosion är framstående kan beskrivas enligt följande. I det första skedet då konstruktionen byggs antas den vara intakt och klarar av att bära full last. Korrosion antas angripa stål-armeringen, och vid en viss nivå måste konstruktionen repareras. Reparationsprocessen består av att frilägga armeringen genom att ta bort betongens täcksikt, varvid armeringen rengörs från korrosionsprodukter. Åtgärden för att återge befintlig beständighet och materialkvalitet är att applicera ett reparationssystem bestående av primer och reparationsbruk för att återgjuta ett nytt täcksikt. I detta läge anses konstruktionen vara reparerad men dess lastkapacitet behöver för den delen inte vara tillfredsställande. Detta kan bero dels på grund av ett minskat armeringsinnehåll pga. korrosion, dels på en förändrad kraftöverföring mellan armeringen och reparationsbruket. Utifall bärförmågan behöver ökas kan konstruktionen förstärkas genom att limma FRP (Fibre Reinforced Polymers) i form av stavar eller laminat, applicera utanpåliggande eller invändiga spännkablar mm.

Ovan beskriva livscykel är simulerad i laboratoriemiljö. Försöksprogrammet och de resultat som studien resulterat i är presenterade i denna licentiatrapport. En probabilistisk ansats är gjord, både genom att beskriva parametrar som stokastiska variabler samt att använda dessa i en beräkning där sannolikheten för brott är beräknad för konstruktionen i olika delar av livscykeln.

Studien har visat att den accelererade korrosionsuppställningen gav en minskning av den dragna böjarmeringens vikt på 12% i det korroderade området. Denna minskning motsvarar en diameterreduktion på i genomsnitt 6% för armeringsstålet. Denna korrosionsskada uppstod efter 75 dagar av accelererad korrosion med en påtvingad korrosionsströmsdensitet på 0,10 mA/cm². Både jämnt fördelad korrosion såväl som korrosionsgröpar hittades på de korroderade armeringsjärnen. Betongbalkens styvhet var mätt till 2980 kNm² före korrosionsprocessen och minskade med 15% pga. korrosion till 2530 kNm². Denna minskning är verifierad både genom att mäta global styvhet med hjälp av lägesgivare samt en lokal mätning där töjningsgivare användes.

Resultaten visar att det finns en stark koppling mellan nedbrytningsprocessen och förändringen i krökning och styvhet, vilket kan vara ett bevis på att detta är en metod att mäta statusen hos konstruktioner. Statusen skulle kunna definieras med hjälp av en prestandafaktor. För den befintliga konstruktionen definieras prestandafaktorn som förhållandet mellan uppmätt storhet, exempelvis styvhet, mellan den befintliga och intakta konstruktionen.

Således blir faktorn 1 för den intakta konstruktionen samt mindre än 1 för den nedbrutna. För en förstärkt konstruktion kan faktorn överstiga värdet 1. Dragprov visade att duktiliteten vid brott av det korroderade armeringsstålet minskade med 55% pga. korrosionsangreppet jämfört med det oskadade armeringsjärnet. Brottöjningen för det korroderade järnet mättes till 10% medan motsvarande siffra för det oskadade järnet var 22%. Minskningen är kopplad till korrosionsgropar, vilka skapar lokala spänningskoncentrationer längs armeringen. Det tidiga brottet uppstår då brottöjningen i något tvärsnitt av armeringen uppnås. Den globala längdändringen av järnet förblir liten eftersom brottöjningen verkar på ett litet område av totala längden. Kloridinitierad korrosion uppvisar ofta korrosionsgropar. Ett brott av ett betongkonstruktionselement vilket är gravt angripet av kloridinitierad korrosion kan därför förväntas vara avsevärt mindre duktilt än för det konstruktionselement som inte är attackerad av korrosion. Global längdändring vid flytning för den intakta stålarmeringen mättes till 0,39 % och för den korroderade till 0,43 % vilket inte är någon utmärkande skillnad.

Brott var definierat som flytning av dragna stålarmeringen för de oförstärkta balkarna och som delaminering av CFRP laminat för den förstärkta balken. Lastkapaciteten för den intakta balken var 79,8 kN. Lastkapaciteten minskade med 15 % pga. korrosionsangreppet till 69 kN. Lastkapaciteten minskade ytterligare 18 % till 60 kN för balken där betongtäcksiktet var avlägsnat. Brott inträffade vid 64,8 kN för den reparerade balken och vid 82,7 kN för den reparerade och förstärkta balken. Stålinnehållet minskade med i genomsnitt 12 % under korrosionsfasen. Under samma tid uppmättes en 15 % minskning av balkstyvheten. En analytisk modell visar att en 12 % minskning av stålinnehåll i tvärsnittet motsvarar en minskning av styvhet med 9 %. Resterande 6 % av styvhetsminskningen kan vara kopplat till krypning. Ett annat viktigt resultat av studien är att den aktuella förstärkningen uppgraderade balkens lastkapacitet så att den klarade högre last än den intakta balken.

Livscykeluppförandet, i form av last mot nedböjningsförhållande, överensstämmer väl med den FE-analys som gjordes innan den experimentella studiens början. Det ska nämnas att analysen inte var gjord på de specifika försöksbalkarna i den här studien, utan tolkas mer som ett generellt resultat. En analys av försöksbalkarna som genomgått livscykeln i det här projektet ska utföras i ett senare skede.

Den probabilistiska ansatsen för att studera sannolikheten för brott i olika skeden i livscykeln visade på att brottsannolikheten ökade två gånger från 10^{-6} för den intakta balken till $2 \cdot 10^{-6}$ för den korroderade balken och vidare upp till $7 \cdot 10^{-6}$ för den reparerade balken. Förstärkningsåtgärden uppgraderade balkarna så att sannolikheten för brott för den reparerade och förstärkta balken återigen låg på en nivå omkring 10^{-6} .

Nyckelord: Betong, nedbrytning, rehabilitering, korrosion, förstärkning, FRP, kolfiber, probabilistisk dimensionering.

Notations and symbols

Roman letters

	<i>Description</i>	<i>Unit</i>
A_{sR}^u	<i>Residual cross sectional area of uniformly corroded steel bar</i>	$[m^2]$
A_{sR}^{up}	<i>Residual cross sectional area of steel bar attacked by pitting corrosion</i>	$[m^2]$
A'_s	<i>Cross sectional area of compressive reinforcement</i>	$[m^2]$
$f_R(r)$	<i>Frequency function describing resistance</i>	$[-]$
$f_S(s)$	<i>Frequency function describing load effect</i>	$[-]$
A'_s	<i>Cross sectional area of compressed reinforcement</i>	$[m^2]$
d'_s	<i>Distance to compressed reinforcement</i>	$[m]$
X_{d_s}	<i>Stochastic variable describing effective height</i>	$[m]$
$X_{f_{st}}$	<i>Stochastic variable describing steel yield strength</i>	$[Pa]$
$X_{A_{s,c}}$	<i>Stochastic variable describing corroded bar cross sectional area</i>	$[m^2]$
$X_{d_{s,c}}$	<i>Stochastic variable describing effective height for repaired beam</i>	$[m]$
$F_{c,gf}$	<i>Compressive force in glass fibre rod</i>	$[N]$
$F_{t,gf}$	<i>Tensile force in glass fibre rod</i>	$[N]$
A_{gf}	<i>Cross sectional area of glass fibre rod</i>	$[m^2]$
E_{gf}	<i>Modulus of elasticity for glass fibre rod</i>	$[Pa]$
A	<i>Atomic weight of steel (56 g/mole)</i>	$[g/mole]$

A_1	Truss element modelling residual cross section area of corroded steel bar	[-]
A_2	Truss element modelling cross section loss due to corrosion	[-]
A_f	Fibre cross sectional area	[m ²]
A_s	Cross sectional area of tensile reinforcement	[m ²]
$A_{s,s}$	Cross section area of stirrups	[m ²]
b	Beam width	[m]
C	Concrete cover thickness	[m]
d	Effective height	[m]
$d_{s,corr}$	Effective height for repaired beam	[m]
E	Modulus of elasticity	[Pa]
E_f	Modulus of elasticity for fibre	[Pa]
E_s	Modulus of elasticity for steel	[Pa]
F	Load	[N]
F	Faraday's constant (96500 A/sec)	[A/sec]
f_{cc}	Compressive strength of concrete	[Pa]
f_{ct}	Tensile strength of concrete	[Pa]
f_d	Strength design value	[Pa]
f_y	Yield stress	[Pa]
$f_{y,s}$	Yield strength of stirrups	[Pa]
g	Permanent load	[N/m]
g	Failure surface	[-]
G	Failure function	[-]
h	Beam height	[m]
h_c	Height of beam	[m]
I_{corr}	Corrosion current	[A]
I_2	Moment of inertia for concrete cross section in stage 2	[m ⁴]
I_c	Moment of inertia of concrete	[m ⁴]
I_s	Moment of inertia for steel	[m ⁴]
k	Coefficient determined from pull-out test	[-]

K_1	Nonlinear spring element modelling remaining bond after corrosion	[-]
K_2	Nonlinear spring element connected to concrete via nonlinear couplings	[-]
L	Free span	[m]
L_{exp}	Length of tensile reinforcement exposed to corrosion attack	[m]
M	Safety margin	
p	Variable load component	[N/m]
P	Probability	[-]
p_f	Probability of failure	[-]
R	Resistance	[Nm]
S	Load effect	[Nm]
S_s	Distance between stirrups	[m]
t	Carbonisation time	[year]
t	Time	[sec]
w	Width of beam	[m]
x_{corr}	Penetration depth of corrosion attack	[m]
x_{carb}	Carbonisation depth	[m]
x	Height of compressed zone of concrete cross section	[m]
X_S	Stochastic variable describing load effect	[Nm]
$x_{upgraded}$	Height of compressed zone of strengthened beam	[m]
a	Surface area of steel reinforcing bar	[m ²]
z	Valence of steel (+2)	[-]

Greek letters

	<i>Description</i>	<i>Unit</i>
τ_{\max}^c	Maximum bond strength between concrete and steel	[Pa]
τ_c	Concrete contribution to bond strength	[Pa]
τ_s	Stirrup contribution to bond strength	[Pa]
δ	Displacement	[m]
κ	Partial factor on material bearing capacity dependent on humidity, load duration etc.	[-]
η	Partial factor considering differences between real property and test (normally equals 1)	[-]
μ	Mean value	
μ	Coefficient determined from pull-out test	[-]
α	Coefficient dependant on type of corrosion attack	[-]
α	Sensitivity factor for stochastic variable	[-]
α_s	Relation between steel and concrete modulus of elasticity	[-]
α_f	Relation between fibre and concrete modulus of elasticity	[-]
β	Coefficient determined from pull-out test	[-]
β	Safety index	[-]
ϕ_0	Nominal diameter of steel bar	[m]
γ_m	Partial coefficient considering uncertainty in model	[-]
γ_n	Safety factor related to safety class	[-]
μ_R	Mean value for load carrying capacity	[Nm]
ϕ_R	Residual diameter of steel bar	[mm]
ϕ_s	Steel bending reinforcement diameter	[m]
μ_S	Mean value for load effect	[Nm]
ϕ_s	Diameter of reinforcing bar	[m]
$\phi_{s,corr}$	Corroded steel bending reinforcement diameter	[m]
σ	Standard deviation	
σ_R	Standard deviation for load carrying capacity	[Nm]

σ_S	Standard deviation for load effect	[Nm]
σ	Stress	[Pa]
σ_c	Stress in concrete	[Pa]
σ_s	Stress in steel	[Pa]
Φ	Standardized normal distribution function	[-]
ε	Strain	[-]
ε_C	Strain in concrete	[-]
ε_s	Strain in steel	[-]
ε_f	Strain in fibre	[-]
ε_{fu}	Ultimate strain in fibre	[-]
ε_{u0}	Strain at underside of concrete beam before strengthening	[-]
ε_{c0}	Concrete strain before strengthening	[-]
ε_{s0}	Strain in tensile steel reinforcement before strengthening	[-]
φ_c	Effective creep number	[-]
$\Delta\varepsilon_{s0}$	Increase of steel strain	[-]
$\Delta\varepsilon_{c0}$	Increase of concrete strain	[-]
$\varepsilon_{t, gf}$	Tensile strain in glass fibre rod at yielding of tensile steel reinforcement	[-]
$\varepsilon_{c, gf}$	Compressive strain in glass fibre rod at yielding of tensile steel reinforcement	[-]
δ	Material loss due to corrosion	[m]
γ	Density of steel (7860 kg/m ³)	[kg/m ³]
ΔW	Steel reinforcement weight loss as a result of corrosion	[kg]

Table of content

1	INTRODUCTION.....	1
1.1	Research questions.....	2
1.2	Aim.....	2
1.3	Limitations	2
1.4	Structure of thesis.....	2
2	PROJECT DESCRIPTION	3
2.1	Studied process.....	3
2.2	Numerical simulation.....	4
2.2.1	Corrosion of reinforcing bars	5
2.2.2	Relation between corrosion and bond deterioration.....	6
2.2.3	Bond stress-slip models	7
2.2.4	Finite element modelling of debonding	7
2.2.5	Calculation example.....	8
3	LITERATURE REVIEW.....	13
3.1	Degradation	13
3.1.1	In general.....	13
3.1.2	Freezing.....	14
3.1.3	Corrosion.....	16
3.2	Repair and retrofitting.....	23
3.2.1	In general.....	23
3.2.2	Adhesive and bonding.....	23
3.2.3	Patch repair	25
3.2.4	Confinement.....	26
3.3	Strengthening	28
3.3.1	Challenges.....	28
3.3.2	Strategies.....	28
3.3.3	Ductility	29
3.3.4	Material	30
3.3.5	Application.....	31
3.3.6	Existing strain fields.....	32

3.4	Monitoring	36
3.4.1	Requirements	36
3.4.2	Fibre optic sensors	36
3.4.3	Curvature measurement	37
3.4.4	Fibre optic sensors in concrete.....	39
3.4.5	Fibre optic sensors in FRP.....	40
4	SAFETY AND PROBABILISTIC APPROACH.....	43
4.1	Structural safety	43
4.1.1	Safety class	44
4.1.2	Partial coefficients	45
4.2	Probabilistic design.....	45
4.2.1	First order second moment reliability method (FORM).....	46
4.2.2	The Hasofer-Lind safety index	49
4.2.3	Parameters.....	51
5	EXPERIMENTAL STUDY	53
5.1	Introduction to experiment.....	53
5.2	Beam specimens	54
5.2.1	Corrosion process	56
5.2.2	Corrosion initiation	58
5.2.3	Accelerated corrosion duration.....	58
5.2.4	Repair procedure.....	60
5.2.5	Strengthening procedure.....	60
5.3	Test setup	61
5.3.1	Long term test	61
5.3.2	Loading	63
5.3.3	Failure load test.....	64
5.4	Monitoring	65
5.4.1	Traditional monitoring equipment.....	66
5.4.2	Fibre optic strain measurement.....	67
5.4.3	Long term test	69
5.4.4	Failure load test.....	70
5.5	Material properties.....	71
6	TEST RESULTS	73
6.1	General.....	73
6.2	Corrosion stage – long term test	73
6.2.1	Loading	75
6.2.2	Midpoint deflection and strain.....	77

6.2.3	Curvature.....	78
6.3	Failure tests	81
6.3.1	Intact beam.....	81
6.3.2	Corroded beam.....	83
6.3.3	Beam where cover concrete was removed.....	85
6.3.4	Repaired beam.....	87
6.3.5	Repaired & strengthened beam	90
7	EVALUATION.....	93
7.1	General	93
7.2	Corrosion stage – long term test	93
7.2.1	Stiffness.....	94
7.3	Failure load test.....	96
7.3.1	Load vs. deflection relations	96
7.3.2	Life cycle behaviour.....	98
7.3.3	Existing strain field	98
7.3.4	Stiffness.....	100
8	PROBABILISTIC EVALUATION	103
8.1	Analytical models	103
8.1.1	Reinforced concrete beam.....	103
8.1.2	Strengthened beam.....	105
8.2	Statistical and deterministic variables	106
8.3	Calculations.....	107
8.3.1	Principle for FORM calculation.....	108
8.3.2	Intact beam.....	109
8.3.3	Corroded beam.....	110
8.3.4	Repaired beam.....	110
8.3.5	Strengthened beam.....	110
8.4	Concluding results.....	111
8.4.1	Distributions.....	111
8.4.2	Sensitivity factors α	115
9	DISCUSSION AND CONCLUSIONS.....	117
9.1	Discussion	117
9.2	Conclusions.....	120
10	SUGGESTIONS FOR FUTURE WORK.....	121

APPENDIX A – MATERIAL PROPERTIES	129
APPENDIX B.1 – INTACT BEAM (A).....	133
APPENDIX B.2 – CORRODED BEAM (B).....	137
APPENDIX B.3 – BEAM WHERE COVER CONCRETE WAS REMOVED (D)	141
APPENDIX B.4 – REPAIRED BEAM (E)	145
APPENDIX B.5 – REPAIRED AND STRENGTHENED BEAM (F).....	149

1 Introduction

Numerous existing concrete structures are showing significantly shorter service life than they were designed for. A reason for this, besides higher demands from the owners and new load regulations, may be that the degradation of concrete and steel sometimes progresses faster than was expected when the structure was designed and built, which for example has led to thin concrete covers. Yet another reason may be that many of structures designed in the mid 50's were built without considering the use of de-icing salts on the roads. Consequently, one severe reason for degradation is due to corrosion caused by de-icing salts. The environment around concrete bridges along salted roads is at times very harsh with high moisture levels. Cracking and spalling of concrete will also allow the chlorides from the icing salts to penetrate the concrete. In addition, the salty water may also be splashed up on the edge beams and perhaps also pour down the side of the bridge deck. Problems will eventually appear when salt water penetrates into the concrete to the depth of the steel bars. Other degradation processes that can affect concrete structures are related to carbonisation, concrete not being resistant to freeze-thaw and swelling ballast due to ASR reactions, just to mention a few. In this thesis focus is on degradation problems related to chloride initiated corrosion.

The investments made today into construction repair and rehabilitation are huge. An estimated amount of approximately 15-20 billion SEK is invested in Sweden every year into this sector of the construction industry according to "Sveriges byggindustrier". In the foreseeable future one may expect even increased need for concrete repair and rehabilitation. Knowledge and procedures to understand and to "give the patient the right medicine" must be further developed so that cost effective remedies can be given. Ideally the deterioration problem must be taken care of before it becomes really serious for the structure, with replacement as the only cure.

Repair and rehabilitation of concrete structures have today evolved into a multi-disciplinary science where it is necessary to master and combine knowledge from a number of different fields such as concrete technology, environmental loadings, transport mechanisms, electro-chemistry, structural mechanics and composite materials etc. Durability research has progressed considerably the last decade, which has evolved into methods and systems to improve the durability of reinforced concrete structures. In spite of the effort, the need for repair and rehabilitation does not seem to have been reduced since various construction errors cause deterioration and damage on the structure.

Many studies have been carried out about degradation, retrofitting and strengthening separately but no study that the author is aware of, has combined these disciplines into a holistic approach.

In the current report this is done, and all stages in the degradation, retrofitting and strengthening processes have been performed and studied one after the other.

1.1 Research questions

Repairing or upgrading an existing concrete structure is often considerably more difficult than building a new one. The following important questions should be asked:

- How do existing loads during repair and strengthening affect the structure?
- Does the stiffness of the structural member decrease due to deterioration issues?
- How can the load carrying capacity be determined by a probabilistic approach?

Answers to these questions must be considered by the owner to guarantee a structure's safety during its remaining life.

1.2 Aim

The work presented in this licentiate thesis are aimed to test, understand and analyse deteriorated, repaired and strengthened concrete beams including a probabilistic approach to answer the above given research questions.

1.3 Limitations

This project will continue after the licentiate thesis has been presented. It is carried out as a collaboration project with Norut Teknologi AS, Norway. At Norut a detailed FE-analysis will be made, based on the tests presented in this report. For that reason it has been decided not to present any detailed FE-analysis at this stage of the project.

It is not rare that steel reinforcement corrosion appears again only a couple of years after repair or strengthening of a structure, especially for patch repairs. This study will however not consider the long term effects caused by the repair procedures.

1.4 Structure of thesis

Chapter 2 describes the project in detail as well as a presentation of an elementary FE-simulation. Chapter 3 presents a literature survey about degradation, repair and retrofitting, strengthening of concrete structures. Also monitoring of structures is discussed in this chapter. In chapter 4 the important topics regarding probability is presented and focus is placed on theory behind probabilistic design and methods to evaluate the safety of a structure. Chapter 5 presents the laboratory test in detail. Test results are presented in chapter 6 and these are then evaluated and discussed in chapter 7. A probabilistic evaluation is performed and presented in chapter 8. Chapter 9 gives an overall discussion and concludes the findings in the project. Finally, chapter 10 gives suggestions for future work.

All material data and detailed information regarding the test specimens are given in Appendix A at the end of the report.

2 Project description

2.1 Studied process

The aim of the project is to experimentally simulate the behaviour of concrete beams enduring a simulated life cycle procedure. The test program will direct the beams from original performance of the intact beam through degradation, repair and upgrading with CFRP (Carbon Fibre Reinforced Polymer) plate bonding to its original load carrying capacity. Several attributes makes this project special. Amongst these should accelerated corrosion, strain measurement using fibre optic sensors and sustained loading during the entire life cycle should be mentioned. The studied life cycle is defined by seven steps, presented in Figure 2-1. Numerical model results are schematically described in Figure 2-8.

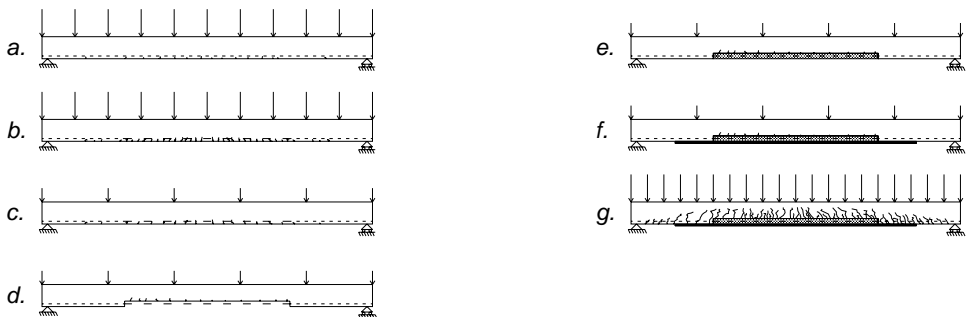


Figure 2-1. Seven defined stages in the entire process (Horrignoe, 1998).

a. Undamaged beam

In the initial stage, the beam is subjected to the full service load (SLS), during which cracking occurs. The deflection increases as the serviceability load is gradually obtained, coming to a halt at a certain level. The load-deflection-curve is not linear, as cracking occurs along the way and changes the beam specimen stiffness. Although, the beam is considered linear elastic as yielding in tensile steel reinforcement or crushing of concrete does not occur.

b. Corrosion of flexural tensile reinforcement

Simultaneously as the serviceability load acts on the beam specimens, an accelerated corrosion setup corrodes the tensile steel reinforcement. The cross-sectional area of the attacked bars is reduced as well as the bond strength between the bars and surrounding concrete. The associated reduction in bending stiffness leads to increased displacements at the same load.

c. Reduced load during repair and strengthening operations

The structure is taken out of service and the variable component of the loading is reduced to the permanent load only. Both load and deflection decrease. The beam should at this point be weakened due to the reduced steel area and bond between steel and concrete.

d. Removal of damaged concrete and repair of reinforcement

Contaminated concrete is removed and the tensile reinforcement is exposed over the entire deteriorated region of the beam. The associated loss of composite action causes additional deflections. Another effect of removing the concrete surrounding the steel reinforcement under load, when the beam is bent, is that the reinforcement will take the shortest way and move towards the centre of the beam. This new position of the bars will be fixed as the repair mortar is casted. Before the repair procedure, attacked bars are cleaned by sandblasting and will have a permanently reduced cross section.

e. Refilling with repair mortar

The removed contaminated concrete is replaced by a repair mortar, which is strain-free at the serviceability load, whereas the neighbouring concrete remains strained and cracked.

f. Strengthening by CFRP plate bonding

If required, additional reinforcement can be introduced. After repairing the beam, it is strengthened with CFRP (Carbon Fibre Reinforced Polymer) plates. This procedure increases the stiffness of the beam specimen without adding any significant weight.

g. Loading until failure

Finally, the beam is gradually loaded until failure occurs. It is possible that the failure load of this beam is higher than the reference beam. The reason for this is that it is strengthened and therefore given greater possibilities to carry the load.

2.2 Numerical simulation

The entire process from intact beam through deterioration and repair has earlier been simulated (Sand, 2001) as a pre-study to predict the general structural behaviour. Simulation models for deterioration and repair history were defined.

The deterioration model involved the reduction of the reinforcing bar section due to corrosion and the relationship between corrosion and bond deterioration. The repair history was established by removing elements in the beam model to simulate removal of the cover concrete, and then adding new and strain-free elements after the repair procedure. In this thesis the beam tests carried out have not in particular been simulated and only the principle behaviour of the beams will be compared with the earlier carried out FE-analysis. However, in the extension of the project the beam tested will also be simulated.

2.2.1 Corrosion of reinforcing bars

The bar attack penetration is estimated from the measurement of corrosion rate, using the polarization technique and applying Faraday's law

$$x=0,0115 \cdot I_{corr} \cdot t \quad (2.1)$$

Where x is the attack penetration in mm , t is the time in $years$ elapsed since the aggressive reacted with the reinforcement and I_{corr} is the average value of the corrosion current in $\mu A/cm^2$ during time t . The residual rebar diameter ϕ can be estimated from the nominal diameter ϕ_0 by

$$\phi_R = \phi_0 - \alpha x \quad (2.2)$$

α is a coefficient dependant on the type of attack. When uniform corrosion occurs, α equals to 2, see Figure 2-2a. The remaining bar diameter is then

$$\phi_R^u = \phi_0 - 2x \quad (2.3)$$

However, when pitting corrosion occurs as shown in Figure 2-2b, α may reach values up to 4-8. A value of the residual section at pits ϕ_R^p can then be predicted by

$$\phi_R^p = \phi_0 - \alpha x \quad (2.4)$$

The cross section area of the reinforcing bar attacked by uniform corrosion A_{sR}^u can be estimated by

$$A_{sR}^u = n \frac{\pi \phi_R^u}{4} \quad (2.5)$$

where n is the number of the tensile reinforcing bars in the concrete beam. If pitting occurs, the residual cross section area of the tensile reinforcement A_{sR}^{up} can be estimated by

$$A_{sR}^u = (n-1) \frac{\pi \phi_R^u}{4} + \frac{\pi \phi_R^p}{4} \quad (2.6)$$

Here, Sand (2001) has given the example that only one rebar is attacked by pitting and the remaining rebars are attacked by uniform corrosion.

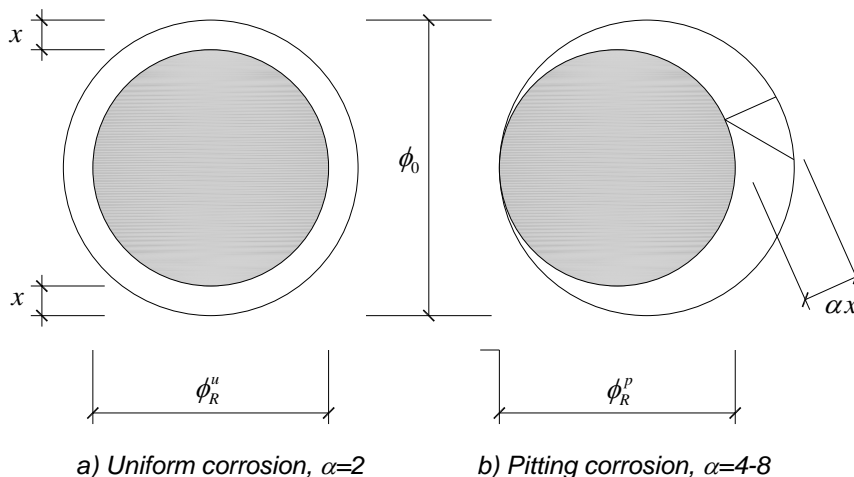


Figure 2-2. Residual reinforcing bar section for a) Uniform corrosion and b) Pitting. Sand, 2001.

2.2.2 Relation between corrosion and bond deterioration

The bond strength τ_{\max}^c is defined as a function of corrosion level x as

$$\tau_{\max}^c = \tau_{\max}^c(x) \quad (2.7)$$

where τ_{\max}^c is the bond strength and x is the corrosion level given by equation (2.1). Sand (2001) has chosen an empirical bond deterioration estimation by Rodriguez et al. (1994), as this model considers the presence of ties, the negative effects of corrosion of the selfsame ties, and the positive effect of support reaction confinement.

$$\tau_{\max}^c = \tau_c + \tau_s = 0,6 \left(0,5 + \frac{C}{\phi_0} \right) f_{ct} (1 - \beta x^\mu) + k \frac{A_{s,s} f_{y,s}}{S_s \phi_s} \quad (2.8)$$

with

$$k \frac{A_{s,s} f_{y,s}}{S_s \phi_s} \leq 1,7 \text{ MPa} \quad (2.9)$$

The bond strength is a contribution from the concrete τ_c and stirrups τ_s .

The contribution from the concrete is dependent on the cover to rebar ratio C/ϕ_0 , the tensile strength of the concrete f_a and the attack penetration depth x . The contribution from the stirrups is dependent on the cross section of the stirrups $A_{s,s}$, the yield strength of the stirrups $f_{y,s}$, and the distance between stirrups S_s . The set of β , μ and k values were determined by considering the results from pull-out tests with concrete with compressive strength equal to 40 MPa, when applying a current density $I_{corr} = 0,1$ mA/cm² to accelerate the steel corrosion. The main bar diameter was $\phi_0 = 16$ mm and stirrup diameter $\phi_s = 8$ mm with spacing S equal to 70 mm and the concrete cover was 24 mm. The resulting values of the constants β , μ and k were 0.26, 0.1 and 0.163 respectively.

2.2.3 Bond stress-slip models

Sand (2001) has used a local bond stress-slip model which was proposed in CEB-FIP model code (1993). This model is given in Figure 2-3a. Castellani modified this model to also consider corrosion effects, see Figure 2-3b.

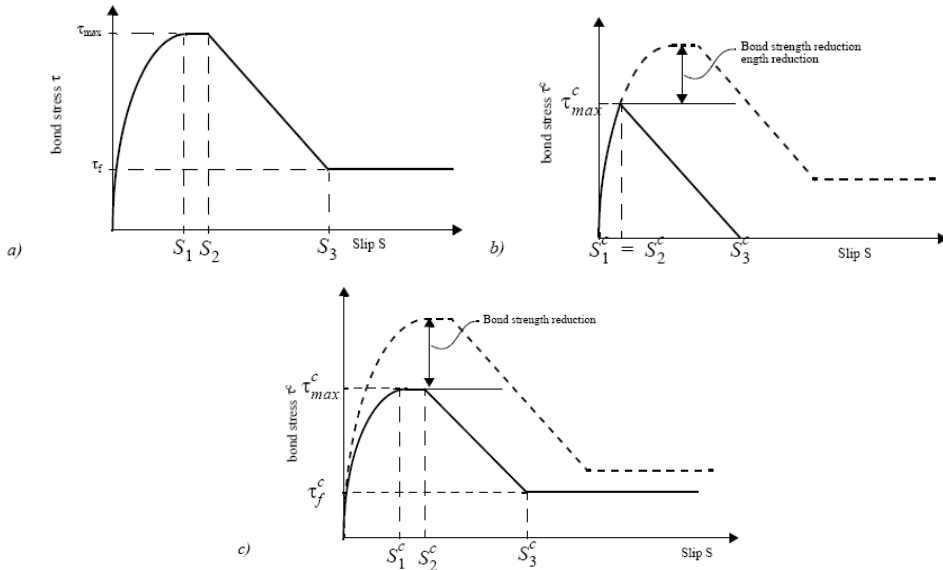


Figure 2-3. Bond stress-slip models. a) CEB-FIP model for reinforcement without corrosion, CEB-FIP (1993). b) Model proposed by Castellani (1999) for reinforcement attacked by uniform corrosion. c) Model proposed by Tørlén et. al (1998) for reinforcement attacked by corrosion. Sand (2001).

2.2.4 Finite element modelling of debonding

Sand concludes that a crucial step in the modelling of debonding between concrete and reinforcement bars is the representation of bond between concrete and steel bars.

Sand used two noded truss elements to model reinforcement, while concrete was modelled with eight noded hexahedral elements. Bond failure is excluded if complete continuity between finite elements, representing concrete and steel bars, is fulfilled. Therefore, the concrete and steel is coupled using interface elements. These elements work as nonlinear springs whose force–displacement characteristics are defined as function of the relative sliding or slip between concrete and the reinforcing bars. The force in the spring can then be expressed as a function of the slip S , that is

$$F(S) = \frac{n}{2} \left(\frac{\pi \phi_s}{2} L_e \right) \tau_s \quad (2.10)$$

where ϕ_s is the diameter of the reinforcing bars, $\tau(S)$ is the bond stress given in Figure 2-3. The concrete beam is reinforced with n reinforcing bars as shown in Figure 2-4.

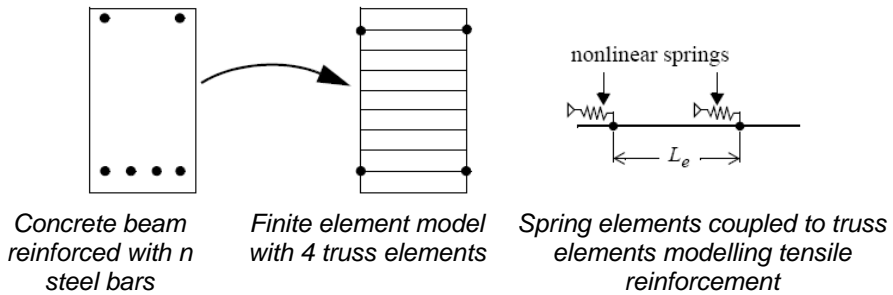


Figure 2-4. Finite element modelling of tensile reinforcement in concrete beams, Sand (2001).

Corrosion leads to loss of the cross section area of the reinforcing steel and reduction of bond strength between concrete and steel bars. To achieve this, Sand modelled the rebars with two sets of truss elements, labelled as A_1 and A_2 . Truss elements set A_1 models the remaining cross section area of the reinforcing bars after corrosion and truss element set A_2 models the cross section loss due to corrosion. The truss element set A_1 is connected to the nodes of the concrete with nonlinear springs labelled as K_1 which models the remaining bond strength after corrosion. Before corrosion takes place, the truss element set A_2 are connected to the nodes on the concrete with the nonlinear springs K_2 via nonlinear couplings. After corrosion takes place, the couplings between the truss element set A_2 and the springs K_2 are removed. Consequently, loss of cross section area and reduced bond strength is achieved.

2.2.5 Calculation example

The approach described by Sand (2001) is illustrated by Sand with a calculation example on a simply supported beam presented in Figure 2-5. The free span is $L = 8,0$ m was subjected to a permanent load $g = 23,75$ kN/m and a variable load component $p = 8$ kN/m. The Norwegian codes gave an ultimate limit load of 41,3 kN/m.

Uniaxial concrete strengths were 16,0 MPa in compression and 1,21 MPa in tension after adjustments with material safety factors. The yield strength and elasticity modulus of the reinforcing steel were taken as 400 MPa and 210 GPa respectively.

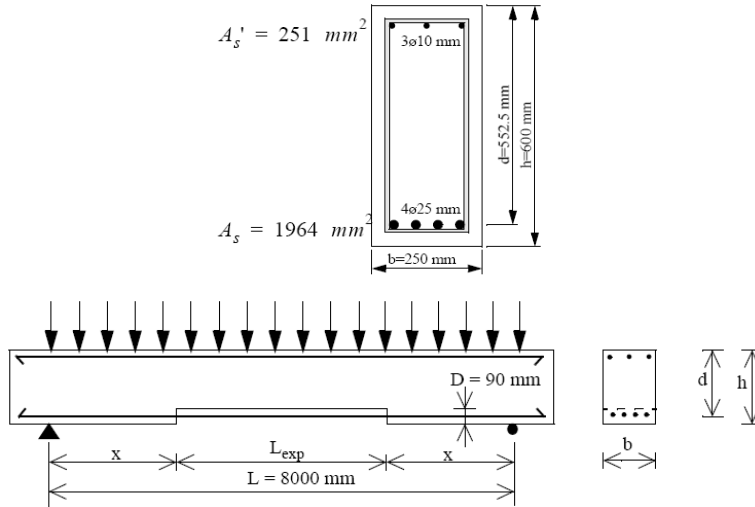


Figure 2-5. Beam specimen used in FE-calculation. Sand (2001).

The concrete beam was modelled with a total of 363 eight noded hexahedral elements and the resulting element mesh is shown in Figure 2-6. The bond stress-slip model described in section 2.2.3 modified by Tørleén et al. (1998) was employed in this example.

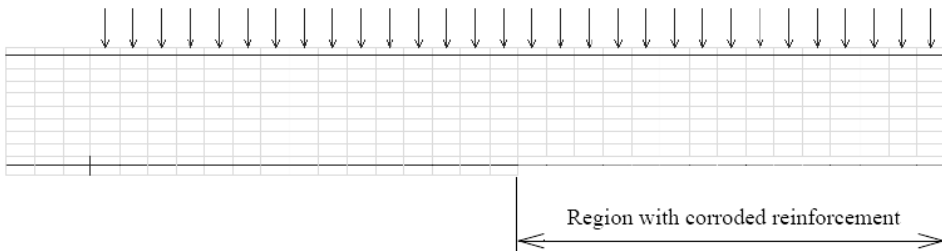


Figure 2-6. Finite element mesh. Sand (2001).

The numerical analyses were designed to simulate the complete life cycle identical to that described in section 2.1. The exposed length L_{exp} of the tensile reinforcement was varied as was the degree of corrosion attack. Figure 2-7 shows the calculated force vs. central deflection for beams where the cross section area of the tensile reinforcement has been reduced by 10% and 25% respectively. In addition, the exposed length L_{exp} during the repair phase was selected in the range 50% to 70% of the free span.

The deteriorated and repaired beams are labelled “B1T- $\beta\%$ U- α L”. The values substituted as α is the percentage of the free span subjected to corrosion attack, and β is the level of corrosion in percent of total tensile reinforcement of beams. In the purpose of comparison, finite element simulation of a sound beam was carried out with the bond stress-slip model specified in CEB-FIP model code and the calculated force vs. central deflection curve, labelled as B1CEB-FIP-S, is also shown in Figure 2-7.

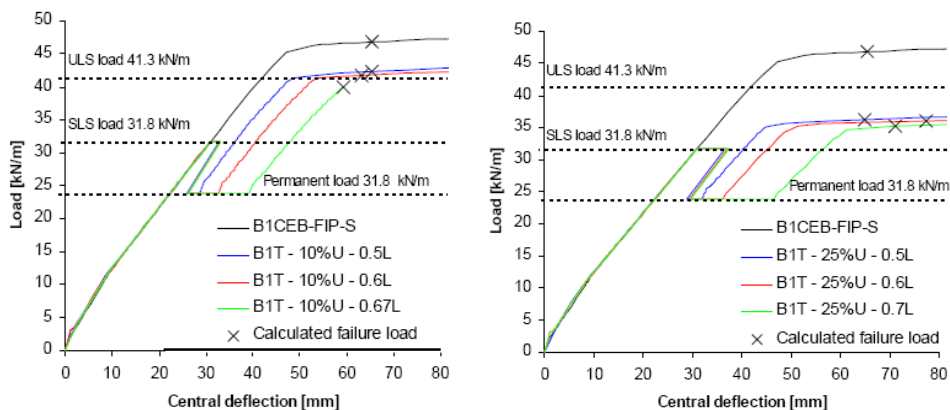


Figure 2-7. Calculated load vs. central displacement curves for beams. Left: with 10% mass loss due to corrosion. Right: 25% mass loss due to corrosion. Graphs from Sand (2001).

The calculated relative failure load from the finite analysis together with information about beams is summarized in Table 2-1.

Table 2-1. Numerical results obtained from finite element analysis of deteriorated and repaired beams compared with results from a sound beam (Sand, 2001).

Beam notation	Exposed length L_{exp} [mm]	Reinforcement reduction of cross section [%]	Calculated relative failure load [-]	Failure mode*
B1CEB-FIP-S	Sound	0	1,00	C
B1T-10%U-0,5L	4000	10	0,91	C
B1T-10%U-0,6L	4800	10	0,89	C
B1T-10%U-0,67L	5360	10	0,86	D
B1T-25%U-0,5L	4000	25	0,78	C
B1T-25%U-0,6L	4800	25	0,77	C
B1T-25%U-0,7L	5600	25	0,75	C

* D: Debonding, C: Crushing of concrete ($\epsilon_c > 3,5\%$),

Figure 2-8 shows the general result from this study in the form of a load-central deflection graph. This result corresponds to the discussion in the previous chapter 2.1. The different stages, *a* through *g*, are marked in the graph in.

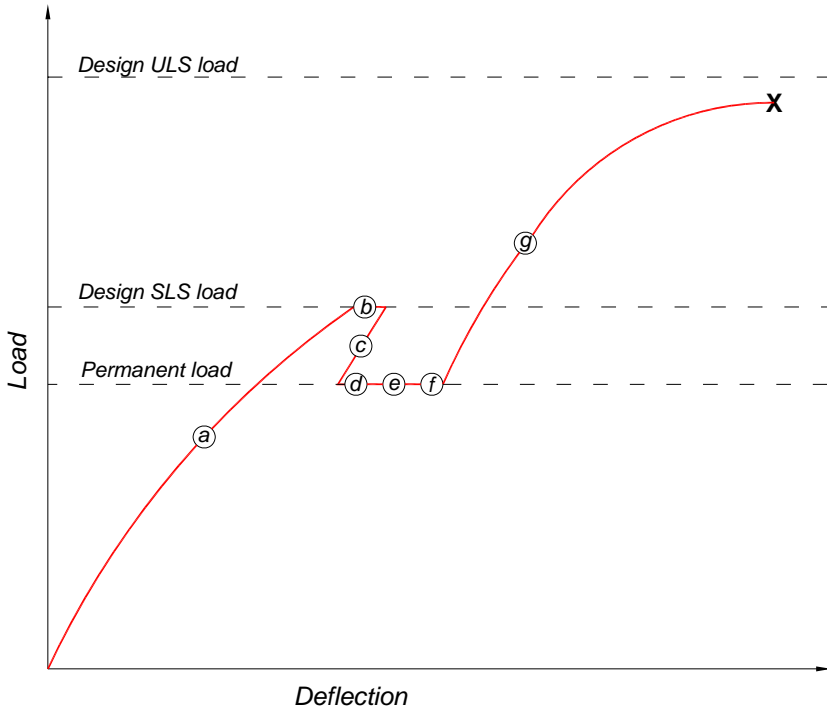


Figure 2-8. Graphical description of general beam behaviour during the repair process (Sand, 2001).

3 Literature review

3.1 Degradation

3.1.1 In general

Concrete structures requiring rehabilitation are often exposed to aggressive environments. Many of these environments are related to cold-climate conditions and factors including freeze-thaw action, exposure to de-icing salts, and sustained low temperatures combined to attack the repaired structure. Due to this the performance of the structure decreases. This is related to material deterioration and/or effects on bond strength between steel and concrete and can be a of mechanical, chemical or physical nature as can be seen in Table 3-1. Performance could be categorized in four groups;

- Function
- Load carrying capacity
- Durability
- Aesthetics

All four of these attributes could be affected by corrosion. However, this project is only focusing on the load carrying capacity and the durability. A concrete structure's performance can decrease of several reasons and an overview of this is presented in Table 3-1, and is further discussed briefly in the next section.

Table 3-1. Examples of causes related to degradation on concrete's structural performance.

<i>Mechanical</i>	<i>Chemical</i>	<i>Physical</i>
<i>Vehicle impact</i>	<i>Aggressive environment; i.e.</i>	<i>Freezing</i>
<i>Overload</i>	<i>chlorides</i>	<i>Heat</i>
<i>Movement, i.e.</i>	<i>Biological deterioration</i>	<i>Salt crystallisation</i>
<i>settlement</i>		<i>Shrinking</i>
<i>Explosion</i>		<i>Erosion</i>
<i>Vibration</i>		<i>Fatigue</i>

3.1.2 Freezing

In general

Every cubic metre of conventional concrete contains between 120 and 180 litres of pores which are so small ($<0,5 \mu\text{m}$), and are structured in such a way, that they are easily filled with water when the concrete is exposed to free water during a long or short time. The pores are filled due to capillary forces and capillary condensation. It is especially the surface concrete area that is filled with water in connection with rain, melting of snow etc. As this water freezes, it expands 9 percent of the original volume, which forces some of the water to neighbouring air-pores. The pressure is evened out as the water spreads in the surrounding concrete. If the concrete does not contain any air-pores, extremely high pressure arises in the concrete. Concrete that is damaged in this way shows signs of inner expansion; for example severe deep cracks, cracking of surface concrete and similar damages.

The pore water freeze temperature is lowered as the pore size gets smaller, as Table 3-2 shows.

Table 3-2. Pore diameter against temperature at freezing (Marina betonkonstruktioners livslängd, 1993).

<i>Diameter [10^{-10} m]</i>	<i>Temperature at freezing [$^{\circ}\text{C}$]</i>
450	-6
280	-10
200	-15
160	-20
115	-30

At normal freeze temperature (0°C) hence no pore water is frozen.

A concrete that contains no air-pores is not possible to create in practice. There is always 1,5 to 2,5 % volume percent of *natural air content* in the concrete. Those pores are large and isolated from each other. They are not easily filled with water and therefore even out the expansion pressure from the freezing water, but not to any extent. The natural air content is almost never enough to protect the concrete and extra pores are needed. An air-pore forming fluid is introduced in the uncured concrete, which creates very small evenly distributed pores in the concrete. Those small pores are also isolated from each other, but the distance between these are shorter than for the large pores. The result is decreased mechanical stresses in the concrete as water freezes, see Figure 3-1 for graphical description.

The factor that is central for freeze-durable concrete is that the distance between the pores is small. Both high air content and small pore size advocate good concrete freezing durability. All concretes with air content below about 2 % show very bad freeze durability. Air content above 3,5 % means that the freeze durability is good (Fagerlund, 1992).

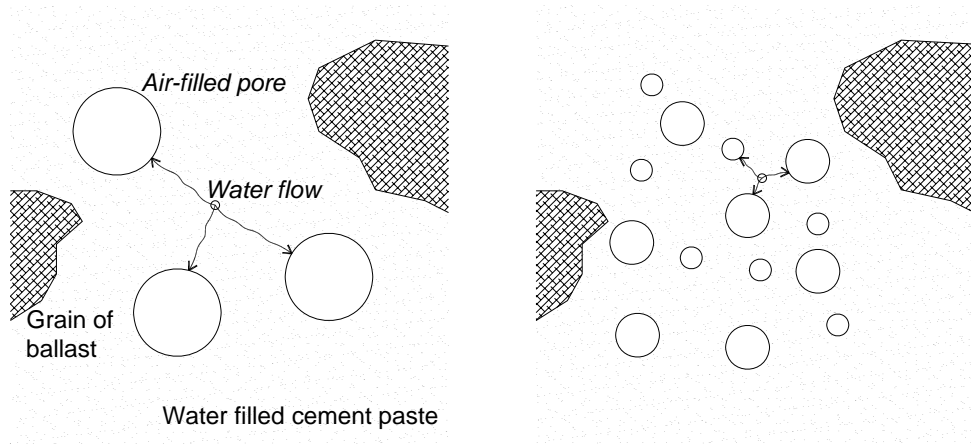


Figure 3-1. Principle of air-pore mixture. Left (without extra pores): Few large pores, long distance between pores. Right (with extra pores): Many small pores, short distance between pores. Based on Fagerlund, 1992.

A reduced water/cement-ratio makes the concrete dense which implies slow water absorption and a small amount of water able to freeze. Both factors work against a freeze resistant concrete. Reduced wct-ratio also involves a finer pore system and decreased pore distance (Fagerlund, 1986). A stiff concrete is not as sensitive to freeze damages as a loose concrete (Bergström, 1955). The cause is the reduced risk of weak separated layers or water filled water separation pockets under large ballast stones. The risk of air content loss during transport and casting is also diminished (Fagerlund, 1992). A longer mixing time is needed, to obtain a homogenous pore distribution with many evenly distributed air pores. The pore system is also more stable by increasing the mixing time (Okkenhaug, 1983).

Freeze attack without chlorides

A freeze damage caused by freezing of pure water is located inside the concrete. The surfaces are though intact as they often are dryer than the inside of the concrete (Fagerlund, 1992). The problem is solved by increasing the air content in the concrete (Marina betongkonstruktioners livslängd, 1993).

Freeze attacks with presence of chlorides

A concrete without extra pores has very small possibilities to withstand freezing when chlorides are present, even at low concentrations. Bridges constructed before 1965 are showing significant damages due to use of de-icing salts.

No additional pores were introduced into the concrete before this time, which gave the concrete no chance to protect it self from the combination of sub-zero temperature and chlorides. Spalling of cover concrete was the main cause of damage, and fall-out of large grains of ballast (Fagerlund, 1992).

Even small concentrations of chlorides causes drastically worsened damages. The peak is at about 2-4% and rapidly decreasing as concentration increases. The damages are reality only after a few freeze cycles, which indicate that the chloride-freeze damages are physically explainable. One possible reason is that an expansion pressure caused by climate dependant structural changes at the salt crystals is the mechanism. However, this hypothesis is not fully accepted and the destruction mechanism is not waterproof. Fagerlund (1992) discuss that the damage is connected to the osmotic pressure that forms due to difference in concentration in chloride containing surface water and the pure water inside the concrete; the higher difference of chlorides, the higher osmotic pressure. The freezable water decreases drastically as the chloride concentration increases further, which decreases the damage. Why the damage is concentrated around the surface is explained by the very slow diffusion of chloride ions inside the concrete.

Smaller distance between the pores in the concrete is required to protect concrete that is exposed to chlorides and freezing at the same time. A concrete structure that will be exposed to both freezing and chlorides, i.e. from de-icing salt of the sea, should always be freeze tested before casting. Slag concrete with high slag content (>65%) has proved to give very high diffusion resistance against chloride intrusion (Fagerlund, 1992).

Structural design

The structural design could have great impact for the freeze-thaw durability. Because of the link between freeze damage and water content in the concrete it is vital that water is not trapped, exposing the concrete structure for a long time. The structure should be designed to let all water drain off, especially if chlorides are dissolved in the water (Fagerlund, 1992).

3.1.3 Corrosion

In general

Good quality concrete will normally offer excellent chemical protection for steel reinforcement against corrosion (Hansson et al, 1985), due to the high alkalinity and the low permeability of the matrix (Mangat & Molloy, 1992). At a pH of 13.5 the interaction between the steel and the hydroxyl ions present in the pore solution, results in the formation of an insoluble Fe_2O_3 layer that makes the underlying steel passive.

Neither the high alkalinity of the pore solution nor the low permeability of the cover can guarantee that the steel will resist corrosion, especially in aggressive environments such as for marine structures. Chloride ions may enter the concrete during mixing or after curing from external sources such as seawater. Once chlorides have reached bar level, they depassivate the embedded steel by locally breaking down the protective layer (Fe_2O_3). Corrosion damage caused by chlorides is concentrated and often severe. The reason is assumed to be that corrosion cells appear where the cathodic surface is large and where the anodic is a comparatively small part of the steel reinforcement. At a big ratio between anode and cathode area and with good oxygen conditions, the corrosion rate can get very high, more than 1 mm per year (Camitz & Pettersson, 1989). The time for the chlorides to break down the protective layer is called initiation period, followed by the propagation period, when corrosion products start to form (Tuutti, 1982) (Austin et. al, 2004). A schematic diagram of the initiation and propagation period can be seen in Figure 3-2. Steel reinforcement that is casted inside of concrete is passive due to the high alkalinity ($\text{pH} > 12,5$). Corrosion is no threat in this situation. The alkalinity is created by alkaline reaction products from cement reactions (sodium hydroxide, potassium hydroxide, calcium hydroxide) which are dissolved in the pore water. The calcium hydroxide alone is 30% of the weight of the reacted cement quantity in an ordinary Portland cement, which is therefore a great base reserve for the concrete. Also the calcium compounds are a part of the base reserve, but they are hard to solve (Fagerlund, 1992). The alkalinity is also affected by the water/cement-ratio (wct). A lower wct implies a lower porosity and less amount of pore water. This gives increased cement content, which enhance the alkali. These two effects give a raised alkalinity at lowered wct, and are especially of interest during chloride induced corrosion. A sufficiently low wct, corrosion is impossible to form due to the high pH (Fagerlund, 1992). The passive steel reinforcement could become passive due to two reasons; chloride intrusion and carbonisation.

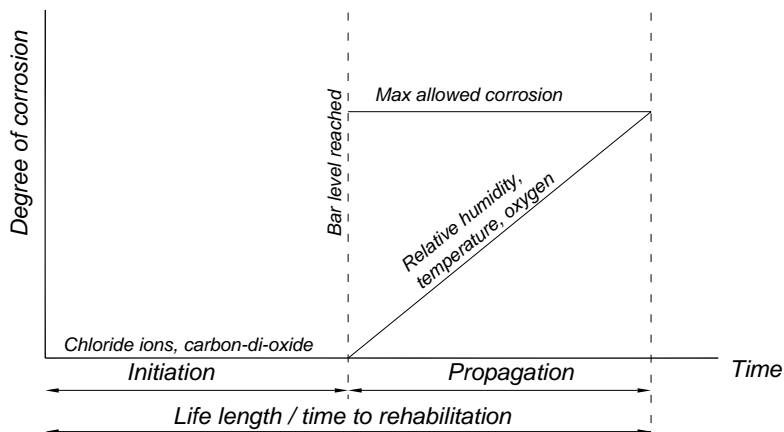


Figure 3-2. Model for reinforcement corrosion. Relative humidity, temperature and oxygen have impact on the corrosion rate. The inclination of the line in the propagation area gives the corrosion rate (Tuutti, 1982).

In general, the propagation period is quite short. The initiation period is really what determines the service life span of the structure. When designing a structure, the service life length is assumed shorter than the initiation period.

The initiation period is divided into two common reasons why corrosion arises; initiation by carbonisation and chloride initiated corrosion. It is not rare that both processes occur simultaneously, which influence the choice of repair or strengthening method.

Corrosion effects

Steel corrosion in RC structures affects both the steel and the concrete. The strength of a corroding steel reinforcing bar is reduced because of a reduction in the cross-sectional area of the steel bar. Pitting corrosion may also reduce the ductility of the steel bar by introducing notches on the surface of the steel bars that lead to a premature necking. This failure is not easy to detect, as this local damage will not reveal itself by additional deflection of other external effects.

While the steel reinforcing bars are corroding, the concrete integrity is impaired because of cracking of the concrete cover caused by the expansion of the corrosion products. Finally, the composite action of the steel and concrete is diminished because of deterioration in the steel-to-concrete interface, caused by the lubricant effect of the corrosion products and by cracking of the concrete cover (Tamer & Soudki, 2005).

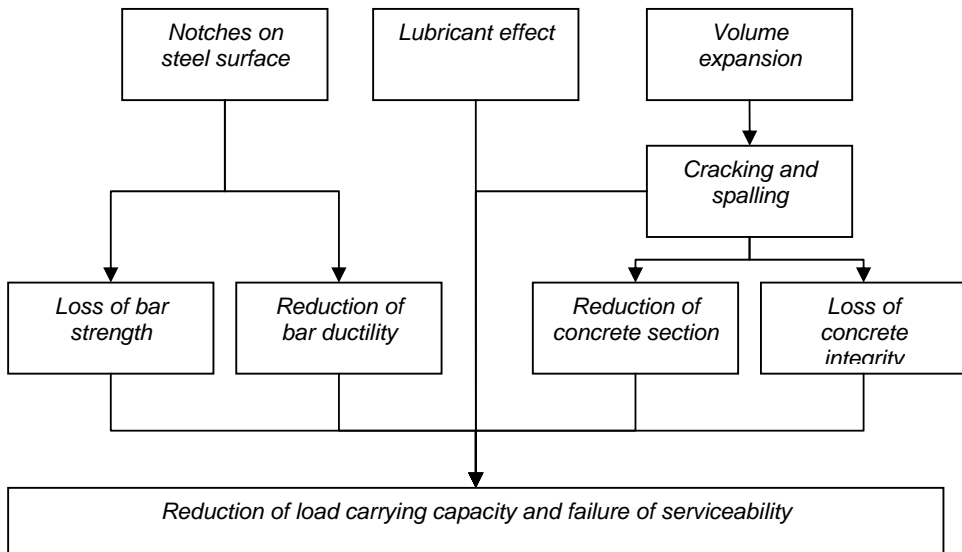
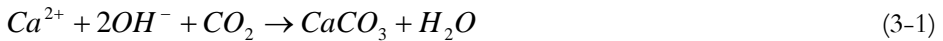


Figure 3-3. Effects of steel corrosion on concrete structures. After Tamer & Soudki, 2005.

Initiation by carbonisation

Carbonisation is a process where carbon dioxide (CO_2) from the surrounding air penetrates the concrete and reacts chemically with the pH-raising calcium compounds and alkali hydroxides that are present in the pore solution. The reaction process is an acid-base reaction, which results in neutralisation of the calcium hydroxide. The hydroxide ion concentration decreases and the pore solution's pH-level decreases from at least 12,5 to about 9. The reaction could be stated:



The reaction is dependant on, which means that there has to be some moist in the concrete for the reaction to occur.

Carbon dioxide is a part of the atmospheric air in concentrations around 0,03% at ground level. In some particular environments, the air content of carbon dioxide is far higher, i.e. in cities, tunnels and garages. This concentration difference creates a driving force for levelling out this difference. Carbon dioxide intrudes into the concrete's capillaries and pores, and is consumed in the reaction above. New carbon dioxide penetrates the concrete until all reactive calcium has been turned into calcium carbonate.

The reaction process propagates with a relatively defined front into the concrete. This front divides the concrete into two zones, the outer carbonised zone ($\text{pH} < 9$) and the inner non-carbonised zone with pH-level above 12,5. When the front reaches steel reinforcement level, the steel is activated due to the low pH-level, and starts to corrode (Fagerlund, 1992). The rate of this front depends on, for example

- The surrounding's CO_2 -concentration.
- The quantity of available Ca-ions, that are eager to react.
- Diffusion rate for the CO_2 -gas.

The biggest influence on the carbonisation rate is from the concrete's diffuseness with respect to carbon oxide. Concrete with a low water/cement ratio (wct) is less sensitive to carbonisation, as the CO_2 -gas does not penetrate to any extent.

The relative humidity (RH) determines the quantity of physically bonded water in the concrete structure. A higher RH gives a higher degree of water filled capillaries. Carbon dioxide can not penetrate an already water filled capillary, which means that a high RH concrete is not affected by carbonisation. The fastest carbonisation occurs when the RH is around 50%. At this RH, the majority of the capillaries are opened for carbon oxide to enter, and there is at the same time enough water for the reaction involving the water phase. Based on the assumption that the carbonisation mechanism is of diffusion type, the rate of carbonisation could be calculated by the following expression:

$$x = k_{carb} \cdot t_{carb}^{1/2} \quad (3-2)$$

This is an empirical equation which will give relevant answers only if the coefficient, k , is chosen correctly. One can nevertheless conclude that the equation indicates that the carbonisation rate decreases ever more as time passes.

Chloride intrusion

Chlorides from seawater or de-icing salts slowly penetrate into the concrete. There is no front, as can be seen during the carbonisation process. Instead, the chloride concentration gradually decays from the surface into the concrete. The corrosion process will not start until the chloride concentration around the steel reinforcement reaches a certain threshold value. Corrosion product forms and often occurring as local pit-corrosion for the chloride initiated corrosion. In unfavourable conditions the corrosion process is very fast. Pre-tensioned steel reinforcement is particularly vulnerable for chloride initiated corrosion. This brings the importance of sustained load during corrosion tests, in laboratory environment in particular, to the surface. The intensity of the corrosion is mainly dependent on how much oxygen (O_2) that can penetrate through the concrete to the steel (Fagerlund 1992). The initiation time for corrosion caused by chlorides is dependant on

- The chloride concentration in the surrounding.
- Diffusion rate for chlorides.
- Concrete's ability to bond chlorides.
- The chloride concentration value for the initiation of corrosion.
- Cover concrete thickness.

The chloride profile is determined from the concrete surface and into the concrete, by cutting out discs of concrete drill cores. An average chloride concentration value is verified for each disc.

Electrochemistry

Corrosion is an electrochemical reaction involving the transfer of electrical charges in the form of electrons in the steel, and ions in the free concrete water. Due to this, there is a change on and around the reinforcing steel surface. To drive an electron current there has to be a potential difference between two separate areas, the anode and the cathode. The anode has greater positive charge than the cathode. At the anode, an oxidation process occurs that implies that material pick up electrons. When the steel at the anode looses electrons, positively charged steel ions are created, which results with the steel being dissolved while emitting electrons. The steel corrodes and is transformed to what is known to as rust. The electrons travel in the steel to the cathode where they are taken care of by oxygen from the air and the water in the concrete. Hydroxyl ions, OH^- -ions, are created as a result from this reaction, see Figure 3-4. The steel in the cathodic area is not attacked, it is passive.

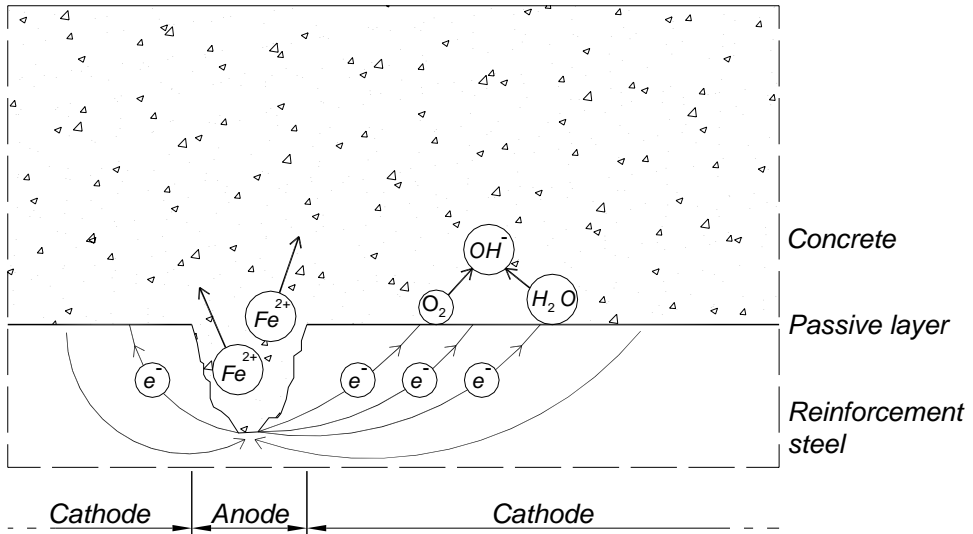


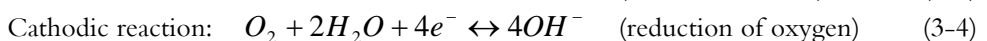
Figure 3-4. Diagram of a corrosion cell in moist concrete.

Anodic and cathodic surfaces always exist on the steel reinforcement, as the steel consists of different material phases, i.e. perlite, ferrite, cementite and carbon crystals. Each one of these material phases has its own potential, which fulfils the demand of potential difference for corrosion to occur.

As the size is small they are called micro cells. Also large areas are created where anodic and cathodic surfaces act on the steel reinforcement, so called macro cells. The potential difference is caused by:

- Inhomogeneous steel surface (entrapments in the steel, pollutions etc.).
- Differences in alkalinity along the reinforcement (pH-difference after carbonisation).
- Varying oxygen or chloride concentrations.
- Cracks in the concrete.
- Macro pores, such as insufficiently consolidated concrete.
- Temperature differences.

The processes at steel corrosion are summarized in the following simplified equations:



All in all, the redox process could be expressed in the following way:



The steel ions, emancipated from the anode, react with the hydroxyl ions from cathode:



Further, Fe^{2+} ions react with oxygen, the steel surpasses from Fe^{2+} to Fe^{3+} . The corrosion product that is visible to the eye is called rust. The following criteria are essential for the continuation of this process:

- An anodic and a cathodic surface are needed in a closed circuit.
- Potential difference between the anode and the cathode.
- Electrolyte (water) should be available (ions should be able to move in the concrete).
- Oxidation substance (oxygen) is present.

If any of these criteria are not fulfilled, the corrosion process is stalled. Generally all four criteria are fulfilled in an outside environment that corresponds to a typical Scandinavian climate. This should therefore mean that reinforcement corrosion always occurs. However, the concrete itself has properties that protect the steel. The cement paste has a high pH-level, at least 12,5, which creates a dense corrosion layer on the surface of the steel. This layer protects the steel from corrosion. The common corrosion process could only begin if this protective layer is put out of function, due to for example loosening up from ion activity, chlorides or destroyed by decreased of pH-level.

In reality, however, the $Fe \rightarrow Fe^{2+} + 2e^-$ reaction is not the only reaction which takes place at the anode. Other reactions occur simultaneously, i.e. anodic evolution of O_2 and possibly Cl_2 (Hearn 1996). The ratio of the charge consumed in the reaction of interest (oxidation of Fe) to the total charge passed is called the current efficiency, N (MacInnes, 1939), and was obtained by comparing the mass of corrosion product determined from the gravimetric method and from Faraday's law.

This value of N was then used to adjust the extent of corrosion determined theoretically at various times during the corrosion process. Value of N was found to be approximately 0,7 at experiments reported in Ballim & Reid (2003), which indicates that the $Fe \rightarrow Fe^{2+} + 2e^-$ reaction is dominate, but not the only one.

Accelerated corrosion

To simulate corrosion of reinforcement, accelerated simulation is often required. Accelerated chloride-induced corrosion techniques are common to reduce the time taken for a critical level of chlorides to reach the reinforcement bars, thus depassivate the steel reinforcement. Three methods are common: Admixed chlorides, impressed voltage/current and wet/drying techniques.

The first two methods are either combined or separate depending on the reason for the study (Austin et al, 2004).

When an impressed current is used to drive corrosion, the amount of mass loss is related to the electrical energy consumed once the steel has become depassive, and can be modelled using *Faraday's law*. This law is expressed:

$$\Delta W = \frac{I_{corr} t_{corr} A t_m}{zF} \quad (3-7)$$

There are other competing reactions, and Faraday's law will only give a true reflection of the extent of the corrosion if the total number of equivalents which have entered in the reaction are used. For example, at an applied potential difference of 6 V only a small portion of the total current can be attributed to rust formation, Faraday's law is adjusted by multiplication with a constant N that is now known to be 0,7, see previous page.

3.2 Repair and retrofitting

3.2.1 In general

The objective with upgrading is to increase the performance of a structure. Performance can be divided into the four previous given criteria; load bearing capacity, function, durability and aesthetic. The load bearing capacity, durability and function are the most vital criteria to consider as a structural engineer. However, an aesthetic appearance is also important, especially for those who own and uses the structure. All four criteria should be fulfilled to consider the upgrading completely successful.

3.2.2 Adhesive and bonding

The most critical link to make a strengthening system work properly is the issue regarding bonding the strengthening material to the structure. A good bond will supply sufficient force transfer between the materials to give an effective system.

Glue is often referred to as adhesive, and is used to bond the strengthening material onto the structure. Glue is a product which normally is in liquid form with good ability to wet the materials intended to be bonded together. Organic or metal-organic compounds are normally considered as interesting substances to use as adhesives. Examples of metal-organic compounds are silicones, titan and tin compounds.

The adhesive is applied on the materials and a reaction with the substrate surface occurs to give a high chemical bond. It is essential that the glue can wet the surfaces and create contact with the materials on a molecular level. The glue is able to wet the material surface if the surface tension of the adhesive is lower than the material surface (Hollaway & Leeming 1999). The surface tension is lowered if the material surface is contaminated by grease or oil, which makes it hard for the adhesive to wet such surfaces. Since epoxy resin has a higher surface tension, of around 35–45 mN/m, than Teflon, 18 mN/m, it is impossible to bond Teflon using epoxy. The same case is for rubber and some plastics. Wood has a surface tension of about 200 mN/m. This makes it ideal to bond with epoxy (Andersson & Spett 2002). Generally, there are four different types of significant bindings:

– Mechanical forces

These forces act entirely mechanically and arise when the adhesive penetrates down into large or small cavities and hooks on to the materials. Mineral based strengthening systems, where the epoxy is replaced by a polymer modified mortar and the sheet or plate of the strengthening material by a net, totally depend on these forces on a macro level.

– Van der Waals forces

These forces occur in between almost all material as long as they are sufficiently close to each other. The adhesive has to come as close as 3–4 Å (1 Å = 1 Ångström = 10^{-10} meters) distance to activate Van der Waals forces in between the materials. These forces are by nature electrical and are created by electrical interactions present in all molecules. Van der Waals forces are relatively weak and the bond strength traced back to these forces has a low capacity to sustain intrusion from water or other materials.

– Polar forces

These forces are typical for materials that except for carbon (C) or silicon (Si) also include oxygen (O). Permanent electrical unbalances are created in those molecule shapes due to the exceptional ability of the oxygen molecule to attract electrons from the rest of the molecule. This unbalance creates a positive, anodic, and a negative, cathodic, side of the molecule just like a magnet. The application of a naturally polar adhesive will create a very strong bond with good durability against the environment.

– Covalent forces

This force creates the strongest bond possibly in between materials. It depends on chemical reactions between two materials during which covalent bindings are created. These forces are aimed to be utilized as much as possible when bonding materials using adhesive, since these bindings are utterly durable against chemical and mechanical impacts. Covalent bindings produce practically completely water-resistant durability in the joint between the bonded materials.

3.2.3 Patch repair

A typical technique to repair corrosion damaged concrete, referred to as patch repair, is removal of the chloride contaminated (or carbonated) concrete surrounding the reinforcing steel bar. The bar is cleaned from corrosion products, and the cavity is then refilled with new chloride-free, high pH concrete. This repair procedure could then be complemented with strengthening of the structural member. See Figure 3-5 to view all stages in the repair process followed by strengthening of the structural member. The composite action between steel reinforcement and concrete is changed when the cover concrete is removed. When new concrete then is introduced in the structural member, it is important to understand the effects caused by the operation. Cross-section strain distribution will surely be modified, as the applied concrete is not subjected to any strain due to dead load of the structure.

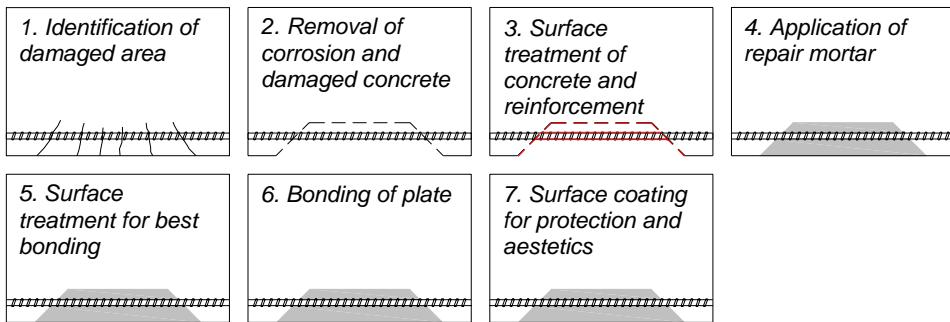


Figure 3-5. Patch repair procedure followed by strengthening of the structural member in flexure (Täljsten, 2003).

Experimental studies show that it is possible to achieve full composite action between the concrete structure and the patch repair concrete. Several authors highlight the importance of similarity between existing and repair concrete; i.e. modulus of elasticity, tensile strength, coefficient of thermal expansion, shrinkage, creep and tensile adhesion to the concrete beam (Mays et al, 1996). The difference in modulus is said to be not more than ± 10 kN/mm² (Hewlett & Hurley, 1985; Emberson & Mays, 1987; Plum, 1989).

After the repair has been performed, the reinforcing steel in these areas are well depassivated. However, the new concrete creates a situation where potential differences appear between the old, chloride contaminated concrete, and the new. This difference in potential is the driving force for new corrosion sites in the chloride contaminated concrete around the repaired area (Ball, 2000), see Figure 3-6. There is no use in protecting the steel bars with corrosion resistive paint at this point, since the critical area is located inside of the old concrete.

However, if a cathodic protection system is used to apply an electrical current which makes the steel reinforcement act as an anode instead of cathode, this problem is solved. The cathodic protection system acts in the opposite way of accelerated corrosion.

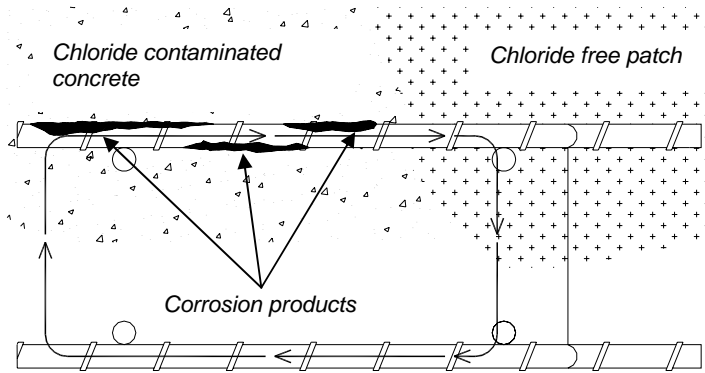


Figure 3-6. Patch accelerated corrosion. Potential difference between patch and chloride contaminated concrete results in accelerated corrosion.

3.2.4 Confinement

When a concrete beam is subjected to corrosion, the corrosion products will create an expansion pressure around the steel reinforcement, leading to cracking and spalling of surrounding concrete. One way to retain strength and to keep the damaged element in one piece is to confine the corrosion damaged concrete member by wrapping it with CFRP material, see Figure 3-7. This technique is directed toward concrete columns, but there is a study where a combination of confinement and longitudinal strengthening is applied on beams subjected to corrosion and bending moment (Soudki & Sherwood, 2000). It should be mentioned that this method does not have a before known effect on the corrosion process. The most beneficial case would be that the corrosion products were confined so much, that further corrosion would be stopped. The worst case scenario would be that the corrosion flourished under the wrapping material, giving an accelerated deteriorating process.

Some authors claim that the presence of cracks in concrete does not necessarily result in intensification of the corrosion process (Andrae et al, 1993). Crack width does not significantly affect the corrosion rate, and many codes require unnecessarily detailed crack control demands in order to limit the corrosion process (Beeby, 1983). The explanation for this is that the corrosion process can stop itself. For concrete columns however, the consolidation and densification of the corrosion products around the reinforcement can be enhanced by adding adequate strengthening. It is possible to achieve effective confinement by wrapping CFRP material around the cracked surface of the concrete column, therefore tightening the concrete in that area, which will contribute to reduced corrosion rate.

In contrast, it is possible that an unhealthy concrete structure that is confined by a FRP system is hiding all visual evidence of the corrosion activity, which can proceed for a long time without any notice (Ball, 2000).

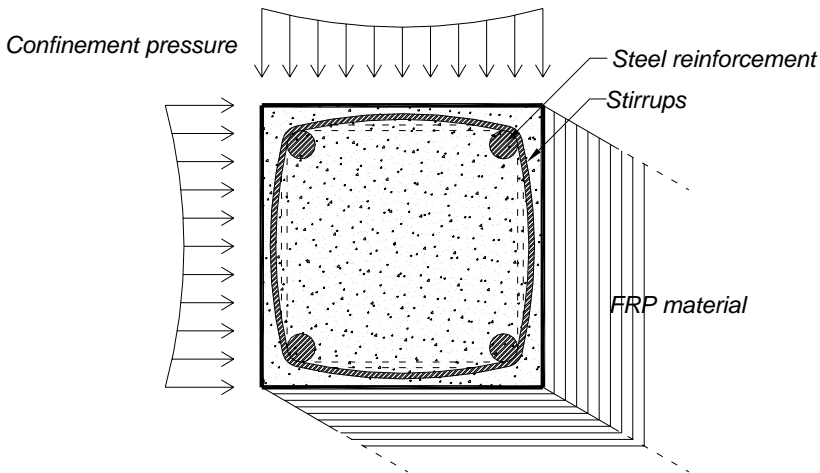


Figure 3-7. Diagram of confinement by wrapping the concrete member with CFRP material.

Positive effects by confinement;

- Increased densification of the corrosion products, which form a barrier that protects the steel reinforcement from more water and oxygen to penetrate to bar level. This will decrease the corrosion rate since the vital aggregates essential for corrosion to occur is fully or partly removed from the concrete/steel interface.
- Confinement of a concrete section lessens corrosion cracking and bond splitting cracks.
- Increased shear resistance to overcome the loss in steel reinforcement cross section.

By combining longitudinal strengthening and transverse (in this case wrapping), increased shear and moment capacity as well as confinement are accomplished (Soudki & Sherwood, 2000). One problem with FRP material bonded with epoxy is that a non-permeable barrier is created, which could trap water and moisture inside of the structural element. The corrosion process could easily be accelerated in the environment created under the strengthened surface. Further, it could be hard to see the extent of the damage of the concrete when it is covered.

3.3 Strengthening

The concept of strengthening with composite materials involves the external bonding of fibre reinforced polymer (FRP) in the shape of plates, to slabs and beams, or the wrapping of RC columns. Interest in these upgrading techniques is widespread and continues to grow because of the ease of installation, low cost and high strength-to-weight ratio of the FRP materials. Further, the method is ideal as it does not increase the structural member's thickness or add any weight to the structure. The FRP strengthening methods are not only useful for concrete structures, as they can also be used for steel and timber structures. In this thesis the focus will be on external strengthening of concrete structures in flexure.

3.3.1 Challenges

Strengthening of existing structures can at first sight be assumed to be a simple procedure. However, while consideration has to be taken to existing materials, deterioration of the structure, loads during strengthening and to existing geometry, it could get quite complicated. When strengthening is undertaken, all different modes of failure have to be considered. Strengthening in flexure could for example lead to brittle shear failure, and not to a desired ductile bending failure. By strengthening one critical member in a structure, another member could become the critical one. Strengthening of one member, thus increasing its stiffness, in an undetermined structural system affects the entire structure. The strengthening should also be designed in respect to maintenance and repair needs, as well as for fire, vandalism, collision etc (Chaallal et al, 1998).

Further, existing documentation of old structures are often poor and it may be necessary to redesign the structure according to the former codes and standards that were in use. Field investigations are often necessary and always provide useful information about a structure's status.

3.3.2 Strategies

When deterioration processes are present it gets more complicated to evaluate the status of the structure, as mentioned above, since the capacity of the structure continuously decreases, see Figure 3-8. The left part of the curve the performance level of the structure is slowly decreasing, but it is still above the design minimum. As new and higher load carrying demands or safety levels are defined, the structure still manages to fulfil the requirements.

At some point the deterioration has affected the structure to a level that it no longer carries the design load, and has to be strengthened. Many aspects affect the choice of the strengthening design; i.e. economy, structural, environmental, remaining service life of the structure etc. There is no use in strengthening one certain part of the structure to last 50 years, if only 5 to 10 years remain of the structure's service life.

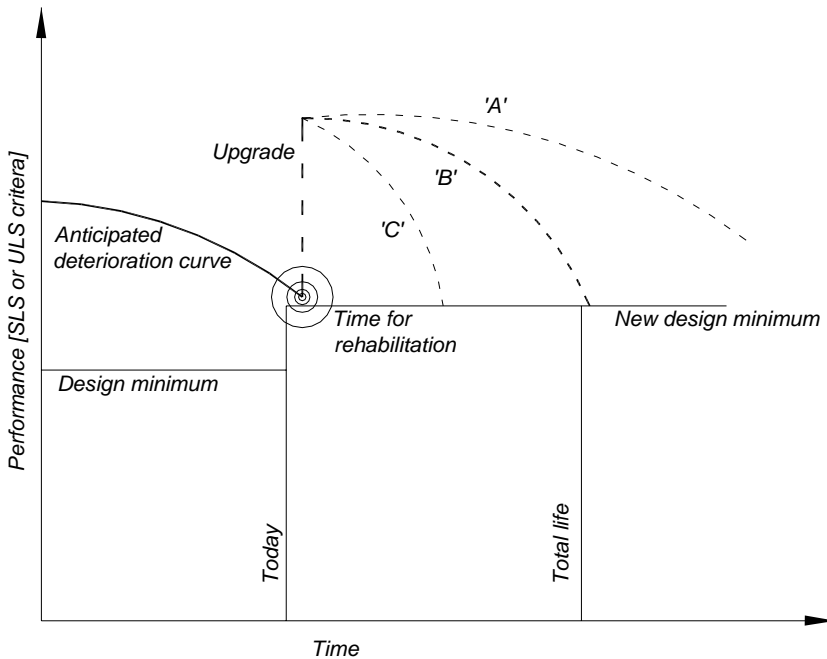


Figure 3-8. Deterioration and strategies for strengthening. Based on Carolin, 2003.

In this general and exaggerated example there are three different upgrading designs. Type 'A' works really well, 'B' gives desired service life but is more cost effective than 'A' and 'C', is for this structure a poor method for this structure and in the given example it even accelerates the deterioration process.

In this case, 'B' is the most suitable upgrade technique since it maintains acceptable performance through the total life of the structure, and is at the same time cheaper than method 'A'.

3.3.3 Ductility

Fibre reinforced polymers (FRPs) are linear-elastic materials. If, for example, a carbon fibre plate is pulled to failure the failure will be brittle, abrupt and without any warning. Due to safety reasons structures are not normally allowed to have such behaviour.

Instead, they should be designed to have a ductile failure, or at least give enough warning signals preceding a possible failure. Ductility can be defined as the capability of a structure to deform while still carrying the load even when the maximum load bearing capacity is exceeded. A structure's behaviour is not easy to predict, as material property and structural ductility are not directly dependant.

Linear-elastic materials may increase the ductility of a structure. For example, a concrete beam reinforced with steel bars is often considered to have a very ductile behaviour. But if the same beam is subjected to fatigue loading, the failure will be a brittle one, as high stresses form in both tension and compressive reinforcement. In spite of the upcoming brittle failure of a fatigue loaded concrete beam, there is no warning about this sudden failure, as it initially behaves similar to a ductile failure. By strengthening such beam with FRP, stresses decrease in tension and compressive reinforcement, leading to a safe structure with ductile failure instead of a brittle one (Carolin, 2003). This ductile concrete beam could also fail in a brittle manner if the steel bars were attacked by pitting corrosion. The brittle behaviour is generated by stress concentrations in cross sections along the steel bar where a corrosion pit reduces the area significantly.

When designing, it is possible to engineer strengthening so that the failure occurs in a place or in a particular mode which gives favourable ductility of the structure. For example, a shear failure is generally thought of as a brittle failure. If strengthening is applied to see to that a bending failure occurs first, the ductility of the element is possibly enhanced.

3.3.4 Material

The FRP consists of two main components, fibers and a matrix. Occurring fibres are carbon, glass or aramid fibres and the matrix are usually epoxy, vinyl ester or phenolic. Because of the ease with which the uncured FRP can be shaped it is possible to create many different products. In civil engineering there are several FRP products that are suitable to use; uni- and multi-directional sheets (which are not blended with any matrix before bonding on a structure), mechanically wrapped strands, rebars, grids, rods and tendons.

FRP can be used in different strengthening scenarios; i.e. tensile, flexural, shear, fatigue, buckling, confinement and blast upgrading.

Carbon fibre is the most adaptable to use in all strengthening scenarios, see Table 3-3, expect for blast upgrading, where aramid fibre is particularly pliable due to its great ability to absorb shocks and high quantities of energy. The reason why aramid fibre is not appropriate to use in civil engineering purposes is because of its sensitivity to moisture and ultraviolet light and it is more expensive than CFRP (Cadei & Holloway, 2002).

CFRP has a high modulus of elasticity, 200–800 GPa. Strain at failure is 0,3–2,5 %. The material does not absorb water and is resistant to many chemical solutions. The fibre behaves very well against fatigue and does not creep under loading.

Table 3-3. Different material behaviour under influence of various factors, + indicates a good behaviour, = indicates an average behaviour, - indicates a bad behaviour. Carbon fibre demonstrates the best properties (Karbhari, 1996).

Criteria	Steel	Aramid fibre laminate	Laminate of carbon fibre	Laminate of glass fibre
Relaxation and creep	+	-	+	=
Moisture resistance	=	=	+	-
Alkalinity resistance	+	=	+	-
Thermal stability	=	=	+	-
Chloride resistance	-	=	+	=
Fatigue behaviour	=	=	+	-
Long time loading	+	-	+	=

3.3.5 Application

Bonding of a CFRP material in the beam's longitudinal direction increases its moment capacity. The fibre material is stretched when the beam deflects; creating a force which is located at the tensile face of the beam cross-section, see Figure 3-9.

When calculating moment capacity, beam response at failure load after strengthening has to be investigated. The failure modes regard whether compressed reinforcement is yielding or not, compressed concrete is crushed or not, and if carbon fibre material fails or not. Each failure mode is related to a certain ultimate strain distribution, affecting generated ultimate moment capacity of the cross-section. When moment capacity is calculated for all possible cases, the one which gives the lowest moment capacity is the expected one occurring. For an accurate design, two stages are studied. In the first stage, the condition before strengthening is studied. The other stage is the design for increased bending capacity, where the initial conditions before strengthening are taken into consideration. Complete guidelines for strengthening with FRP can be found in Täljsten (2004).

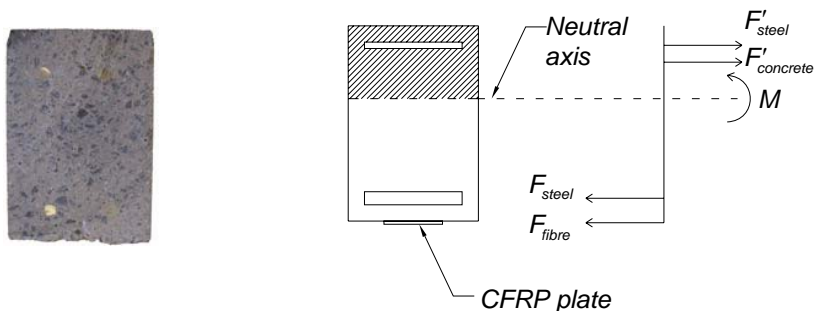


Figure 3-9. Forces acting on a CFRP strengthened concrete beam cross-section subjected to a moment, M .

3.3.6 Existing strain fields

When repairing or strengthening an existing concrete structural member, often parts of the structure is removed. This could be done by water jetting, jack hammering or other similar methods. New concrete is then cast into the old concrete area. If the structure is loaded, i.e. by dead load, when refilling is carried out, stresses (or strains) will act on the existing structure but not on the newly added material. This means that stresses are created at the interface. This behaviour is shown in Figure 3-10, where the strain distribution for a rectangular beam during repair and when loaded is shown. If the resulting strain field exceeds permitted strain levels, steel yielding or concrete compression failure might occur.

In Figure 3-10a, the cover concrete is removed and the beam is subjected to the bending moment acting during the repair procedure. Note that the strain in the repair mortar is zero. Figure 3-10b shows the strain distribution when applying an arbitrary moment, M . Those two strain fields are then super positioned to result in the actual strain distribution for the repaired beam when further loaded, as presented in Figure 3-10c.

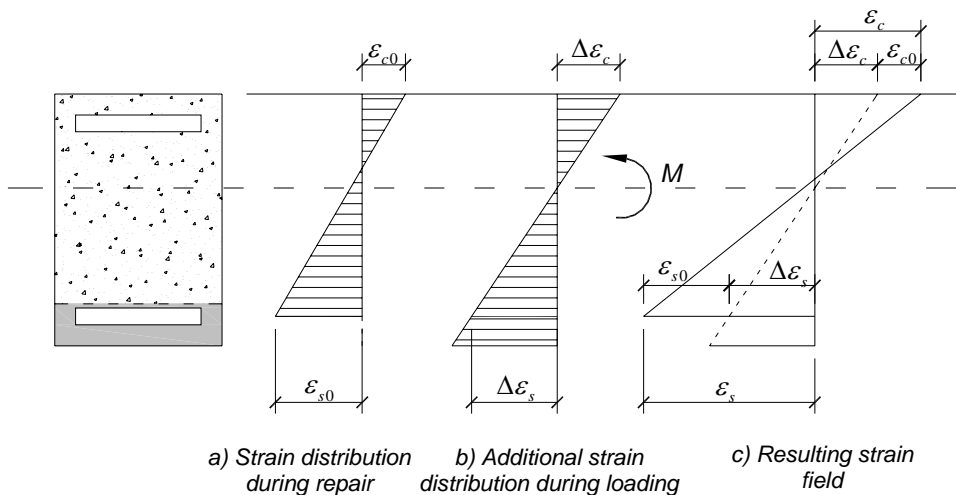


Figure 3-10. Diagram of how to take consideration to strain field created during the repair procedure.

Near Surface Mounted Reinforcement

This method consists of increasing moment capacity by adding FRP or steel products on the tensile face of a beam. This method is particularly appropriate when upgrading a structure, not when building a new one, since the material is added on the surface. This means that it is reasonably easy to add the material. FRP material could either be plates bonded on the surface of the structural member, or rods which are bonded in cut slots in the concrete. See Figure 3-11 for a diagram over an NSMR strengthened beam.

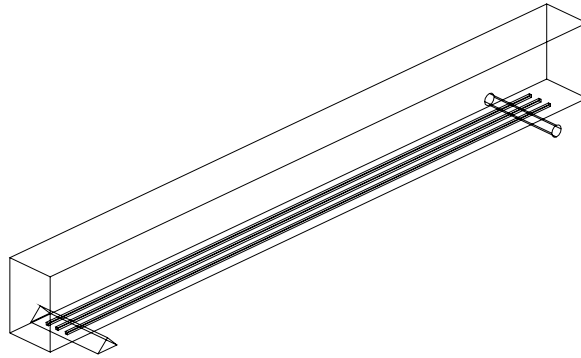


Figure 3-11. Near surface mounted reinforcement (NSMR) rods attached to the tensioned side of the concrete beam.

One important effect when strengthening is that the compressed zone of the concrete cross section is increased. This increases the strain and force in the concrete, see Figure 3-12.

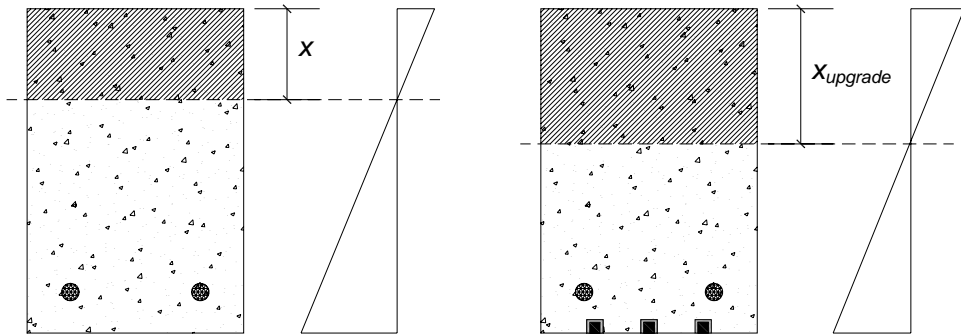


Figure 3-12. The compressed zone of the concrete beam is increased for the strengthened beam.

Pre-stressing of strengthening material

The pre-tension is achieved by applying a tensile force on the CFRP during the curing process, which is then released when a sufficient amount of strength has built up in the adhesive layer. The effect of this is inbuilt tensile stresses in the carbon fibre material, although the beam member is not externally loaded. The result is that the strength in the CFRP material and resin is used more efficient, leading to higher crack load and failure load. Another effect of pre-stressed strengthen material is that the compressed zone is increased even more (Nordin, 2003).

In similarity to the existing strain field during repair, a change in strain distribution for a structural member will also occur when it becomes pre-stressed. This is principally shown in Figure 3-13. The cross sectional strain distribution for a concrete beam which is strengthened with a pre-stressed FRP material and also subjected to a bending moment is seen in Figure 3-13a, and is created by superposition of the strain distribution created by the applied bending moment given by Figure 3-13b and the pre-stressing force given in Figure 3-13c.

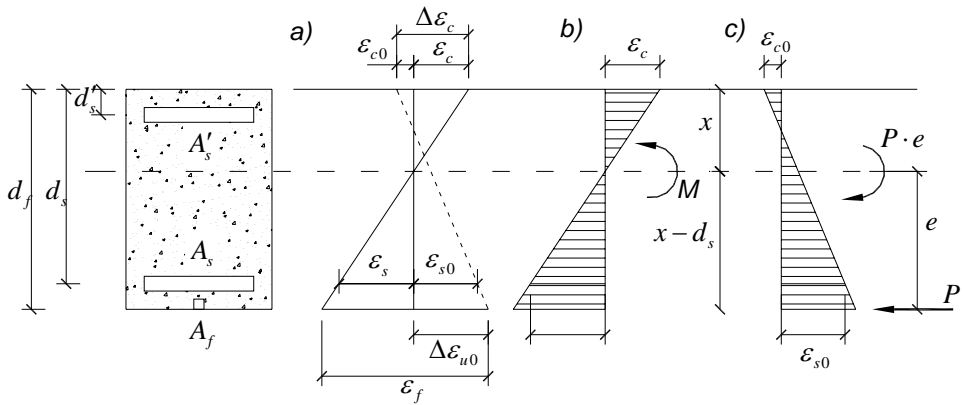


Figure 3-13. a) Strain distribution in the loaded beam cross-section, where the CFRP is pre-stressed, is achieved by super-positioning of b) and c). b) Strain distribution when applying a bending moment on the non-strengthened cross-section. c) Gives the initial strain field when applying a pre-stressed strengthening material.

Opposite to the negative effect from the existing strain field during traditional concrete repair a beneficial contribution will be achieved by pre-stressing, in particular when concrete cracking and steel yielding is considered

Pre-stressed tendons

The third application is to place cables or rods on each end of the beam, made of steel or FRP material. It is then pre-stressed and secured at each end. They are positioned along the tensile part of the cross-section to contribute to the moment capacity, see Figure 3-14.

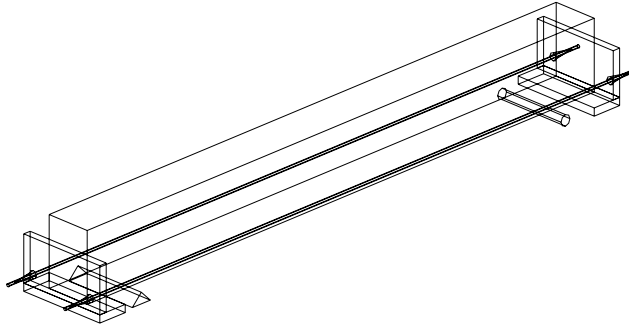


Figure 3-14. Pre-stressed cables are installed to improve moment capacity.

Another possible solution is to place the tendons dropping down to the underside of the beam in mid-span and fastened at beam ends. See Figure 3-15. This solution works well even if the concrete beam is considerably deflected at mid-span. If large deformations are present in the first example the lever for the cable decreases in mid-span, reducing the effectiveness of the strengthening system.

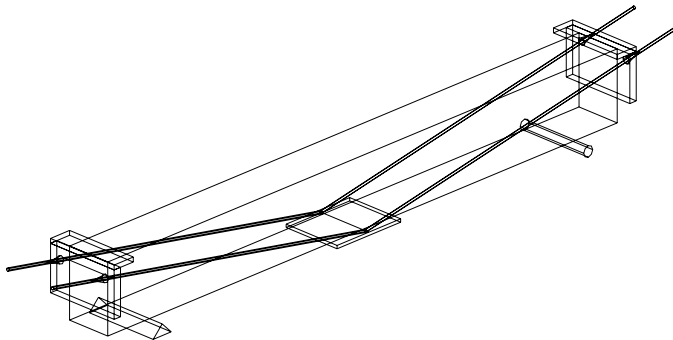


Figure 3-15. Another way to place pre-stressed tendons in order to enhance the flexural capacity of the beam member.

A weak link is the fastening of the CFRP or steel tendon in the beam ends, as great forces have to be controlled at those points. The NSMR method does, however, not ensure that bond failure between carbon fibre and concrete does not occur. Especially at the ends of the carbon fibre, leading to possible delamination that progresses along the beam. The performance of above discussed NSMR and pre-stressed tendon strengthened concrete beams has been studied at Luleå University of Technology by Nordin (2003). Load/displacement curve for reference beam, beam with non pre-stressed NSMR reinforcement and beam with pre-stressed NSMR reinforcement is presented in Figure 3-16.

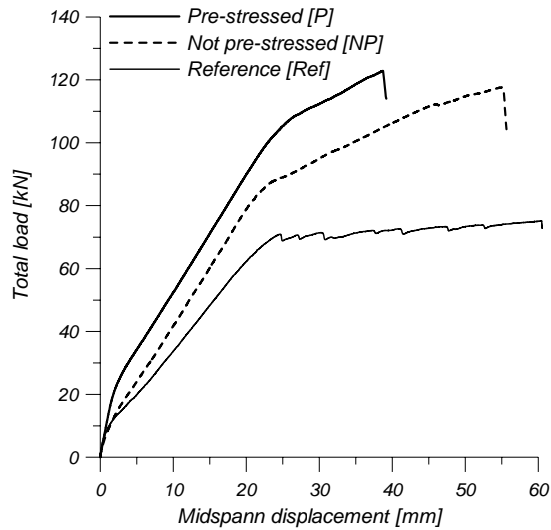


Figure 3-16. Load-displacement graph for pre-stressed, not pre-stressed and reference beam. The study shows that strengthening increase crack load and failure load (Nordin, 2003).

3.4 Monitoring

3.4.1 Requirements

Behaviour over a large time period is interesting to monitor when a concrete structure or a member is subjected to both long-time loading and corrosion, such as in the tests performed in this study. To be able to pick up this interesting information during all the tests the equipment has to be functional during the entire period.

The demands on the equipment are highly dependent on how the surrounding environment affects it. For example, say that the artificially created corrosion aggressive environment is concentrated around the tensile steel reinforcement. If that specific monitoring equipment is placed in that area, it has to sustain that environment. Humidity, corrosion and the long-time use will make it critical how to integrate the sensor onto the beam specimen. If the sensor is chosen to be placed in the part of the cross-section that is subjected to accelerated corrosion and replacement of damaged concrete, this has to be taken into consideration. It is possible to use non-corrosion resistive monitoring equipment if it is placed outside that area, and is electrically isolated from the concrete specimen. One sensor that theoretically fulfils the requirements is the fibre optic sensors, which can be placed anywhere in the beam cross-section by insertion before casting.

3.4.2 Fibre optic sensors

Traditionally monitoring has been accomplished by a network of electrical strain gauges attached at various points on a structure.

Over the past decade, application of fibre optic sensors (FOS) in civil engineering structures has grown to be a serious alternative to the traditional strain gauges. Distributed strain sensing technology has several important advantages over more conventional sensors that make it very attractive for structural health monitoring. In particular, the ability to monitor a virtually unlimited number of locations on a structure using only a single optical fibre and the ability to dynamically choose these locations offers great flexibility (DeMerchant et al, 2000). Other features of such sensors that make them particularly advantageous over their foil gauge counterparts include immunity to electromagnetic interference, corrosion resistance, reduced cabling, excellent sensitivity and small size (Kalamkarov et al, 2000). There are mainly two types of distributed strain sensing systems that are used today in structural monitoring applications, Bragg grating sensors and Fabry-Perot sensors.

The Bragg grating sensor is the most common and easiest for civil structural monitoring (Utsi, 2001). Very small gratings are created, often with UV-light onto the fibre. By choosing a distance between the gratings a certain wavelength of light is reflected back. This makes it possible to apply several sensors onto one fibre, as long as two sensors do not cross each others wavelengths. The measurement range decreases as the number of sensors increase due to this reason. In the case of sending in a broad band light into the fibre, a specific wavelength of the light is reflected back when it hits the gratings while the rest of the light passes. See Figure 3-17 for the Fibre Bragg Grating principle.

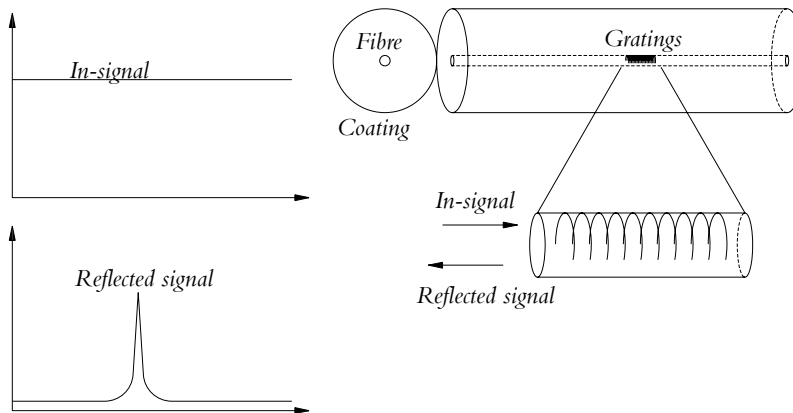


Figure 3-17. Fibre Bragg Grating principle.

3.4.3 Curvature measurement

Curvature is a measure which has theoretical significance in terms of structural stiffness. Stiffness is a measure with which the structural health could be interpreted. It is possible to measure curvature locally using strain readings in two points of the cross section; it is also possible to measure through global curvature using displacement readings.

In bending, the advantage of measuring curvature globally increases with the decrease in the structural thickness. For thick structures it is easier to measure strain. The reason for this is that strain is small and curvature big on a thin structure, and the other way around for a thick structure. One should, however, always consider the difficulties with measuring tension strain in cracked concrete, since the strain readings could be heavily dependant on where the gauge is placed in respect to surrounding cracks. Figure 3-19 shows the benefit of measuring curvature as the structural thickness decreases (Djordjevich et al, 2001). The break-even thickness depends on the instruments' sensitivity. This thickness is 50 mm for the current development state of the curvature gauge with respect to a strain gauge sensitive to 10 microstrain. Thin plates and shells used widely in modern structures (advanced composites in particular), is one area for application of the curvature gauge as the need for extremely high accuracy for strain measurement would be eliminated. In contrast to the strain measurement, curvature measurement is position independent. This property of the curvature measurement concept is beneficial since the exact sensor position within the structure need not be assured. Being able to place the curvature gauge at the neutral axis, where strain is zero, makes measurement on, for example, two ply composite materials possible. Curvature gauges provide preferential sensitivity about a chosen axis, and are sensitive to curvature with arc radii in excess of 3 km (Djordjevich et al, 2001). Such minute curvatures with radii in the kilometre range are of interest in structural applications, which is the intended primary domain for curvature gauges. In practice, this could be described by loading a 67 cm cantilever beam at its free end. The tip deflection with 3 km arc radii is then 0,07 mm. On thick structures it is possible or even preferable to measure curvature by inserting two or more optical strain fibres in the structural cross-section. By doing this, it is possible to calculate strain distribution and curvature by looking at strain in the points of the inserted fibres.

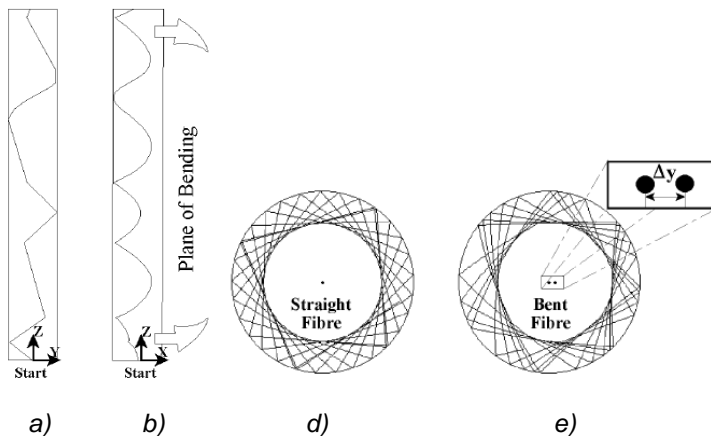


Figure 3-18. a) Shows the light ray path for an unbent fibre, b) is for the bent fibre. c) shows the typical result for an unbent fibre, and d) gives the result for a bent fibre. From Djordjevich (2001).

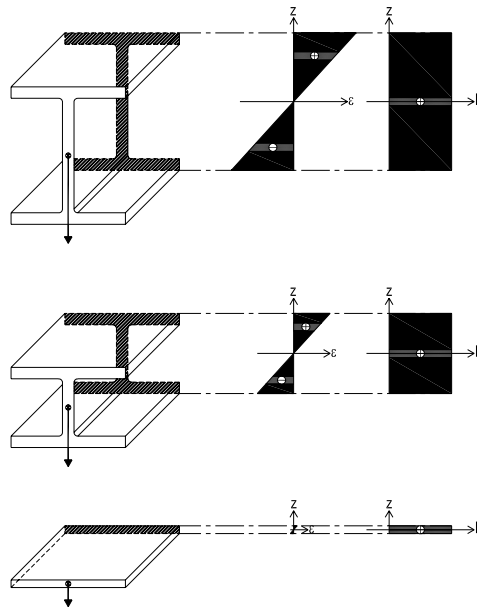


Figure 3-19. Strain is small and difficult to measure in thin structures, whilst curvature is not.

If curvature is measured using strain sensors, an efficient transfer of the strain of the structural member to the measuring gauge is vital for pleasing significance of the results. Optical strain sensors have to be stretched or compressed by the applied load, and the fibre resists this deformation with force. This force has to travel from the optical fibre to the structure (adhesive in the sensor/structure interface, resin, fibre protective coating etc.) which will also deform. This is commonly not taken into consideration, and if there is a strain loss the result will indicate that the measured curvature is less than the actual.

In contrast, optical fibres have negligible bending stiffness. The problem with strain loss during transfer from structure to optical fibre is hence also negligible.

3.4.4 Fibre optic sensors in concrete

The embedding of fibre optic sensors in concrete requires both chemical and mechanical durability due to

- Mechanical attacks when pouring fresh concrete and growing of cement stone crystals onto the fibres during the settling process.
- Chemical attacks during the entire life-span of the structure, caused by high alkaline chemical environment.

Preassembled or embedded sensors minimise the probability of sensor drop-out both during field installation and long-term usage, but they have to withstand the highly alkaline environment.

The only protection to the optical fibre against the surrounding environment is a polymer coating. The coating has to be strong and resistant to the environment that damages the optical fibre, and ideally with Young's modulus close to the glass fibre. Fluorine-thermoplastic has been shown to give excellent protection to the optical fibre. The greatest threat for an optical fibre is the concrete pouring phase, when the fibre could easily be damaged. If the fibre survives this phase without damages, the chance is great that it will work for a long time (Utsi, 2002).

The most common coatings have an elastic modulus that is lower than for the glass fibre. The result is that some of the strain is absorbed in the coating layer, as shear deformation, and only a fraction of the real structural strain is transferred to the fibre core (Utsi, 2002). One way to assure that the optical fibres are not damaged is to embed them in either what is called a 'pultrusion' process (where the fibres are inserted in a FRP product during manufacturing), this is explained more in detail in the next section. Another way is to cut slots in the finished FRP product, and then bond the FOS in the slot.

In practice it is necessary to perform calibration tests, where the optical fibre is subjected to a known strain. By this calibration the ratio between real strain and fibre output is determined.

3.4.5 Fibre optic sensors in FRP

As the optical fibres are very thin and long they are suitable for embedding in different kinds of materials, for example in FRPs. The fibre is embedded along the length of the fibres in the FRP, and makes it possible to monitor the strain in the FRP-material for a long time (Utsi, 2002). The embedding is performed by a process called pultrusion, see Figure 3-20. In the pultrusion of thermosetting resin composites, the reinforcing fibre roving are pulled from a fibre rack or creel into a resin bath containing the liquid resin together with appropriate catalysts and promoters. Then the resin-impregnated fibres travel through several stations, where the fibres are put together in the right directions and finally enter the pultrusion die, which has the form of the finished product. Electric strips attached to the die give the necessary heat to initiate the curing process. Strain sensors are put into the FRP component right before the fibres enter the resin bath. Pultrusion is one of the fastest and most cost effective composites manufacturing processes. The basic operation of pultrusion is simple in concept but quite complex in detail because of the number of mechanical, chemical, and physical factors that are simultaneously involved in the process (Kalamkarov et al, 2000). Embedding optical fibre sensors in FRP-products during manufacturing makes it possible to supervise the construction during its lifetime and save money because of the manufacturing process (Utsi, 2002). However, there might be problems using the pultrusion process. Pre-moulded CFRP materials, such as rods, tubes and plates, require a temperature above that which is safe for the cladding protecting the optical fibre. This is a remaining issue that needs to be solved before optical fibre easily can be pultruded in FRP-materials. The principle of pultrusion is given in Figure 3-20, and a picture which illustrates the problem with this kind of process is viewed upon in Figure 3-21 where the melted white cladding is coming out around the base of the optical fibre.

A way to overcome this problem is to integrate the optical fibre into pre-made slots in the composite by bonding. This method is used in this study, and has also been used in a project concerning a failure test on the Ö-viks bridge in Sweden.

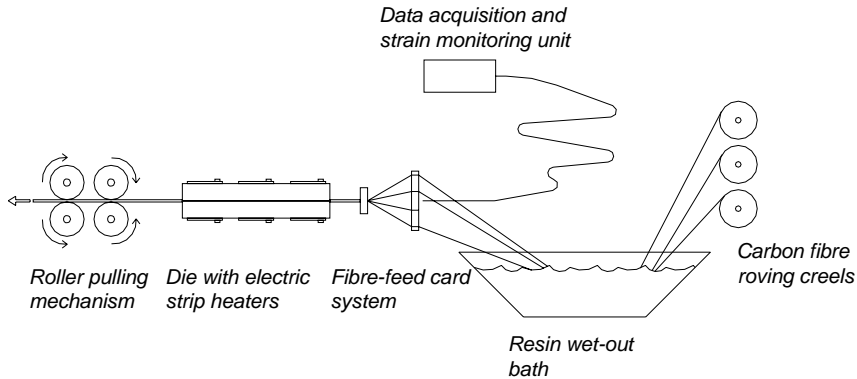


Figure 3-20. Diagram of the manufacturing of FRP-material with embedded optical fibre sensors.

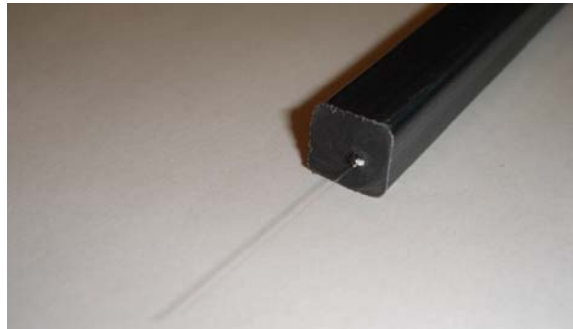


Figure 3-21. CFRP rod with a pultruded optical fibre. The cladding around the fibre has melted and is seen in the base of the fibre coming out from the rod.

One example where FOS has been integrated into a CFRP rod and used practically was during a loading test to failure on a concrete trough bridge located in Örensköldsvik in the middle of Sweden. The test was carried out during the summer 2006. The bridge was intended to be put out of service and demolished on site. Before the bridge was taken down the Swedish rail authorities together with the European founded project Sustainable Bridges (www.sustainablebridges.net) wanted to investigate the shear capacity. However, for a reasonable placement of the load bending failure would occur. Therefore it was decided to strengthen the bridge with NSMR. To monitor the strain during loading, fibre optic sensors (FOS) were integrated in one of these rods.

A comparison was then made between the FOS results by testing a similar rod on which traditional strain gauges were attached. The result from this comparison showed comparable results, and will be reported in coming report. The bridge is seen in Figure 3-22.



Figure 3-22. Ö-vik bridge in Sweden during failure test in the summer of 2006.

4 Safety and probabilistic approach

The probability of failure for a newly constructed structural member, designed in safety class 3 according to the Swedish codes, should by definition be equal or less than one in a million on a yearly basis. The other way around says that, only one out of one million structural members should fail every year. The safety of the member may however change during the lifetime as degradation might occur. For example, corrosion of steel reinforcement will affect the safety and behaviour of the structure negatively, as well as a decreased effective height caused by removal of damaged concrete during loading. If these mechanisms are taken into consideration the safety could sooner or later become deficient. In contrast to this, strengthening of the structure will increase the safety.

This chapter presents briefly the theory behind probabilistic design of structural members. This theory is used later in the evaluation of the test data, see chapter 8, to determine the change in probability of failure for all stages of the life cycle.

4.1 Structural safety

Risk could generally be defined as a combination of probability and negative consequence coupled to an event during a defined time period. Safety is the opposite of risk. It is hard to define safety but it could be said that safety refers to the low probability of failure in a structure or a structural member at a certain limit state.

The safety of a structure is traditionally verified by two parameters, a resistance parameter, R , and a load effect parameter, S . R and S originate from the French words *résistance* and *solicitation*. The basic structural design criteria is generally written as

$$R - S \geq 0 \tag{4.1}$$

Similar methods are used both in the ultimate limit state as well as in the serviceability limit state, i.e. when considering deflections. The problem gets probabilistic when some or all of the variables are stochastic. Now, the question has advanced from a deterministic answer, *yes* or *no*, to a more describing answer given by the probability of failure. The basic structural problem is rewritten to

$$p_f = P(R - S \leq 0) \tag{4.2}$$

Where p_f is the probability of failure.

R and S are respectively described by a stochastic variable. Bearing capacity, R , is described by $f_R(r)$. Load effect, S , is described by $f_S(s)$. Figure 4-1 shows a general case where distributions for load carrying capacity and load effect overlap.

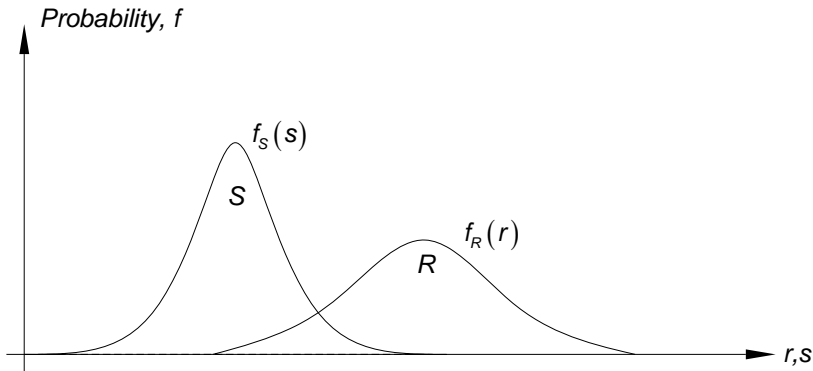


Figure 4-1. Distributions for R and S .

The structural performance of a whole structure, or a member of it, should generally be described with reference to a specified set of limit states which separate desired states of the structure from undesired states. The limit states are divided into the following two categories

- Serviceability limit states (SLS), which for concrete structures concerns crack widths and deflections
- Ultimate limit states (ULS), which corresponds to the maximum load-carrying capacity or, in some cases, to the maximum applicable strain or deformation.

The effect of exceeding a limit state may be irreversible or reversible. In the irreversible case, the damage or malfunction associated with the limit state being exceeded will remain until the structure has been repaired. In the reversible case, the damage or malfunction will remain only as long as the cause of the limit state being exceeded is present. As soon as this cause ceases to act, a transition from the undesired state back to the desired state occurs.

4.1.1 Safety class

In this study Swedish design codes have been used. Other codes or standards, for example ACI or Eurocodes, could however also be used. According to the Swedish design code, “*Boverkets konstruktionsregler 1994*”, the choice of safety class should regard what the extent of human injuries would be in the event of the failure of a building or building element. Safety class 1 is used for cases where there is no risk of severe injury.

Safety class 2 is used when there is some risk of severe human injury and safety class 3 when the risk for human injury is large. Each safety class is assigned a probability of failure, according to Table 4-1.

Table 4-1. Translation between safety class, safety index β and probability of failure, p_f .

Safety class	1	2	3
Probability of failure, p_f	10^{-4}	10^{-5}	10^{-6}
Safety index, β	3,72	4,26	4,75

Safety index, β , which is related to either serviceability or ultimate limit states, should be calculated on yearly-basis. Theoretically, this means that, in safety class 3 with $p_f=10^{-6}$, one out of one million identical structures will reach failure in current limit states. The actual probability of failure is in practice often higher than what the calculation gives. One reason is that, in practice, the dimension above the requirement is chosen. For example, four steel reinforcing bars are chosen even though the calculation requires only 3,5.

When considering a probability of 10^{-6} in philosophic terms, this is referred to as *de minimis*. This means that, in reality, that the risk cannot be sensed and therefore neglected.

4.1.2 Partial coefficients

Today's design codes are built up using partial coefficients on loads and material properties. For example, in equation (4.3) the characteristic stress capacity, f_k , is reduced through γ_m and γ_n to the design value, f_d . κ considers the load carrying capacity of the material and is dependant on the moisture content, duration of the load etc. η considers the systematic difference between a test specimen and a value in the structure. These coefficients are determined from statistical analysis such that the safety of the entire structure reaches a reliability close to an aimed safety. The β -index, which also is a measurement of the safety, could be determined for the specific structure if the distribution of all varying parameters is established.

$$f_d = \frac{f_k \kappa}{\gamma_m \gamma_n \eta} \tag{4.3}$$

The design of structures with the partial coefficients is approved in practically all design cases. If the partial coefficient method is accepted, then it is also okay to apply probabilistic design.

4.2 Probabilistic design

As described above, the deterministic design criteria in equation (4.1) describes that the resistance should be greater than the load effect parameter to avoid a failure.

The problem becomes probabilistic when statistical distributions of the variables are taken into account.

There are three detail levels when talking about theoretical probabilistic methods. The first method considers the uncertainty with one parameter per *uncertain* variable. The generally accepted *Partial Coefficient Method (PCM)*, i.e. used in Euro codes, falls into this category. The PCM is calibrated against other probabilistic methods and is really not a probabilistic method. The next method, called *first order second moment reliability method, FORM*, considers the uncertainty with two parameters, mean value and variance, for each uncertain parameter. A measure of the safety is given by the safety index, β . The risk of failure could be estimated by

$$p_f = \Phi(-\beta) \quad (4.4)$$

The third and most fundamental theory utilize the exact statistical properties for all variables. This method gives the most realistic measure of the probability of failure, p_f , and requires often numerical methods to be solved.

One method which utilizes the exact statistical properties of all variables is the *Monte Carlo (MC)* method. This is really a simulation method which randomly picks numbers in pair from the R and S distributions. Each pair of numbers is compared in between. If failure occur, when $R < S$, the result is 1 otherwise 0. Mathematically this will be expressed by an indicator function, $I(\cdot)$, which returns 1 if the failure function is less than zero, $G(x) \leq 0$, otherwise it returns 0. This leads to an approximation about the failure probability, p_f , and variance, given by

$$p_f \approx \hat{p}_f = \frac{1}{N} \sum I(G(x) \leq 0) \quad (4.5)$$

$$\text{Var}|\hat{p}_f| = \frac{1}{N} p_f (1 - p_f) \quad (4.6)$$

4.2.1 First order second moment reliability method (FORM)

This section presents a basic introduction to the FORM concept. A method for solving the problem is also suggested. For further information regarding this probabilistic method see, for example, Schneider (1997).

If considering Figure 4-1, the probability that a load effect, S , falls into a infinitesimal interval ds at s is

$$f_S(s) \cdot ds \quad (4.7)$$

The probability that R falls in or under this interval is

$$\int_{-\infty}^s f_R(r) \cdot dr \quad (4.8)$$

The probability that S falls in this interval ds when $R \leq S$ equation (4.7) and (4.8) happens at the same time, is

$$f_S(s) ds \cdot \int_{-\infty}^s f_R(r) \cdot dr \tag{4.9}$$

The equation, finally, giving the probability that $R \leq S$ is

$$p_f = P(R - S < 0) = \int_{-\infty}^{\infty} f_S(s) \cdot \left(\int_{-\infty}^s f_R(r) \cdot dr \right) ds = \int_{-\infty}^{\infty} f_S(s) F_R(r) ds \tag{4.10}$$

This could be viewed upon as the volume of the two dimensional joint density functions from the failure surface, and can be seen in Figure 4-2. R and S are plotted as probability functions on the r and s axes. The limit state equation, $G=R-S=0$, separates the safe from the unsafe region, dividing the volume into two parts. The volume of the part cut away and defined by $s > r$ corresponds to the probability of failure. The design point $(r^*; s^*)$ is located on this straight line where the joint probability density is greatest. If failure is to occur it is likely to be there.

The desired safe state is above the failure surface, defined as $R-S=0$, and undesired failure state is below.

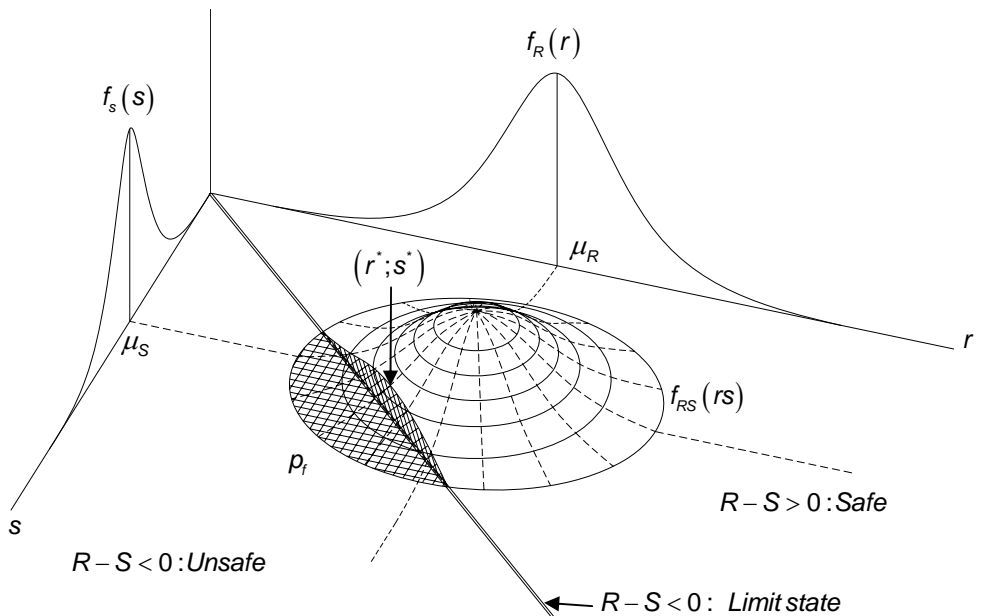


Figure 4-2. The 3-D view of two random joint density function $f_{RS}(rs)$.

If R and S are normal distributed and statistically uncorrelated, then

$$R \in N(m_R, \sigma_R) \quad (4.11)$$

$$S \in N(m_S, \sigma_S) \quad (4.12)$$

The safety margin, M , is defined as

$$M = R - S \quad (4.13)$$

Then it is also valid that

$$M \in N(m_M, \sigma_M) \quad (4.14)$$

Where $m_M = m_R - m_S$ and $\sigma_M = \sqrt{\sigma_R^2 + \sigma_S^2}$

The distribution of M is schematically given in Figure 4-3. Failure occurs when $M < 0$.

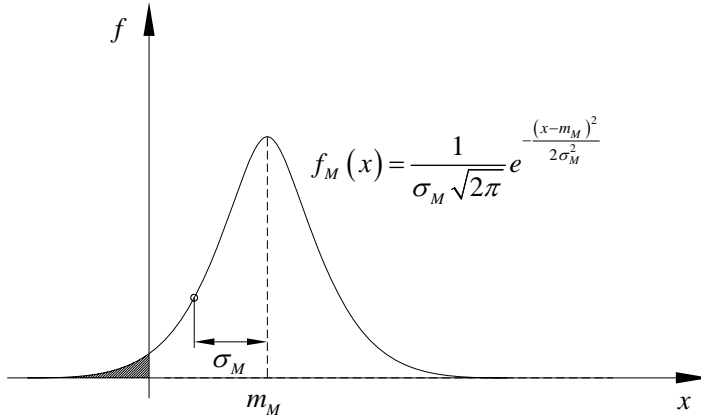


Figure 4-3. Distribution for the variable M . Failure occurs when $M < 0$.

$$p_f = P(M < 0) = \int_{-\infty}^0 f_M(x) dx = \frac{1}{\sigma_M \sqrt{2\pi}} \int_{-\infty}^0 e^{-\frac{x-m_M}{2\sigma_M^2}} dx \quad (4.15)$$

Now, let

$$\frac{x-m_M}{\sigma_M} = y \Rightarrow \frac{1}{\sigma_M} dx = dy \quad (4.16)$$

$$p_f = P(M < 0) = \frac{1}{\sqrt{2\pi}} \int e^{-\frac{y^2}{2}} dy = \Phi\left(-\frac{m_M}{\sigma_M}\right) = \Phi(-\beta) \quad (4.17)$$

$\Phi(\cdot)$ is the standardized normal distribution function. This function, given in Figure 4-4, has mean value 0 and standard deviation 1. If R and S are normally distributed, the safety index, β , is calculated as

$$\beta = \frac{m_M}{\sigma_M} = \frac{m_R - m_S}{\sqrt{\sigma_R^2 + \sigma_S^2}} \quad (4.18)$$

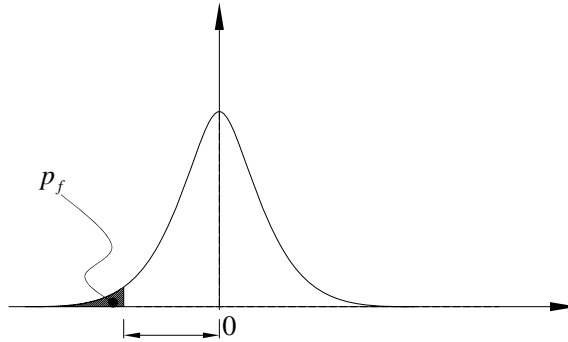


Figure 4-4. The standardized normal distribution function. Safety index, β , is connected to a certain probability of failure, p_f .

4.2.2 The Hasofer-Lind safety index

The procedure when defining the Hasofer-Lind safety index, β , is described as follows. The first step is to normalize the basic variables, which is done by

$$Z_i = \frac{X_i - m_i}{\sigma_i} \Rightarrow Z_i \in N(0,1) \quad (4.19)$$

The second step is to express the failure function with the normalized basic variables.

$$g(Z) = g(z_1, \dots, z_n) \quad (4.20)$$

The safety index, β , is defined as the shortest distance from origin in the z -coordinate system to the failure surface $g(z_1, z_2) = 0$ as can be seen in Figure 4-5. In the failure point the failure function, $g(z_1, \dots, z_n) = 0$ is approximated with $g(\alpha_1 \beta, \dots, \alpha_n \beta) = 0$, where α is the sensitivity factor for which the following is valid

$$\alpha_1^2 + \dots + \alpha_n^2 = 1 \quad (4.21)$$

The normal vector to $g(z_1, \dots, z_n)$ in the failure point $(\alpha_1 \beta, \dots, \alpha_n \beta)$ is given by the vector

$$\frac{\partial g(\alpha_1 \beta, \dots, \alpha_n \beta)}{\partial z_1}, \dots, \frac{\partial g(\alpha_1 \beta, \dots, \alpha_n \beta)}{\partial z_n} \quad (4.22)$$

The length of this normal vector is

$$\sqrt{\left(\frac{\partial g(\alpha_i \beta_i, \dots, \alpha_n \beta_n)}{\partial z_i}\right)^2 + \dots + \left(\frac{\partial g(\alpha_i \beta_i, \dots, \alpha_n \beta_n)}{\partial z_n}\right)^2} \quad (4.23)$$

In the failure point the normal vector coincides with the unit vector $(\alpha_i, \dots, \alpha_n)$

$$\alpha_i = \frac{\frac{\partial g}{\partial z_i}}{\sqrt{\left(\frac{\partial g(\alpha_i \beta_i, \dots, \alpha_n \beta_n)}{\partial z_i}\right)^2 + \dots + \left(\frac{\partial g(\alpha_i \beta_i, \dots, \alpha_n \beta_n)}{\partial z_n}\right)^2}} \quad (4.24)$$

This calculation is done to obtain an α for each primary parameter up to the last parameter, n

$$\alpha_n = \frac{\frac{\partial g}{\partial z_n}}{\sqrt{\left(\frac{\partial g(\alpha_i \beta_i, \dots, \alpha_n \beta_n)}{\partial z_i}\right)^2 + \dots + \left(\frac{\partial g(\alpha_i \beta_i, \dots, \alpha_n \beta_n)}{\partial z_n}\right)^2}} \quad (4.25)$$

In the general case, a non-linear iterative method is used to calculate the safety index β and the sensitivity factors α_i to α_n . Usually the Newton-Raphson method gives a good convergence. There is computer software which can perform the above presented calculation. Amongst these VaP (Variable Processor) could be mentioned. The α -values are visualized in Figure 4-5 in the 2-dimensional case when the distributions Z_1 and Z_2 create the failure surface.

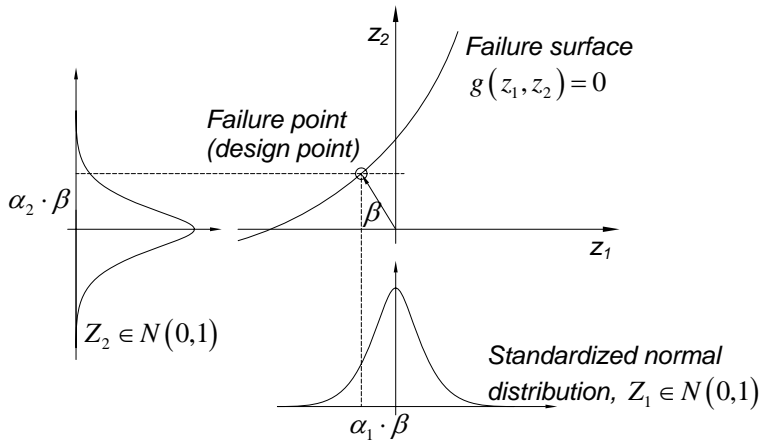


Figure 4-5. A failure surface is created by Z_1 and Z_2 . The sensitivity factors, α_1 and α_2 , are related to the failure point along the failure surface.

The sensitivity factor, α_1 and α_2 , could be interpreted as a measure which describes where on the Z_1 and Z_2 distributions, respectively, a failure most likely would occur. If the α -value, for example corresponding to the structural resistance, is large it means that the failure point (design point) is located considerably below the expected value of the distribution. This is taken care of by introducing a reduction coefficient when designing using a deterministic model. Generally, the resistance is calculated using a model which depends on several primary variables. Each variable is connected to a certain α value, and each variable could principally be reduced with a coefficient if corresponding sensitivity factor is significantly separated from zero.

In modern design codes this reduction coefficient is referred to as a partial coefficient.

4.2.3 Parameters

Focus is generally put on distributions for material properties and geometries on the real structure, as these parameters tend to be assumed as the crucial ones. Indeed, those parameters are important when designing or retrofiting. Especially this goes for old materials, which properties are hard to translate to modern materials. Old steel in bridges built from 1800 to 1960 could, for instance, show a large variance (Larsson, 2006). One should however not forget to analyze the load situation. If the load distribution is poorly established the probabilistic model will give unreliable answers.

There is a variety of distributions that could be chosen to describe a certain parameter. Take for instance the log-normal distribution. It may be suitable if the values from the studied quantity are not allowed to be less than zero, although the mean value is close to zero. One example of this is the tensile strength of concrete. Geometrical variables and modulus of elasticity is normally well described by the common normal distribution. When considering the maximum value of wind load or snow load on annual basis, it is shown that the *Gumbel* distribution, a type-I distribution, may be suitable (Thoft-Christensen & Baker, 1982). Figure 4-6 shows general examples of normal, Gumbel and log-normal distributions.

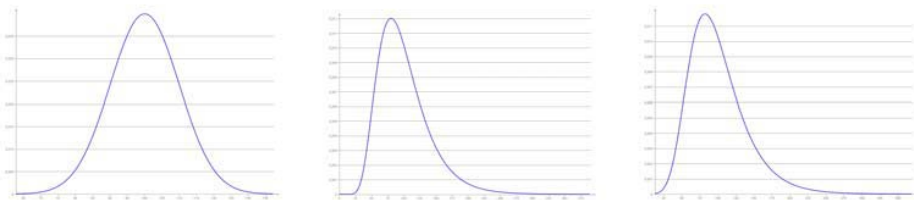


Figure 4-6. Left: Arbitrary normal distribution. Middle: Arbitrary log-normal distribution. Right: Arbitrary Gumbel distribution.

5 Experimental study

5.1 Introduction to experiment

In brief, the experimental study carried out at Luleå University of Technology, division of structural engineering, investigates the behaviour of four meter long concrete beams when they are subjected to a simulated structural life cycle. The life cycle is simulated by accelerated corrosion tests, removal of damaged concrete and corrosion products, repair procedures and finally CFRP strengthening. All stages have been carried out under loading. After a complete life cycle the beams were loaded to failure. The main objective was to compare the beams in different stages in the life cycle and to investigate if it is possible to strengthen a deteriorated concrete beam to attain its original load carrying capacity.

The test is divided into two major parts. The first part, part *I*, is the long term preparation of beams in different stages in the life cycle, and the second one, part *II*, is the load test to failure. The test setup is different for part *I* and *II*, i.e. different test setups and also a slightly different monitoring setup. For example additional strain gauges were attached on the steel reinforcement on the beams where the cover concrete was removed, revealing the corroded steel. In total, seven RC beams are tested, see Table 5.1. Each beam is assigned a particular label, also given in Table 5-1, and it relates to each beam throughout the test. Failure load tests are performed after stages *a*, *b*, *d*, *e* and *f* to give data such as the traditional load versus deflection up to failure load. Monitoring setup is presented for both part *I* and *II* in section 5.4. In the next sub-chapter a more detailed description of the beams is given.

Table 5-1. Test matrix describing how the test series were performed. *F* indicates failure test.

Beam Stage	Beam <i>A</i>	Beam <i>B1</i>	Beam <i>B2</i>	Beam <i>D</i>	Beam <i>E</i>	Beam <i>F1</i>	Beam <i>F2</i>
<i>a</i>	<i>F</i>	↓	↓	↓	↓	↓	↓
<i>b</i>		<i>F</i>	<i>F</i>	↓	↓	↓	↓
<i>c</i>				↓	↓	↓	↓
<i>d</i>				<i>F</i>	↓	↓	↓
<i>e</i>					<i>F</i>	↓	↓
<i>f</i>						<i>F</i>	<i>F</i>

5.2 Beam specimens

The original concrete beam specimen is four meter long, with 300 mm high and 200 mm wide cross section. The steel reinforcement scheme is shown in Figure 5-1 and Figure 5-2. The tensile longitudinal reinforcement was designed with a bend in each end to prohibit anchorage failure. To make the removal of the damaged concrete in the midsection as easy as possible the zone with the constant bending moment has few stirrups. However, outside this zone a considerable amount of shear stirrups were used. The shear resistance of the cross section was high enough to avoid shear failure even during the time when concrete was removed. For all beams the concrete cover was 30 mm, which then coincides with aggressive environment due to the Swedish guide (BBK 04).

Material properties are summarized in the end of this chapter. All material data is presented in Appendix A.

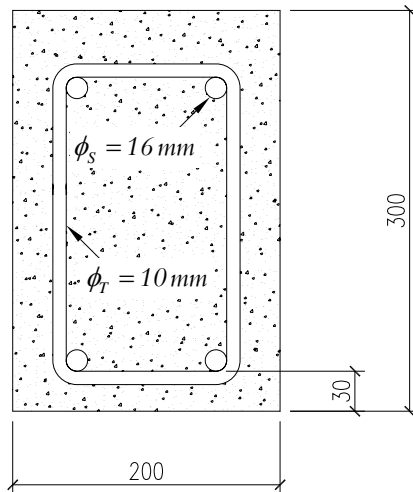


Figure 5-1. Cross sectional view of beam specimen.

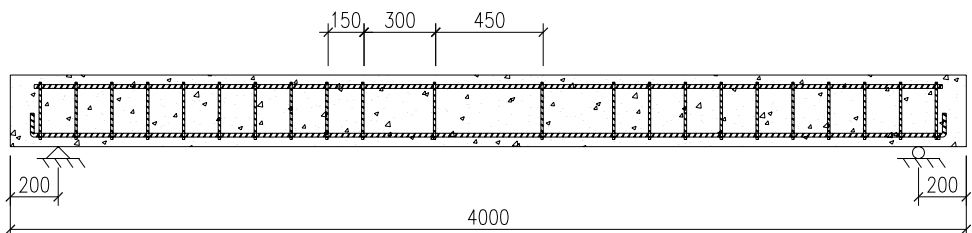
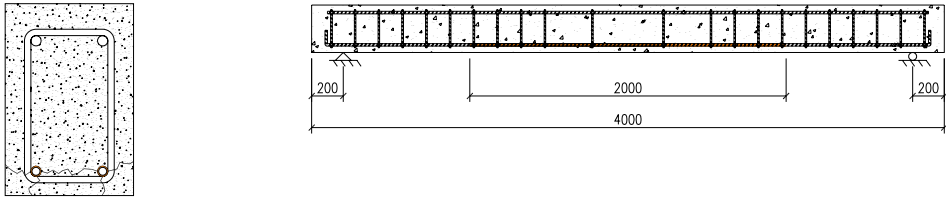


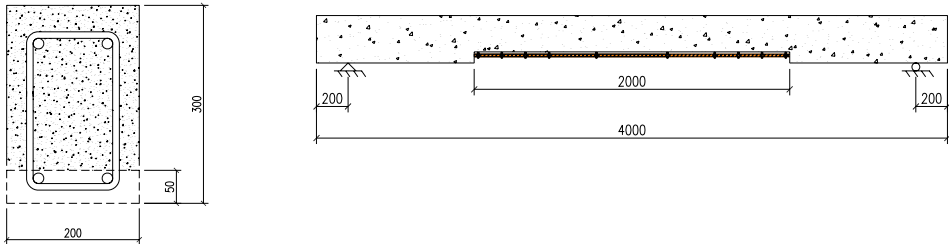
Figure 5-2. Longitudinal view of beam specimen.

Table 5-2. Schematics of corroded, repaired and repaired & strengthened beams.

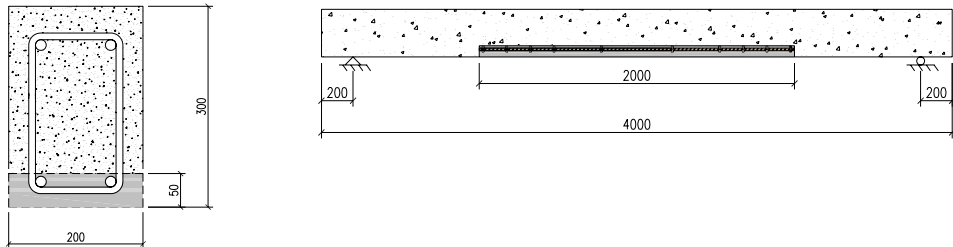
Two metres of the tensile steel reinforcement was corroded in beam mid-span. This beam is referred to as “B”.



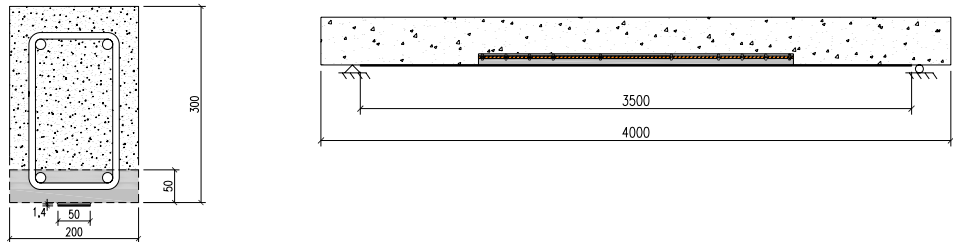
Cover concrete was removed to a depth of 50 mm in the first stage of the rehabilitation process. This beam is referred to as “D”.



The cavity created by removal of cover concrete was filled with repair mortar. This beam is referred to as “E”.



The repaired beam was strengthened by bonding of CFRP plate. This beam is referred to as “F”.



The beam notations are chosen in respect to the point in the life cycle given by Figure 2-8 in section 2.2.

As mentioned earlier, six beams were exposed to accelerated corrosion of the tensile steel reinforcement. Four of these beams were at a later stage repaired, and two of the repaired beams were also strengthened with CFRP plates. The following subchapter describes the preparation of these beams. The test beams were placed upside down during part I. This was to make it easier to work with the tensile side of the concrete beam specimen, especially when repairing and strengthening but also to make it possible to place the pond on top of the corroding beams.

5.2.1 Corrosion process

Accelerated corrosion by electrochemistry is a method to study the effects of corrosion on steel reinforcement in RC structures. The electrochemical principle shown in Figure 5-3 below was used in this experimental study and is called *ponding*. The electrolyte, which distributes the electric current to the steel reinforcement, is placed on the concrete. It would also be possible to lower the entire specimen in the electrolyte, but that would significantly decrease the oxygen supply and instead simulate deterioration for submerged concrete structures opposite to this study which focuses on concrete structures located on land or above water. Silicone was used during part I to prevent that the electrolyte from pouring down into the cracks formed by the applied load.

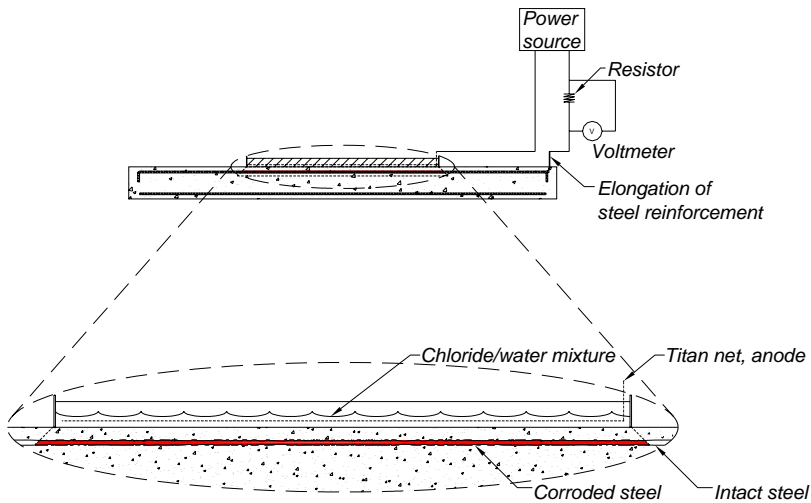


Figure 5-3. Schematic diagram for accelerated corrosion setup.

This first stage of the corrosion process, where chlorides travel through the cover concrete to eventually reach bar level by diffusion, is called the initiation period. This could take several decades to occur for a correctly designed concrete structure.

It is however possible to force chlorides to reach bar level by applying an electrical current using the same setup as described in Figure 5-3. It would also be possible to introduce chlorides in the concrete beams by blending salt into the concrete before casting. This is however not appropriate in this case, since it will require two castings for each beam to delimit corrosion to a certain area. With the chosen method it is relatively easy to direct the corrosion attack to a particular area of the structure. For hardened concrete the chosen concrete cover and concrete quality give considerable corrosion resistance and it could take a relatively long time to achieve corrosion. Therefore in the tests, the chlorides are driven to bar level when the concrete is in the fresh stage, just one day after casting, when the resistance against chloride intrusion is relatively low. A measurement that insures that chlorides have actually reached the steel bars is if the potential difference between steel and the surface of the concrete beam is negative when the applied current is switched off. Another indication is that the electrical current increases.

Ordinary longitudinal steel reinforcement was used. There was no electrical connection between transverse and longitudinal reinforcement since the stirrups were protected by epoxy. For this purpose StoBPE Lim 417 (A+B) was used. Each stirrup was dipped down into a bucket of adhesive to form the coating for corrosion protection. The protective layer reached 100 mm up along the part of the stirrup that was supposed to be near the tensile steel reinforcement as can be seen in Figure 5-4. The adhesive was left to harden for five days at an average temperature of 16 °C and a relative humidity of around 70%. The beams were finally cast. The concrete quality was equivalent to Swedish standard concrete; C28/32, which correspond to a compressive strength of about 40 MPa. Material testing showed however that the actual compressive strength was higher. Material properties are presented in section 5.5.



Figure 5-4. Stirrups were protected against corrosion with a coating of epoxy adhesive. Here they are seen when left to harden.

5.2.2 Corrosion initiation

The initiation process was commenced one day after casting, while the beams were left in the casting frames. The length of the ponds was determined by reducing the area which was intended to be corroded by 200 mm (100 mm in each end). This was done since the chlorides were assumed to spread along the reinforcement bars. The ponding bath length was 1800 in mm this case. A view of the corrosion initiation procedure is given in Figure 5-5.



Figure 5-5. Left: Full view of initiation setup. Right: The anodic titan net placed in the water bath on top of concrete beam.

The current going through the steel reinforcement and the cathode was measured by inserting a resistance between anode and cathode, and was calculated by using Ohm's law. The voltage was held at a constant level until a current increase was noticed. At this stage, the current was turned off and it was said that the chloride intrusion was enough to depassivate the steel reinforcement. The steel reinforcement was considered depassivated after 9 days. After that the beams were left to harden for 28 days.

5.2.3 Accelerated corrosion duration

The corrosion process was accelerated by applying an electrical current to the steel reinforcement. The duration of the accelerated corrosion process was determined by utilizing a theoretical approach based on Faraday's law.

Faraday's law states that the relation between corrosion current and weight loss due to corrosion could be determined by

$$\Delta\omega = \frac{AIt}{ZF} \quad (5.1)$$

The weight loss due to corrosion could also be calculated as

$$\Delta\omega = a\delta\gamma \tag{5.2}$$

The corrosion current could be expressed

$$I = ia \tag{5.3}$$

Equation (5.2) and (5.3) into (5.1) gives

$$\delta = \frac{Ait}{\gamma ZF} \tag{5.4}$$

Since R is defined as material loss per second, this results in

$$R = 3,69155 \cdot e^{-5it} \tag{5.5}$$

This expression provides the basis for predicting the duration of the accelerated corrosion process to a certain corrosion level and at a particular corrosion current density. The result from the calculations is presented in Table 5-3.

Table 5-3. Calculated duration for accelerated corrosion stage for different diameter reduction and applied current (Arntsen, 2004).

Diameter reduction %	Time in days for			
	0.10 mA/cm ²	0.15 mA/cm ²	0.20 mA/cm ²	0.25 mA/cm ²
1	25	17	13	10
2	50	33	25	20
3	75	50	38	30
4	100	67	50	40
5	125	84	63	50
6	150	100	75	60
7	176	117	88	70
8	201	134	100	80
9	226	150	113	90
10	251	167	125	100

A diameter reduction of 4% was chosen to be a relevant corrosion level in this study, corresponding to an 8% area reduction. The accelerated corrosion current was selected as low as possible to 0,10 mA/cm². The reason was that corrosion created by a low current for a longer time is more realistic than corrosion which is created fast with a high current.

The corrosion length was chosen to 2000 mm, which is 55% of the free span. The accelerated corrosion procedure kept on going for 98 days, and was then considered complete

5.2.4 Repair procedure

After 75 days of accelerated corrosion, the cover concrete was removed to a depth of 70 mm along the attacked section to uncover the steel reinforcement. This was carried out with the use of jack hammers – shown in the left part of Figure 5-6.

Before new concrete mortar was cast on to the beams, corroded steel reinforcement was brushed clean using a steel brush. Then the concrete surface was cleaned by pressurised air and primed using primer StoCrete TH. The object with priming is to bind dust and also to wet the dry concrete surface for good bonding between the repair mortar and the existing concrete. A frame was built around the cavity. The cavity was then refilled with a repair mortar up to the level of the removed concrete, using a spackle, as can be seen by the right part of Figure 5-6. The repair mortar used was StoCrete GM1. The primer was applied just before the repair mortar. The repair mortar was left to harden 28 days while covered by plastic to prevent dry cracking. The mortar was kept wet the first week by adding water to the surface. Material properties are found in section 5.5. No primer was used on the steel reinforcement, which normally is used for these types of repair procedures for corrosion mitigation. The reason is that this study does not consider the long term results of the repair procedure.



Figure 5-6. Left: Cover concrete was removed using jack hammer. Right: The cavity was refilled with repair mortar.

5.2.5 Strengthening procedure

The strengthening procedure included the following steps: removal of weak concrete layers by brushing using steel brush, cleaning by means of pressurised air, application of a primer, StoBPE 50 Super (A+B) for the strengthening system used and finally bonding CFRP plates to the concrete surface. The plates used were StoFRP Plate E50C and the adhesive used was StoBPE Lim 465.

Material properties are found in section 5.5. The primer was left to harden for 24 hours before the CFRP plates were bonded.

The peel-ply on the CFRP plates was first removed and then the adhesive applied using a special tool to obtain the correct amount of adhesive on the plates – i.e. an average thickness layer of 2 mm, this tool is shown more clearly in the left part of Figure 5-7. The temperature during the strengthening work was 21 °C and the humidity approximately 45%. After these preparations, the CFRP plates were placed on the beams, as can be seen in the right part of Figure 5-7.



Figure 5-7. Left: Adhesive tool to apply the right amount of adhesive to the plates. Right: Concrete surface, adhesive layer and CFRP plate.

5.3 Test setup

This section explains in detail the test rigs and the test setups. In addition the procedure to generate the load during the corrosion test is presented.

5.3.1 Long term test

The test rig is designed to load the beams in a 4-point bending system. Sketches of the test rig can be seen in Figure 5-8 and Figure 5-9 below and a photo of the test rigs is shown in Figure 5-10. The load is generated by a hydraulic jack placed 200 mm from the beam end, one per beam. Two supports are placed each 500 mm from mid-span. Beneath these is a leverage beam placed to keep all support loads at the same level. The support to the far left in the figure is placed at 200 mm from the other beam end, preventing the beam end from deflecting upwards.

The beam is freely supported, which in practice means that the bending moment is zero at the end supports. In addition, the one-meter section in between the mid-span supports gives a constant bending moment without any influence of shear forces. The benefits of placing the tensile flexural reinforcement facing upwards during repair and strengthening operations has influenced this design.

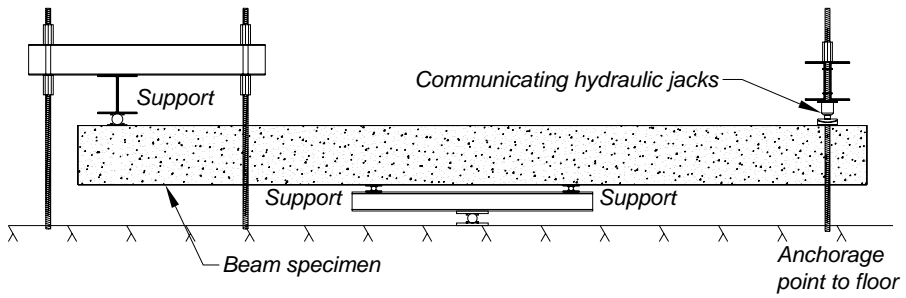


Figure 5-8. Test rig presented from the side.

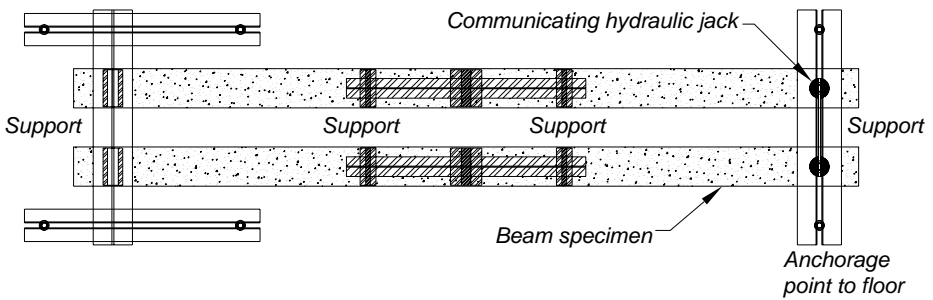


Figure 5-9. Test rig with two beams loaded, presented from above.

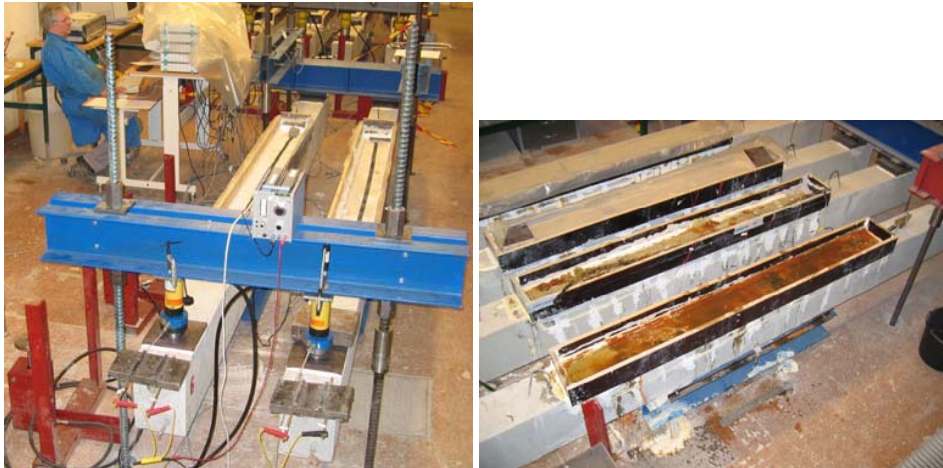


Figure 5-10. Left: Picture taken of the small test rig carrying two beams. Right: Side view of the large test rig carrying four beams.

5.3.2 Loading

One very important part when simulating the life cycle behaviour is to create a realistic load situation during all stages. Considering the real structure in terms of load situation reveals that two load levels are interesting during the service life. Those are service load and dead load. The service load is the sum of dead load and the variable load. The variable load can be different for different structures, but is represented foremost by traffic on a bridge structure.

The load history according to Figure 5-11 is employed to adopt these thoughts into the test. The service load will be engaged in the first stages of the test. The load level is then decreased to dead load during repair and strengthening procedures, and the life cycle for the test beams is completed by loading the beams until failure occurs.

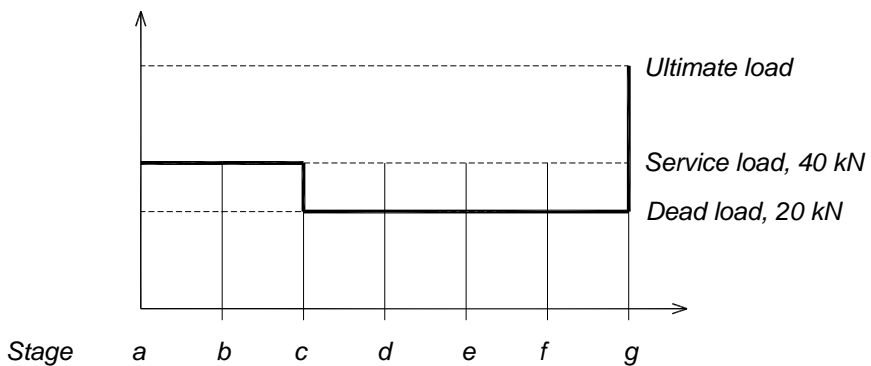


Figure 5-11. Load levels throughout the test.

The serviceability load is defined as the load corresponding to an average crack width of 0,2 mm for the reference beam. Crack width measurement and pattern from reference beam testing gave this load level.

The load was generated by communicating hydraulic vessels. The principle of the communicating vessel is shown in Figure 5-12. An applied load on the small piston gives a pressure in the hydraulic tube. When this pressure acts on the ten times larger cross section area of the large piston, the load is enlarged ten times in relation to the applied load on the small piston.

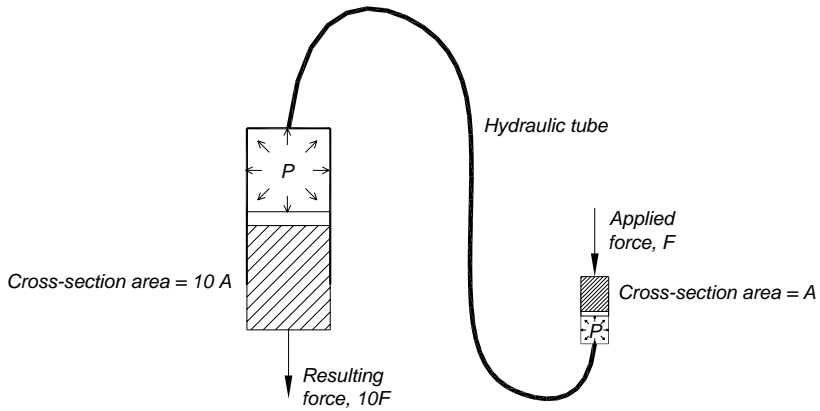


Figure 5-12. Principle of communicating hydraulic jack. The pressure generated by the applied load on small piston gives a 10 times higher resulting force at the large piston.



Figure 5-13. Left: The applied load is placed on the small piston. Right: The resulting load is created through a hydraulic cylinder.

5.3.3 Failure load test

The test setup for the failure load test is seen as a sketch in Figure 5-14 and in the photo in Figure 5-15. The mid-span loads are now applied from above, and the applied load is generated by highly accurate hydraulic cylinders. The deformation speed was set to 0,02 mm per second and the test was performed displacement controlled.

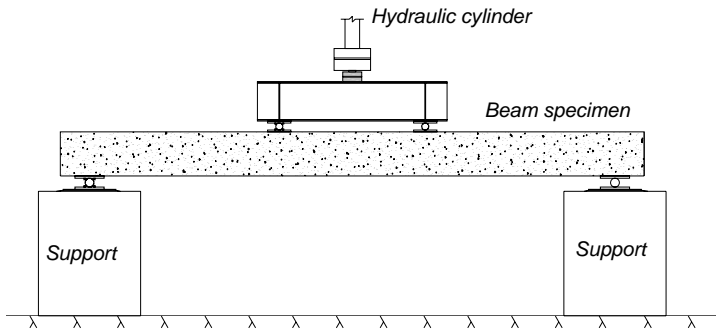


Figure 5-14. Schematic diagram of the test setup used for the failure test.



Figure 5-15. Picture taken on test setup during failure test.

5.4 Monitoring

Much effort has been invested on the monitoring systems. The traditional monitoring systems including load cells, linear voltage displacement transducers (LVDT) and electrical strain gauges (FTGs) are complemented with fibre optic strain sensors. This chapter will present sensor locations and also which type of sensor used for different applications. Further information regarding sensor locations is presented in Appendix B.1 through B.5 for each beam specimen.

5.4.1 Traditional monitoring equipment

Deflections were measured using Linear Voltage Displacement Transducers (LVDTs). The strains were measured with Strain Gauges (FTGs); on the concrete using 67 mm glued FTGs. On the steel reinforcement, glass fibre rods and CFRP plate 5 mm glued FTGs were used, see Figure 5-16. The application of the 5 mm long FTG onto a steel reinforcing bar is shown in Figure 5-17.



Figure 5-16. Top: Gauge used to measure strain on concrete with a length of 67 mm. Bottom: Gauge used to measure strain on glass fibre rod, steel reinforcing bars and CFRP plate. Scale 1:1.

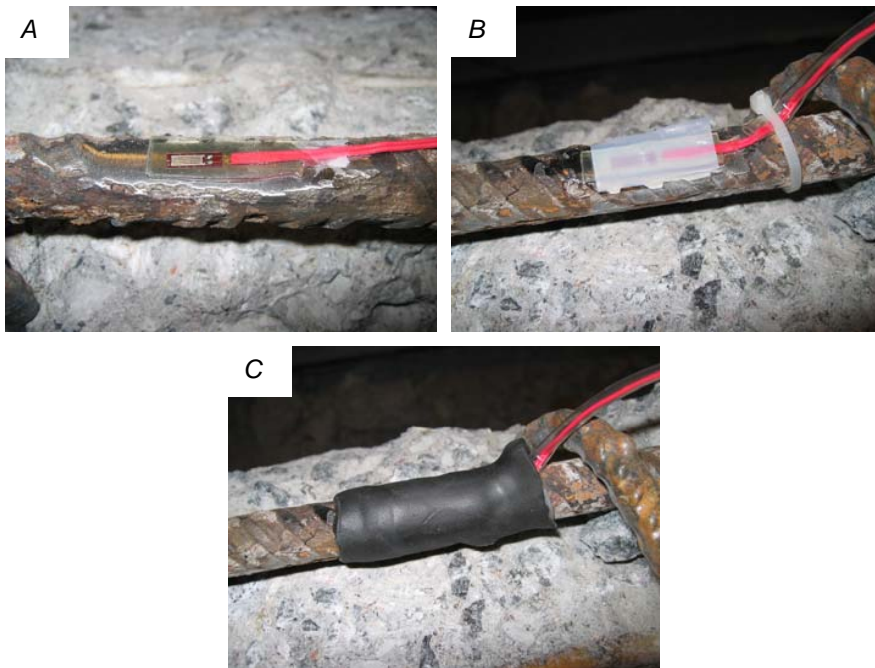


Figure 5-17. Electrical strain sensor attached onto steel reinforcement after removal of cover concrete. A) Sensor glued onto steel reinforcement, B) Teflon sheet placed on the sensor to minimize force transfer on the wrong side of the gauge, C) Rubber protection covering the sensor.

5.4.2 Fibre optic strain measurement

The measuring system must sustain harsh conditions when conducting experiments that incorporate both a long loading period as well as accelerated corrosion. Strain sensors made out of glass fibre are suitable for use in such applications, as they are corrosion resistant. Therefore, strain was also monitored in addition to the traditional strain gauges by Fibre Optic Sensors (FOS), in this case a Fibre Bragg Grating system. The instrument ready for testing is seen in the left part of Figure 5-18. The device which produces the gratings is viewed in the right part.

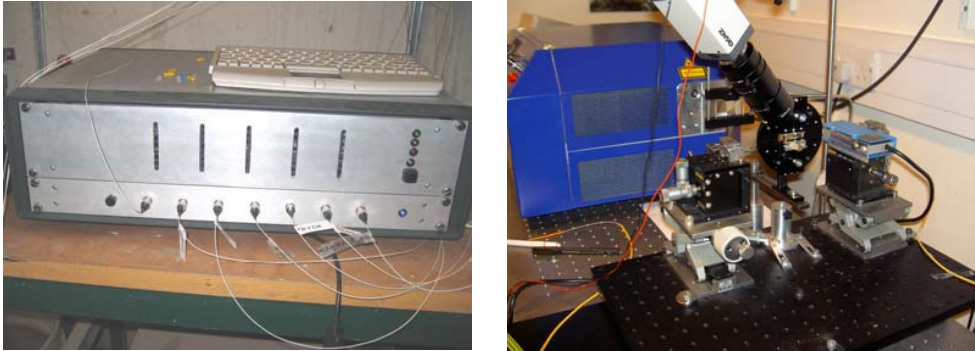


Figure 5-18. Left: Instrument ready for laboratory test. Right: Sensors created by producing gratings along the optical fibre using such device.

The optical fibre used consists of a fibre core surrounded by cladding and finally a layer of coating. The diameter of the optical fibre is about 250 micrometer, see left part of Figure 5-19. The fibre is especially sensitive to shear forces, so it is normally also protected by another plastic coating for easy handling. If the fibre accidentally breaks, it is possible to mend it using a splicing tool, see right part of Figure 5-19.

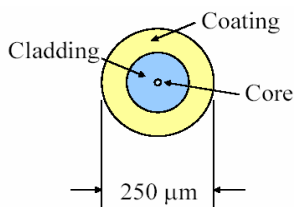


Figure 5-19. Left: Cross sectional view of optical fibre. Right: Splicing tool used to mend broken fibre.

Eight sensors were located along each fibre. The locations are given in Figure 5-20. Additional protection against physical harm was created by inserting the fibre in a 10 mm diameter glass fibre rod, Figure 5-21 A and B. The optical fibres were placed at two points in the beam cross-section; see Figure 5-21 C).

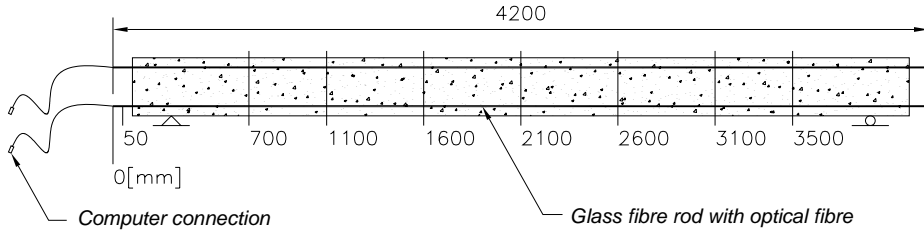


Figure 5-20. Fibre optic sensor location along beam axis.

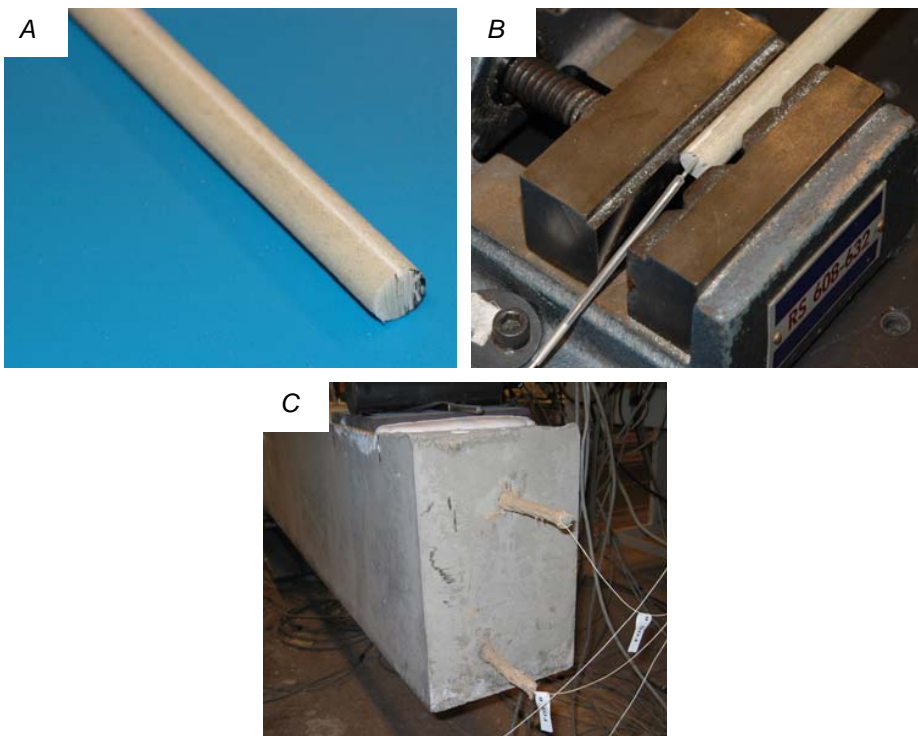


Figure 5-21. A) Glass fibre rod for protection of optical fibre, B) Optical fibre glued in a slot along the glass fibre rod, C) Protective glass fibre rods exiting the beam end with optical fibres sticking out.

5.4.3 Long term test

One LVDT was placed at the deflecting beam end. Another one was located in mid-span measuring deflection between a point on the beam and a steel L-profile attached on each mid-span support. The last LVDT measurement setup gives the possibility of measuring curvature. In addition, two traditional strain gauges were attached in mid-span on each of the glass fibre rods, see Figure 5-22 to view sensor placement and Figure 5-23 to view the curvature measurement setup.

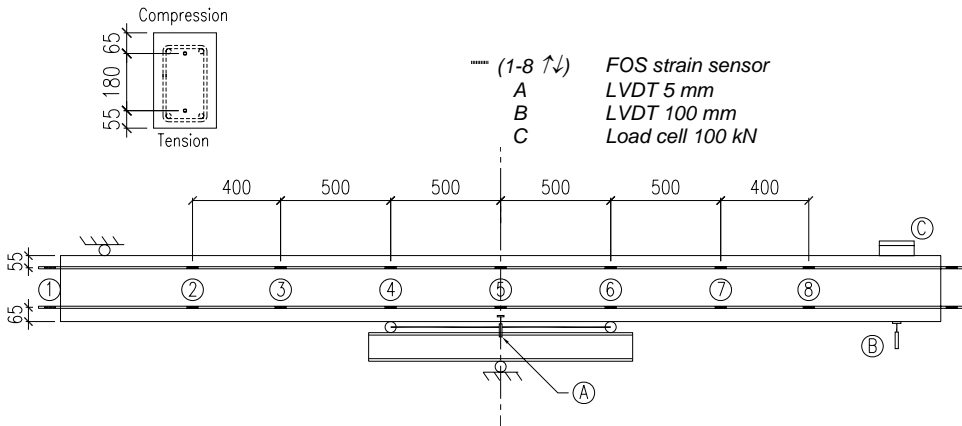


Figure 5-22. Monitoring setup for the long term test.

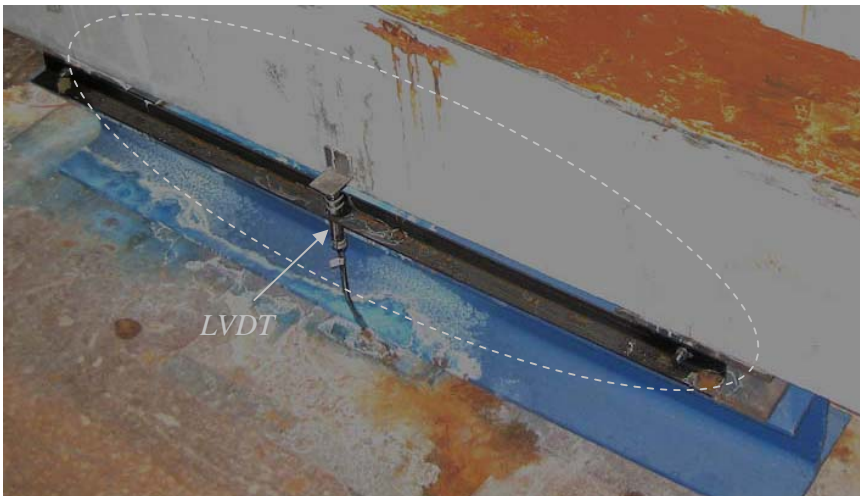


Figure 5-23. Curvature measurement setup using LVDT during corrosion stage.

5.4.4 Failure load test

The monitoring setup during the failure load test for the reference beam and the corroded beams is schematically given in Figure 5-24.

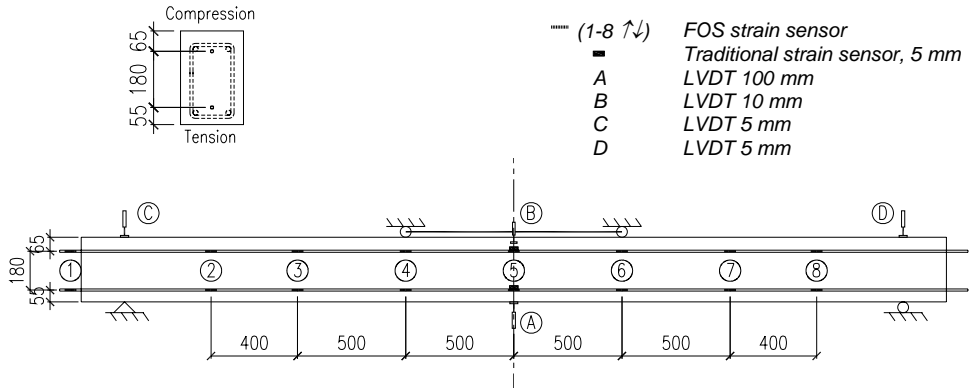


Figure 5-24. Monitoring setup for the reference beams and the corroded beams.

Figure 5-25 gives the monitoring setup for beams where cover concrete has been removed, repaired and repaired & strengthened. Additional strain sensors were attached on the steel reinforcement on these beams.

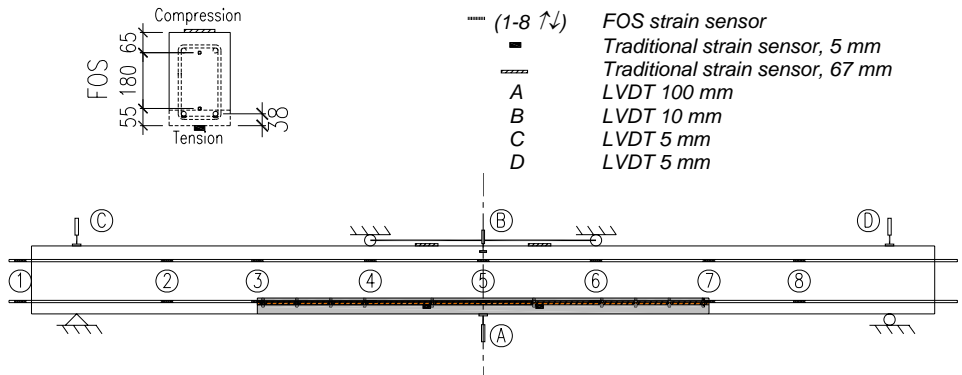


Figure 5-25. Monitoring setup for beams where the cover concrete was removed, repaired and strengthened.



Figure 5-26. Curvature measurement setup using the 10 mm LVDT mounted on a steel profile reaching in between the loading points. Mid-point deflection is measured using a 100 mm LVDT.

Electrical strain sensors were attached onto steel reinforcement after removal of cover concrete. This was done to measure strain on the actual steel rebar. There were also damages on the sensors attached on the glass fibre rod caused by the removal of damaged concrete.

5.5 Material properties

The concrete chosen as C28/32 according to Swedish norms had an average compressive strength of 64,9 MPa. The average tensile strength of the concrete was recorded to 4,3 MPa. Concrete from the same batch was used for all beams.

The properties of the repair mortar are very similar to the concrete with an average compressive strength of 65 MPa and an average tensile strength of 3,9 MPa. This is good in terms of material compatibility when adding a new material to the structural member.

The results from testing undamaged and corroded steel reinforcement, with 16 mm diameter and Ks500 quality revealed a 55% loss of ductility of the corroded steel bar specimens compared to the undamaged steel bars. The yield stress was determined to 524 MPa for the undamaged steel reinforcing bars and 514 MPa for the corroded. The modulus of elasticity was 186,7 GPa for the intact steel, and 141,1 GPa for the corroded steel.

The CFRP material showed an ultimate stress of 1860 MPa and an ultimate strain of 1,2%. The average stiffness was recorded to 150 GPa. Complete results from material testing are summarized in Appendix A.

6 Test results

6.1 General

This chapter presents the results from the experimental work and is divided into two subchapters

- Corrosion stage (long term test) or initiation stage
- Failure test

6.2 Corrosion stage – long term test

The result of the accelerated corrosion procedure is presented in terms of observed damages on the beams, steel mass loss and visible corrosion damage on the steel bars.

The left part of Figure 6-1 shows the ponds which hold the electrolyte during the corrosion stage, while the right part of Figure 6-1 presents an external view of the beams after corrosion. The corrosion products seen in the electrolyte in the later part of the corrosion stage were extensive.

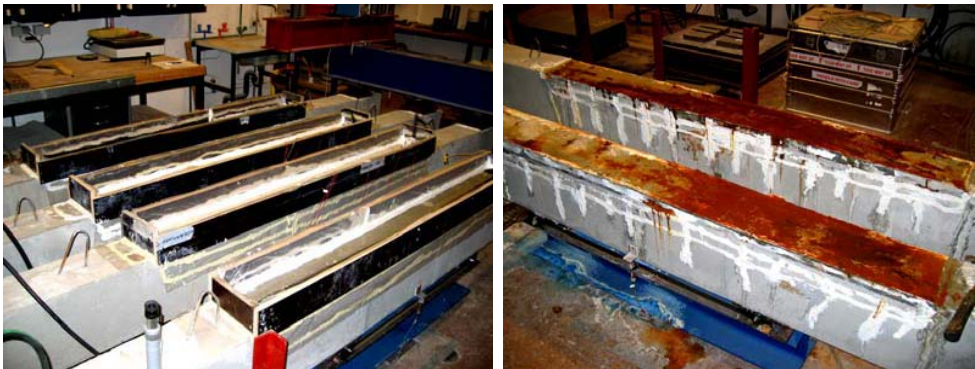


Figure 6-1. Left: Ponds holding chloride water placed onto beams. Right: External look of beams after finished corrosion stage.

Removal of concrete was facilitated by severe cracking around the steel reinforcement due to corrosion. Both pitting as well as distributed corrosion was observed, both of them were expected to arise due to the initiated corrosion process. A clear view of a typical pit is seen in the left part of Figure 6-2, surrounded by distributed corrosion.

The significant degree of corrosion of the steel reinforcement made the bars look quite deteriorated. It is also worth mentioning that a distinct interface between the corroded and the non-corroded sections in the right part of Figure 6-3 could be noticed on the steel bars. This proves that it is possible to damage selected regions with this method.



Figure 6-2. Left: Both evenly distributed corrosion as well as pitting corrosion was observed on corroded steel reinforcement bars. Right: Failure surface for corroded and undamaged steel reinforcing bars after material test.

It is obvious that the bond between steel and concrete is decreased when visually comparing corroded and undamaged steel bars as in the left part of Figure 6-3. Almost all signs of the ridges are erased on the corroded bars.



Figure 6-3. Left: Corroded and undamaged steel reinforcement. Right: The interface between the corroded and the undamaged steel section.

One way to measure the corrosion level would be by a procedure in which each corroded steel bar was gradually lowered into a cylinder partially filled with water. Not only the total weight loss but also the variations in cross sectional area along the axis of the corroded bar could be established. However, Horrigmoe and Sæter (2006) found that this method was unsuccessful in the sense that the production tolerances of the steel bars were too large to obtain meaningful measurements of the variations in cross

sectional area along the bar axis. Hence, the corrosion level was determined by comparing the unit weight of a quantity of un-corroded and corroded steel bars. The result is presented in Table 6-1. The unit weight is decreased to 90% and the bar diameter to 95% compared to the undamaged bar. The actual diameter reduction was in average hence 0,32 mm more than what was planned. This is considered as a very good result when regarding the uncertainty coupled to the corrosion rate discussed earlier.

Table 6-1. Unit weight data is presented for non-corroded and corroded steel reinforcement.

	Weight [kg]	Length [m]	Unit weight [kg/m]	Diameter [mm]
<i>Non-corroded steel reinforcement</i>	72,24	43,2	1,67	16
<i>B1</i>	2,96	1,97	1,50	15,2
<i>B2</i>	2,50	1,64	1,52	15,3
<i>D</i>	4,69	3,13	1,48	15,1
<i>F1</i>	5,68	3,77	1,51	15,2
<i>Relation (corroded/undamaged)</i>			90%	95%

6.2.1 Loading

The applied load was aimed at the service load during the corrosion stage. The service load was established by finding the load at 0,2 mm average crack width of the intact beam, and was found to be 40 kN. Dead load was thought of as the load of an overlying bridge deck, and was defined to 20 kN in the test.

Table 6-2. Real service load and dead load acting on beam specimens during simulated life cycle.

	Service load during corrosion		Dead load during rehabilitation	
	Mean value	Standard deviation	Mean value	Standard deviation
<i>B1</i>	40,2	1,0	22,0	2,3
<i>B2</i>	41,7	0,6	25,4	1,4
<i>D</i>	40,2	0,7	27,8	0,7
<i>E</i>	38,5	0,9	23,3	1,0
<i>F1</i>	33,9	0,9	23,6	1,4
<i>F2</i>	35,8	1,1	19,7	0,7
<i>Average</i>	38,4	3,1*	23,6	3,0*

* Standard deviation calculated in between load levels for all beams.

The developed loading equipment used gave an excellent load situation, even though some fluctuation and variation in the applied total load was noticed. The reason is coupled to internal friction in the hydraulic jacks.

This can be seen in Table 6-2 and graphically in Figure 6-4. In spite of the fluctuation the average load for the corroding beams was close to the desired 40 kN service load, and about 23 kN during repair and strengthening operations.

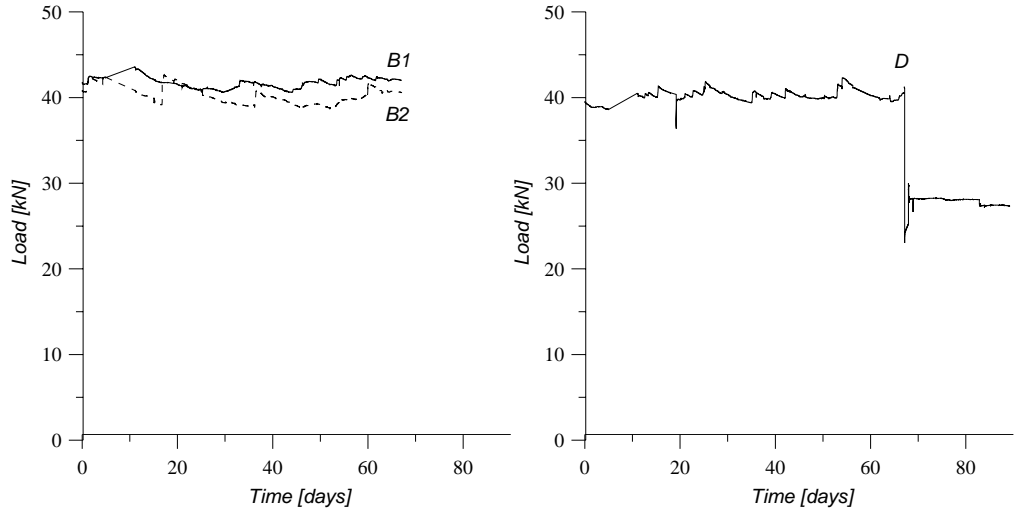


Figure 6-4. Left: Applied load during corrosion stage for the corroded beams B1 and B2. Right: Applied load during the corrosion phase and the time for removal of concrete for beam D, where cover concrete was removed.

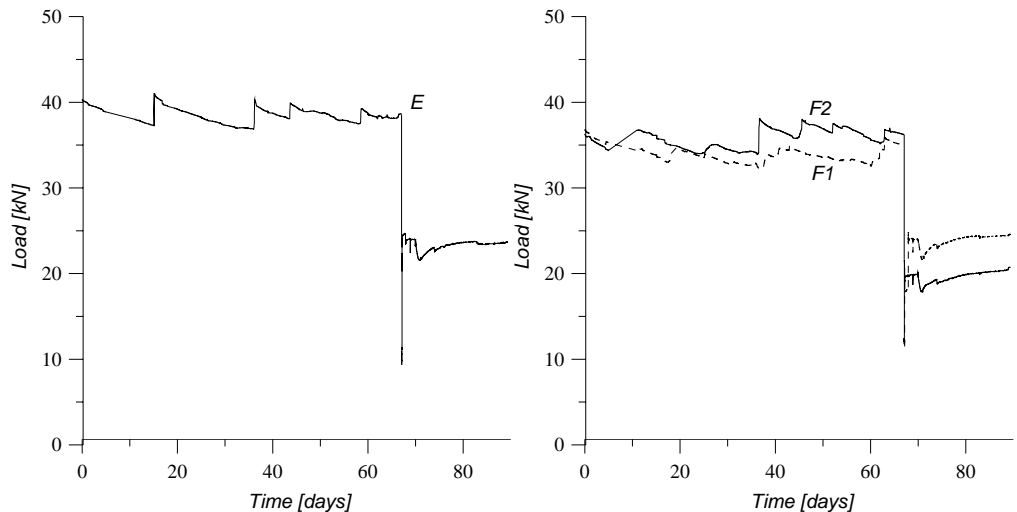


Figure 6-5. Left: Applied load during the corrosion and repair phase for the repaired beam, E. Right: Applied load during the corrosion phase and the rehabilitation phase for the repaired and strengthened beams, F1 and F2.

6.2.2 Midpoint deflection and strain

Midpoint deflection was measured during the long term test on beams *B1*, *B2*, *D* and *F* during the corrosion phase. The deflection for the is presented in Figure 6-6. Measured strain from FOS during the corrosion stage for two of the corroded beam specimens is given in the right part of Figure 6-6.

There is a quite large difference in deflection after finished corrosion stage, measuring from 5 mm to 11 mm. It could be concluded that the beam subjected to the highest load has also the highest midpoint deflection, when comparing the load subjected on each of these beams and the midpoint deflection. Two mechanisms could be pointed out to give this result. The first is that the creep effect is enlarged when the load is increased; the other is that the corrosion process is increased when the tensile force in the corroding steel is increased. By comparing steel mass loss in between beams *B2*, *D*, *B1* and *F* in Table 6-2 and deflection in Figure 6-6, it is found that the difference in deflection is not related to a varying steel mass loss due to corrosion in between the four beam specimens.

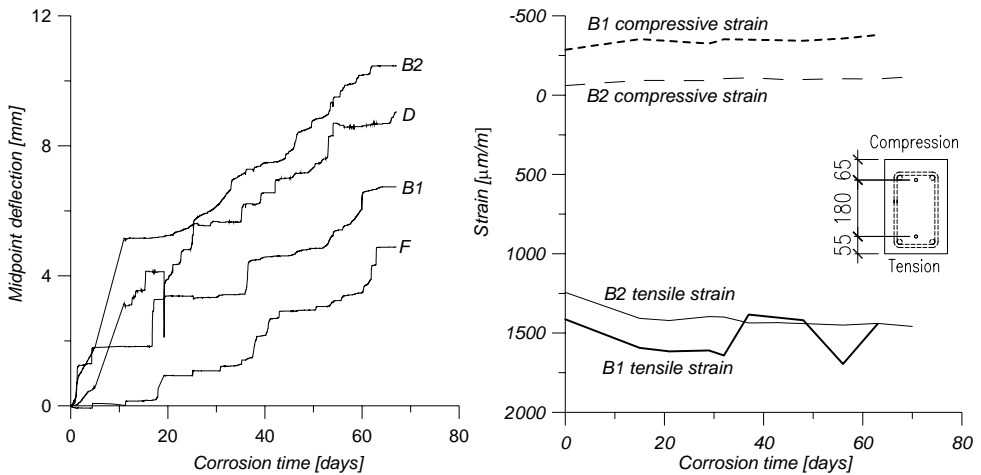


Figure 6-6. Left: Long term behaviour in terms of midpoint deflection. Right: Recorded strain along the tensile and the compressive glass fibre rod during the corrosion phase for two of the corroded beam specimens.

The strain distribution during the repair and strengthening procedure was recorded according to Figure 6-7. This will be taken into consideration later on when the strain distribution during the failure load test is evaluated.

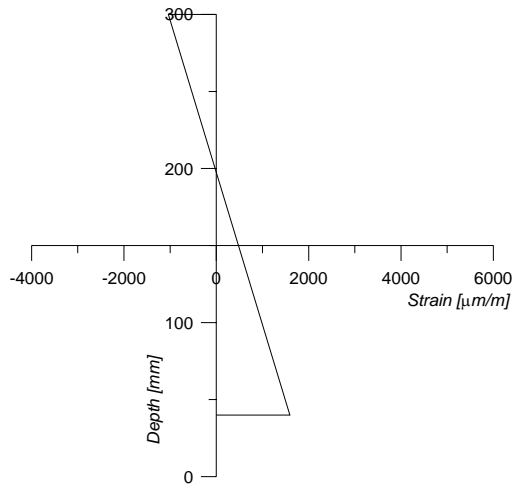


Figure 6-7. Cross sectional strain distribution during the repair and strengthening procedure.

6.2.3 Curvature

Curvature was measured both by the LVDT setup and the fibre optic strain sensors. The relation between strain and curvature for the FOS setup is

$$\kappa = \frac{\varepsilon_c + \varepsilon_t}{D} \quad (6.1)$$

Where ε_c is the monitored strain in the compressed part of the cross section, ε_t is the strain in the tensioned part of the cross section and D is the distance between the points where ε_c and ε_t are measured.

The result from the FOS measurement showed that the optical fibres broke easily, even at moderate strain levels. This was observed for all beams, and a typical result from the failure test is given in Figure 6-8, where the tensile strain in mid-span for the corroded beam is visualised. The optical fibre broke at 2600 microstrain in the particular case at a beam deflection of 6,5 mm, which makes the FOS strain measurement more or less useless during the failure test. However, the low strain level during the corrosion stage made it possible to measure strain distribution for the beam specimen *B1* and *B2* during at least this stage of the life cycle.

The cause of the fibre failure was found to be an insufficient depth of the slots along the glass fibre rod, where the fibre was placed. Although it was possible to measure strain on beam *B1* and *B2* during corrosion it should be mentioned that a majority of the sensors failed during this phase of the test.

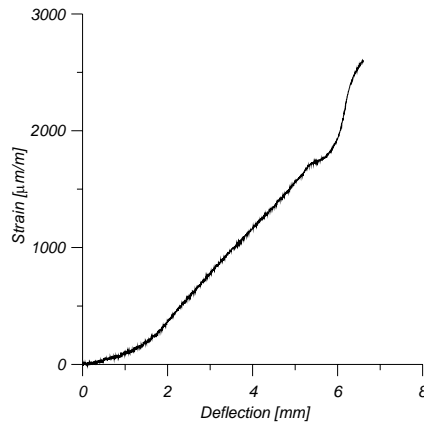


Figure 6-8. Tensile strain in mid-span of the corroded beam on the glass fibre rod.

The curvature for the LVDT setup is determined by the relation

$$\kappa = \frac{2\delta}{\delta^2 + \frac{L^2}{4}} \quad (6.2)$$

Where δ is the recorded uplift between the loading points measured by an LVDT and L is the distance between the loading points, according to Figure 6-9. The figure presents the curvature radius, which is the inverse of the curvature.

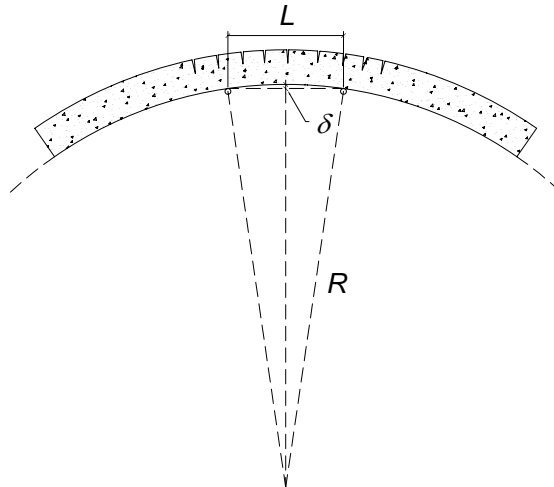


Figure 6-9. Schematic diagram of curvature measurement using the LVDT setup.

Curvature of the corroded beam specimens, *B1* and *B2*, are presented in the left part of Figure 6-10. Both results from the LVDT and FOS are presented for comparison. The right part of Figure 6-10 presents curvature for beam specimen *D*. Left part of Figure 6-11 presents curvature for beam *E* and the right part curvature for beam *F1* and *F2*.

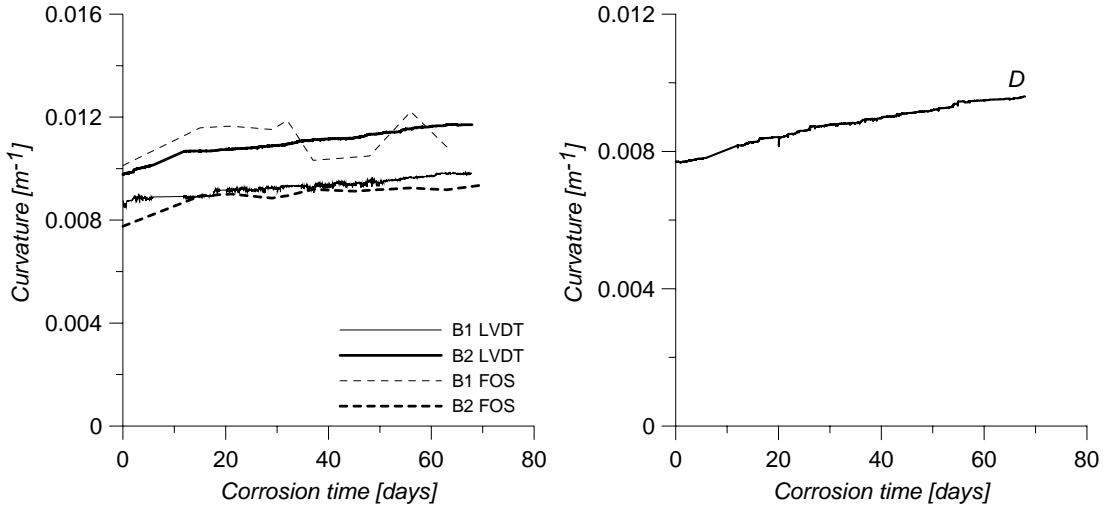


Figure 6-10. Left: Curvature of beam specimen *B1* and *B2* during the corrosion phase using the LVDT as well as the FOS setup. Right: Curvature of beam specimen *D* during corrosion phase using the LVDT setup.

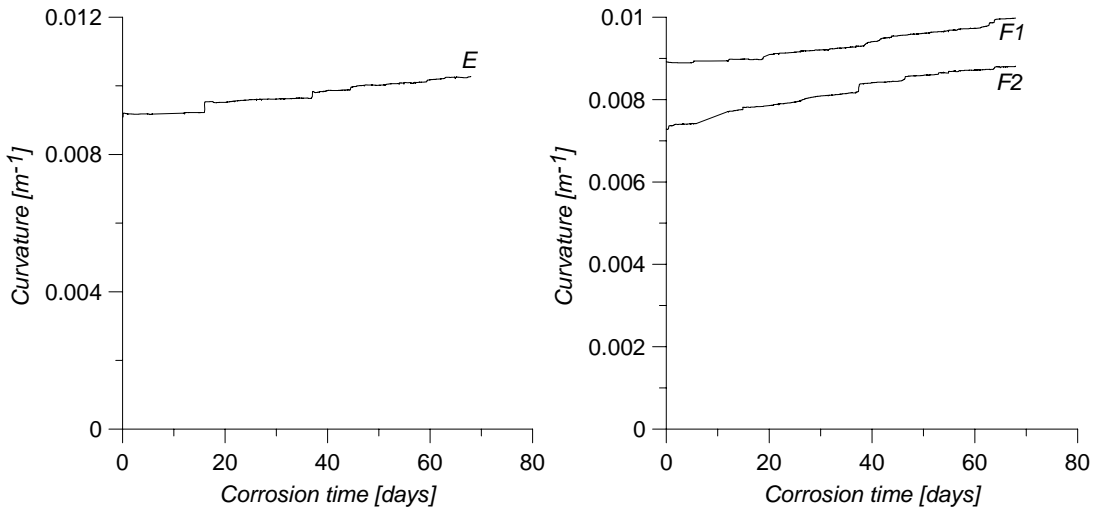


Figure 6-11. Left: Curvature of beam specimen *E* during the corrosion phase using the LVDT setup. Right: Curvature of beam specimen *F1* and *F2* during corrosion phase using the LVDT setup.

6.3 Failure tests

This subchapter presents results from the failure load test. Visual inspection of beam cross-sections was done by cutting out 50 mm thick slices from the beams after the test. The slices were cut out in a section of the beam without any bending cracks.

6.3.1 Intact beam

There were some suspicions that plastic cracks formed during hardening of the concrete. However, as the intact beam cross section shows no signs of cracking, as can be seen in Figure 6-12, these suspicions were eliminated.

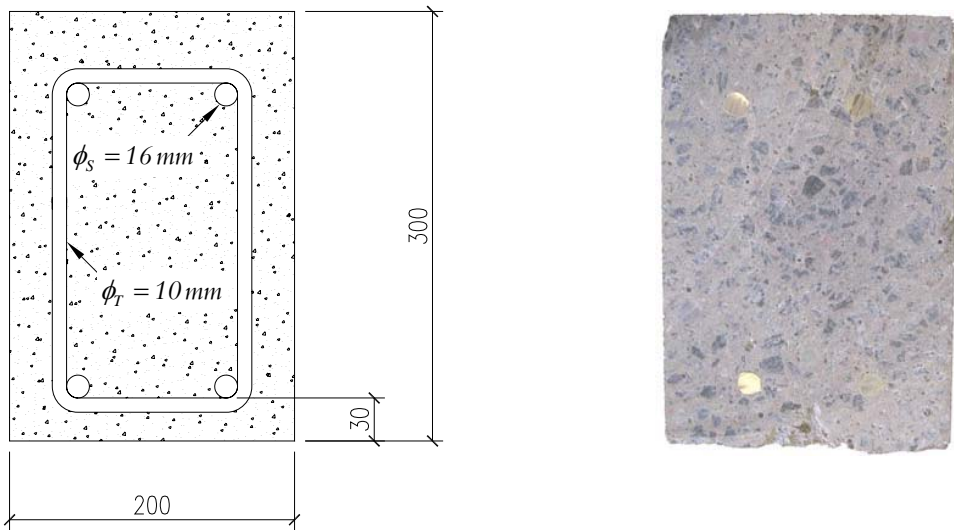


Figure 6-12. Left: Cross sectional view of intact beam. Right: Cross section of real intact beam.

The service load was defined as the load level at an average crack size of 0,2 mm, which occurred at 40 kN. The crack pattern after the failure load test is given in Figure 6-13. Information regarding average crack width at different loads levels is given in Table 6-3.

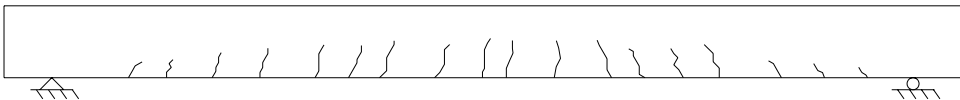


Figure 6-13. Longitudinal view of intact beam with crack pattern after failure load test.

Table 6-3. Crack width measurement during failure load test of intact beam indicates that maximum crack width with respect to serviceability occurs between 40 and 45 kN.

Load	Average crack width	Number of cracks
0		
5		
10		
15	0.05	4
20	0.08	6
25	0.10	13
30	0.15	13
35	0.17	15
40	0.18	17
45	0.21	17
50	0.26	17
55	0.28	18
65	0.34	18

The crack load for the intact beam was 6 kN. The post yielding region indicated that the beam has an obscured ability of carrying more and more load. This behaviour is related to the glass fibre rod inserted into the tensile part of the cross section. The load vs. deflection curve is seen in Figure 6-14. The test was aborted at 50 mm of deflection. No sign of total failure was noticed when aborting the test. The load vs. deflection graph for a beam without glass fibre rods is seen in the right part of Figure 6-14.

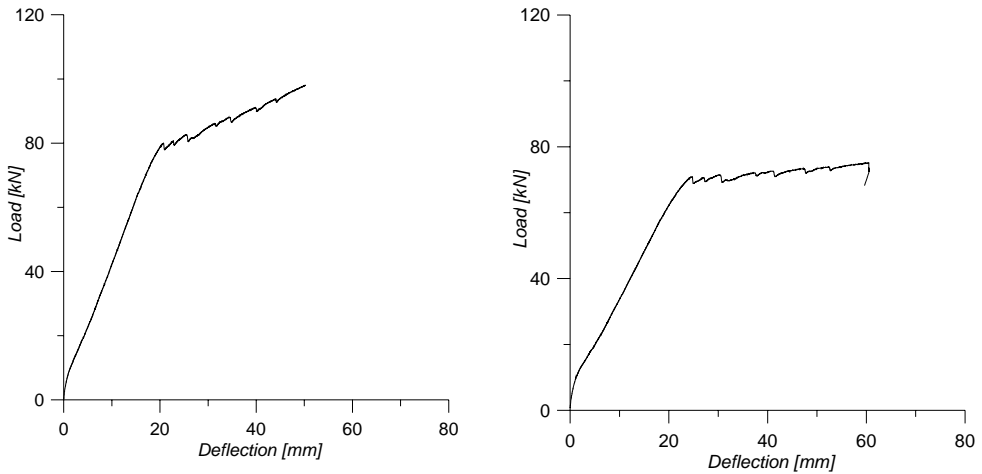


Figure 6-14. Load vs. deflection relation for intact beam.

Yielding of steel reinforcement occurred at 79,8 kN according to the left part of Figure 6-15 and the strain distribution over the cross section is given in the right part. The figure shows that the compressive zone of the concrete is 80 mm.

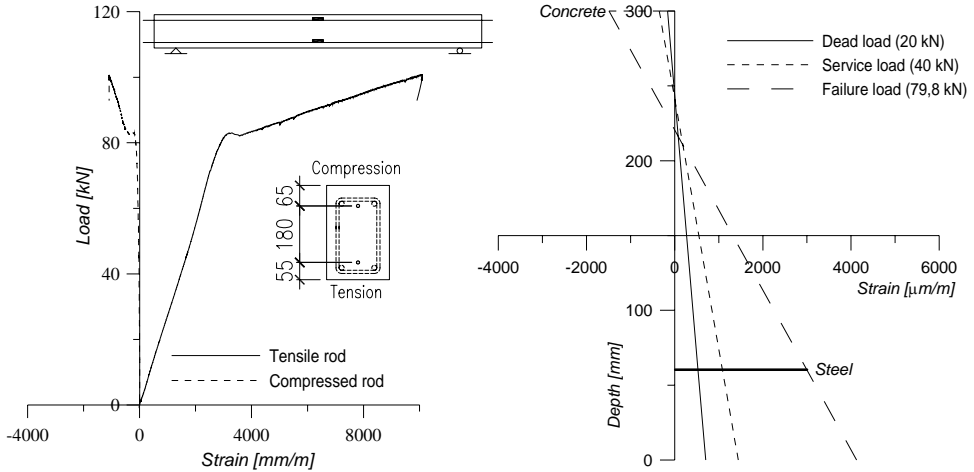


Figure 6-15. Left: Strain in tensile and compressed glass fibre rod. Right: Strain distribution, ϵ_x , through the beam thickness in mid-span.

6.3.2 Corroded beam

The crack pattern after failure test is given in Figure 6-16 for the corroded beam. Longitudinal cracks were found along the tensile steel reinforcement, both on the side of the beam as well as along the under side, in the region of steel corrosion. These cracks are obvious also when looking at the beam cross section in Figure 6-18.

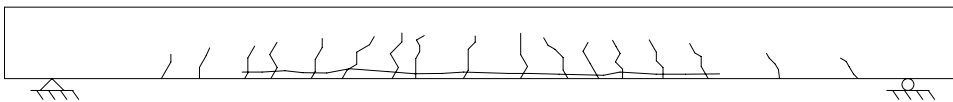


Figure 6-16. Crack pattern for corroded beam after failure load test.

No crack load was observed when testing the corroded beam, obviously because the cross section already was cracked from the loading during the corrosion stage. When dismantling the beam from the long term test rig, some deflection remained from the long term load related to creep. The deflection was measured to 7 mm in mid span. This initial deflection is taken into consideration by starting the load vs. deflection graph in this point. Yielding of steel reinforcement occurred at 69 kN. The failure test was aborted at 55 mm. No sign of total failure was observed when aborting the test.

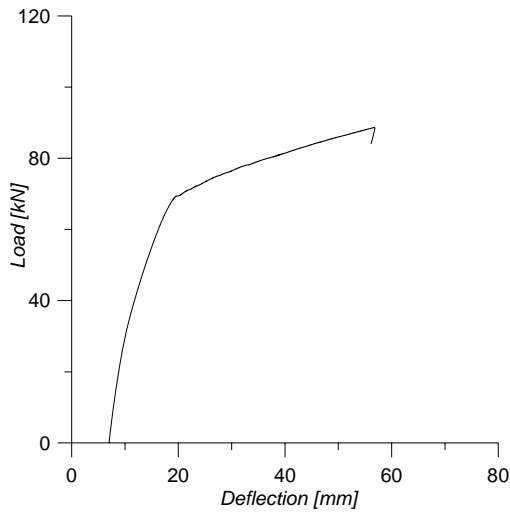


Figure 6-17. Load vs. deflection relation for corroded beam.

The cross section from the beam where tensile reinforcement was attacked by corrosion reveals severe damages in the form of cracks spreading out from the reinforcement. These cracks have arisen due to the expansion pressure created by corrosion products that are more voluminous than steel.

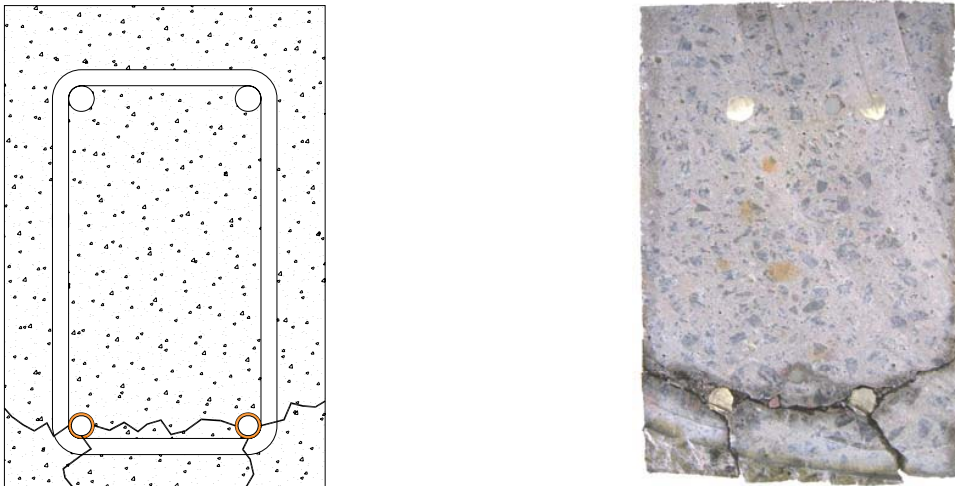


Figure 6-18. Left: Schematic diagram of corroded beam cross section. Right: Actual corroded beam cross section.

6.3.3 Beam where cover concrete was removed

Cover concrete was removed to a depth of 50 mm as can be seen in Figure 6-19. The steel reinforcement did not touch the concrete at any point after the cover concrete was taken away, during when the beam was loaded with the dead load.

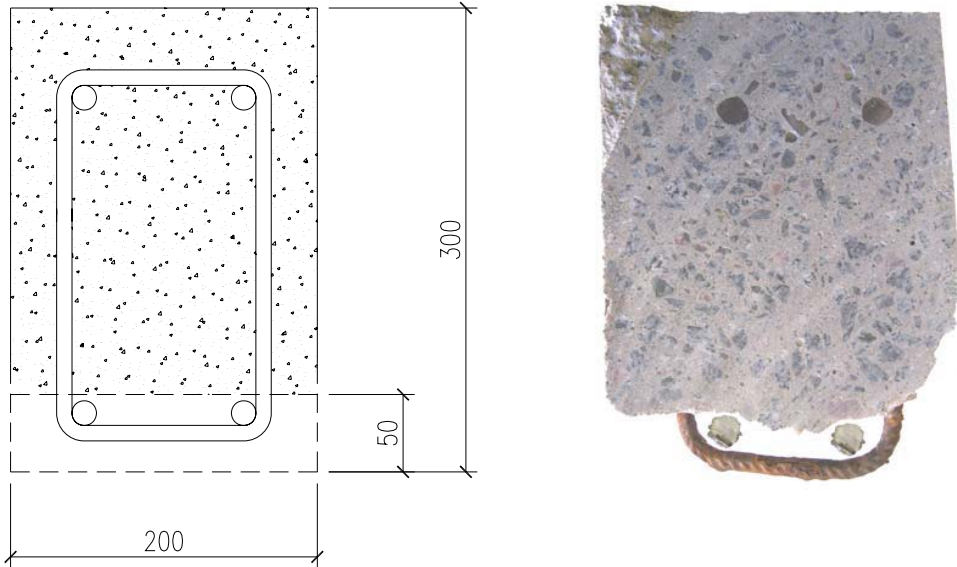


Figure 6-19. Left: A sketch of the cross section of the beam where concrete to a depth of 70 mm was removed. Right: Cross section of real beam where concrete was removed.

The steel reinforcement moved toward the centre of gravity during the failure test until it reached the concrete surface where it stopped. Cracks formed as given in Figure 6-20.

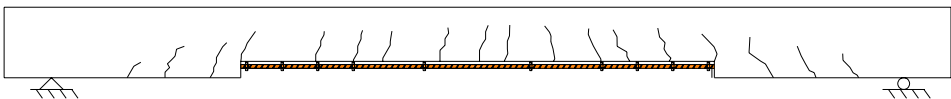


Figure 6-20. Cover concrete removed in the region of corrosion (2000 mm in mid-span).

No crack load was observed for this beam for the same reason as for the corroded beam. Yielding of steel reinforcement occurred at just below 70 kN.

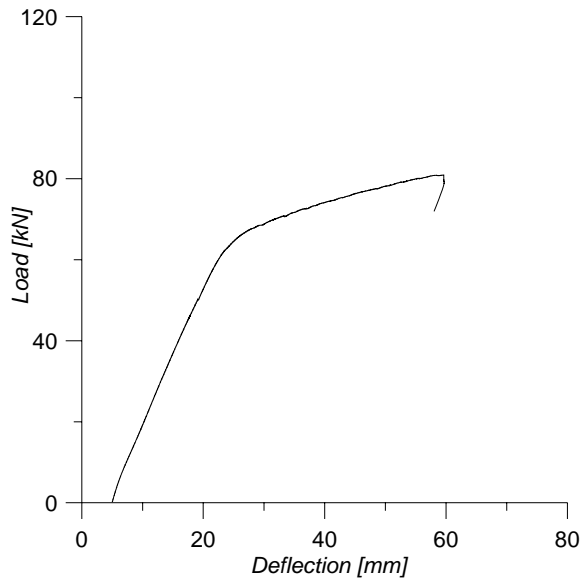


Figure 6-21. Load vs. deflection relation for beam where cover concrete is removed.

Yielding of steel reinforcement occurred at 60 kN according to the left part of Figure 6-22. The height of the compressed zone is established to 100 mm from the strain distribution in the right part of Figure 6-22.

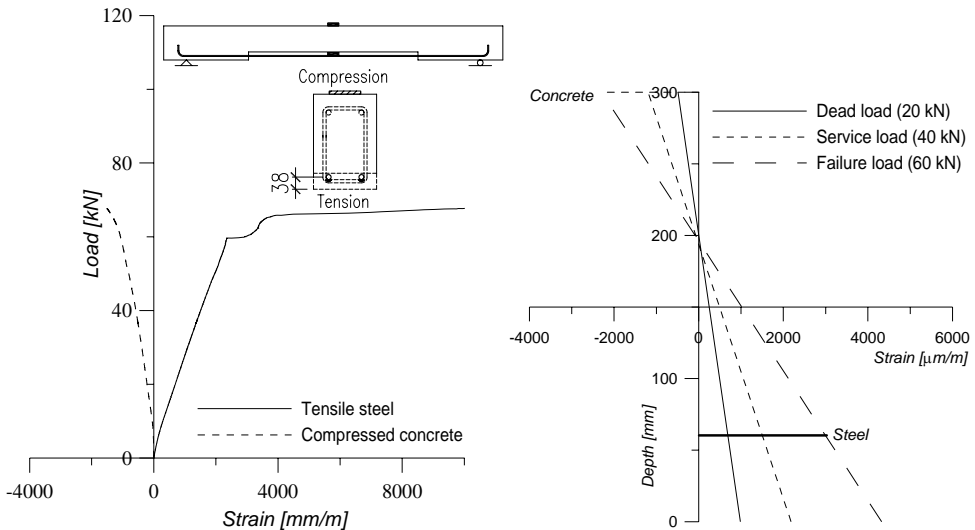


Figure 6-22. Left: Strain readings on tensile steel reinforcement and compressed concrete on beam where cover concrete is removed. Right: Strain distribution between tensile steel reinforcement and compressed concrete surface.

One important result from the failure test of the beam where cover concrete was removed is that the tensile steel reinforcement moved towards the neutral axis as seen in Figure 6-23.

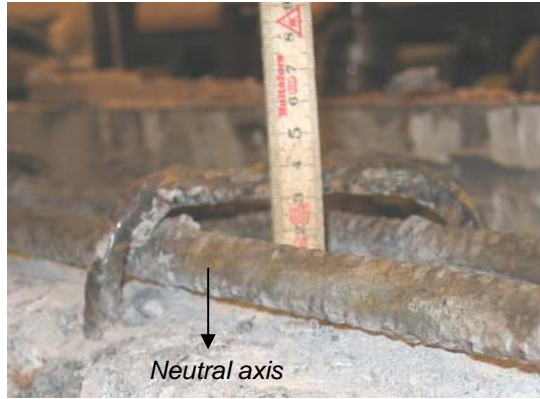


Figure 6-23. The effective height was reduced as the longitudinal reinforcement lost some distance to neutral axis when concrete was removed.

6.3.4 Repaired beam

Repair mortar was cast in the cavity left behind the removed deteriorated concrete cover as described in the left part of Figure 6-24. The result of the operation is given in the right part of Figure 6-24.

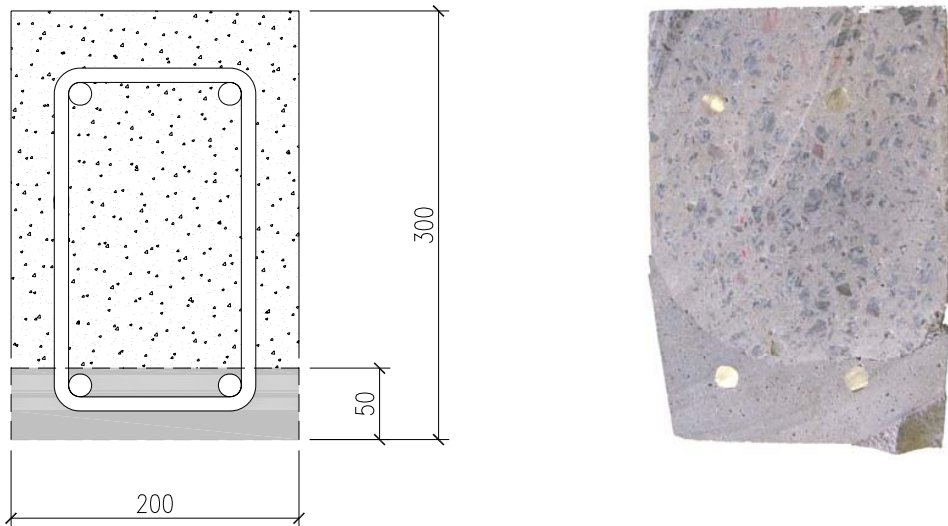


Figure 6-24. Left: Schematic of cross section of repaired beam. Right: Cross section of real repaired beam.

Large cracks formed in the repair mortar, and the crack width was consequently also large and in sizes around one to two millimetres at abortion of failure test. It seems like the fibre reinforced repair mortar does not give a beneficial crack pattern, which should consist of many small cracks. The large cracks are not advantageous when considering durability aspects, such as keeping chlorides away from steel reinforcement, see Figure 6-25 for crack pattern of the repaired beam. Figure 6-26 gives two pictures of cracks in the repair mortar.

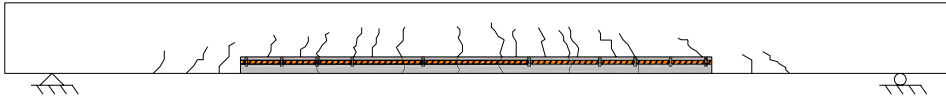


Figure 6-25. The cavity is refilled with repair mortar.



Figure 6-26. Large cracks formed in the repair mortar during failure test.

The initial deflection of the repaired beam after the corrosion stage was 8 mm. Yielding of steel reinforcement occurred at 64,8 kN. The linear increase of load after yielding of steel is the same as for the previous beams. The failure test was aborted at 64 mm. No observations of total failure of beam were noticed at this stage.

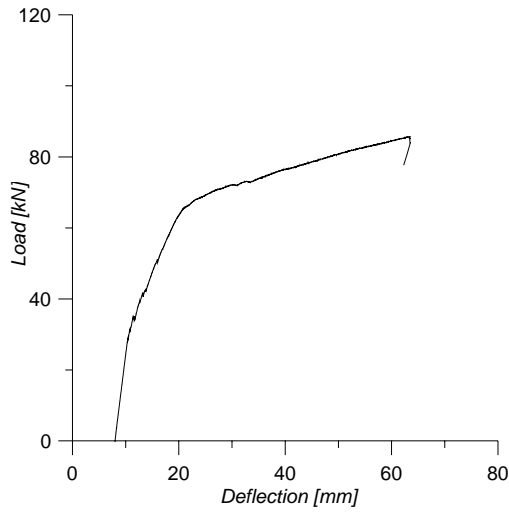


Figure 6-27. Load vs. deflection relation for repaired beam.

Yielding of steel reinforcement was noticed at 64,8 kN according to the left part of Figure 6-28. The height of the compressed zone is 90 mm for the repaired beam as can be seen in the left part of the figure.

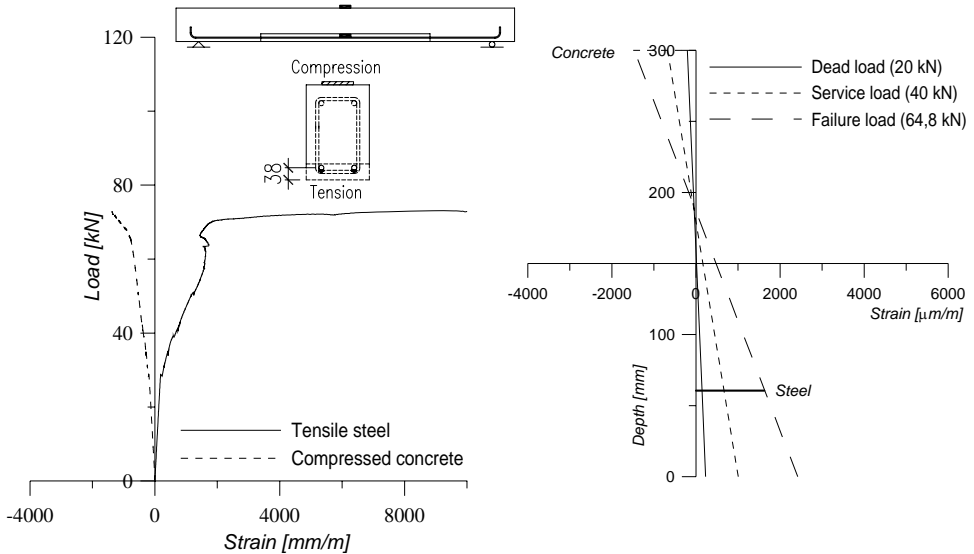


Figure 6-28. Left: Strain readings on tensile reinforcement and compressed concrete on repaired beam . Right: Strain distribution for repaired beam at dead load, service load and failure load.

6.3.5 Repaired & strengthened beam

The cross section of the repaired and strengthened beam is shown in the left part of Figure 6-29, the actual cross section is shown in the right part. The debonding failure occurred in the interface between adhesive and concrete, and is considered as premature. The surface preparation consisted of brushing with steel brush. The reason why this method was chosen was due to the risk of damaging surrounding monitoring cables, and also because of a limited workspace. This method was shown to give a deficient result compared to traditional surface treatment, such as sand blasting or grinding. Other possibilities for why debonding occurred prematurely was that the repair mortar does not have the same surface properties as ordinary concrete, and that the interface between the original concrete and repair mortar is not perfectly plain. Figure 6-30 clearly shows that the interface between original concrete and repair mortar will give changes in adhesive thickness, and also curvature of the CFRP plate when bonding it to the surface. This might give rise to increased peeling stresses.

Left part of Figure 6-31 shows the beam after failure, where the CFRP plate was bonded. The right part shows that only epoxy and primer was left on the CFRP plate after debonding.

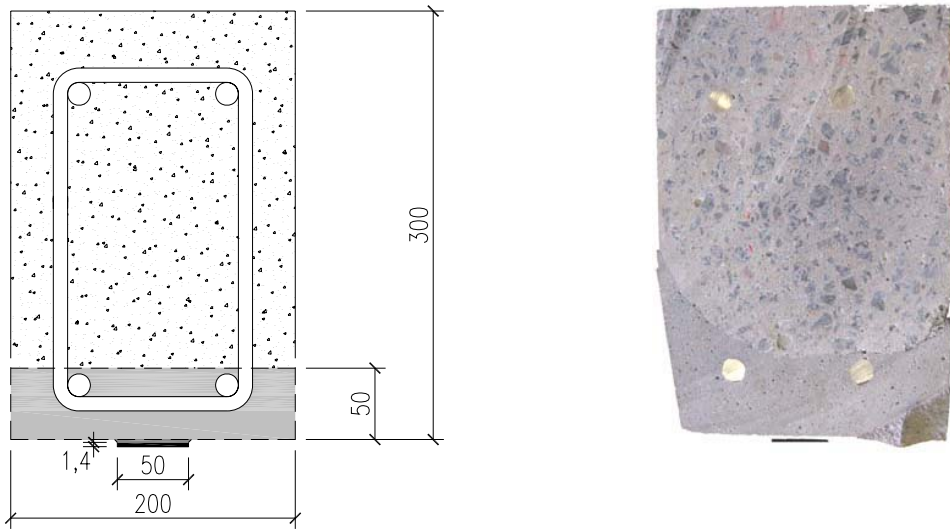


Figure 6-29. Left: Schematic of repaired and strengthened beam cross section. Right: Real cross section of repaired and strengthened beam.



Figure 6-30. Left: Interface between original concrete and repair mortar. Right: CFRP plate bonded to the repaired beam.



Figure 6-31. Left: The failure occurred in the interface between adhesive and concrete. Right: Only epoxy and primer was left on the CFRP plate after debonding.

Large cracks were observed in the repair mortar, similar to the repaired beam. The crack pattern is shown in Figure 6-32. Cracks as wide as 2 millimetres were spotted in the repair mortar.

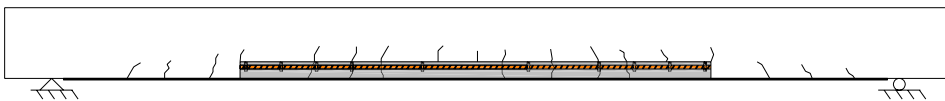


Figure 6-32. Crack pattern for repaired and strengthened beam specimen after failure test.

The initial deflection was measured to 8 mm. The failure occurred as debonding of CFRP plate at 82,7 kN. The residual capacity after debonding was measured to 75 kN.

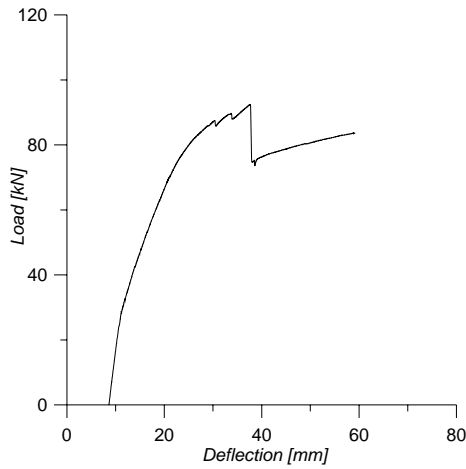


Figure 6-33. Load vs. deflection relation for repaired & strengthened beam.

Debonding of the CFRP plate occurred at 82,7 kN according to the left part of Figure 6-34. The height of the compressed zone is recorded to 150 mm for the repaired and strengthened beam.

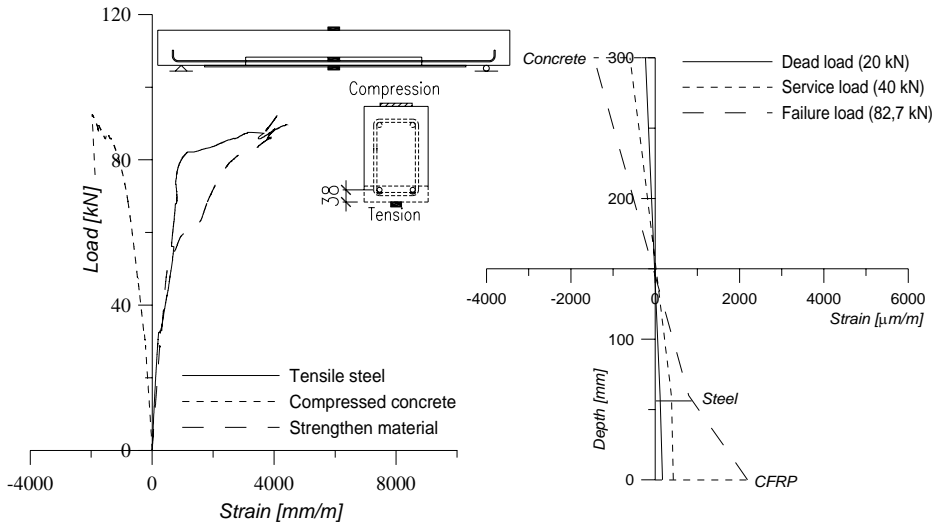


Figure 6-34. Left: Strain readings on tensile steel reinforcement, compressed concrete and CFRP plate for repaired & strengthened beam. Right: Strain distribution between compressed concrete, tensile steel reinforcement and CFRP plate.

7 Evaluation

7.1 General

This chapter focuses on evaluating the result material from the experimental work and is divided into three subchapters; corrosion stage, short term test results and visual inspection of cross sections in different stages in the life cycle.

7.2 Corrosion stage – long term test

Pitting corrosion will generally decrease the ductility of the structural element, due to the decreased ductility of the steel reinforcing bar. This was confirmed by performing material testing on three cut-out corroded steel reinforcing bars from one of the corroded test specimens. The test indicates a 55% decrease in ultimate strain capacity, from 22% of the intact steel bar to 10% of the corroded steel bar according to Figure 7-1. The corroded steel bar loses strength right after yielding occurs, probably as the stress in a certain cross section where a pit damage is located reaches ultimate stress and fails. “No chain is stronger than the weakest link”-philosophy reminds us.

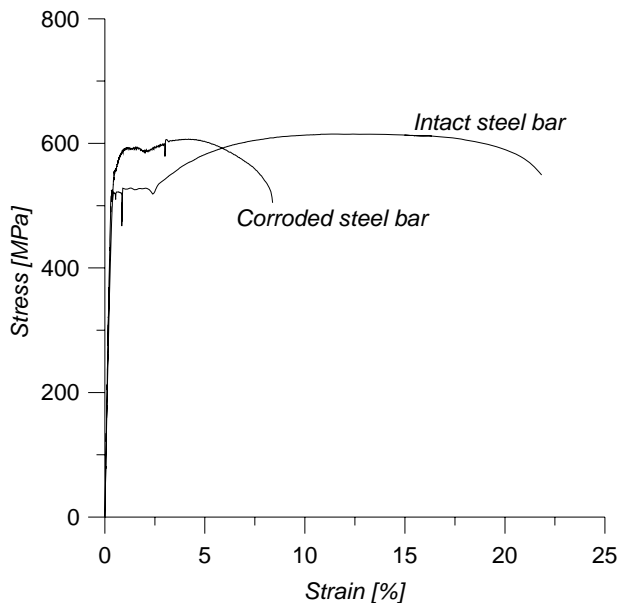


Figure 7-1. Stress vs. strain diagram for intact steel bar and corroded steel bar. Reduction of ductility of corroded steel bar is obvious.

7.2.1 Stiffness

Beam stiffness is determined during the corrosion phase by the relationship between curvature and moment as

$$EI = \frac{M}{\kappa} \quad (7.1)$$

Where M is the acting bending moment and κ is the curvature. Stiffness determined by the LVDT setup is presented during the corrosion phase in the left part of Figure 7-2. All six corroded beams are plotted in the graph, as well as a calculated average stiffness. The stiffness decrease of 15% from 2980 kNm² to 2530 kNm² during the corrosion stage is determined by plotting an average curve. The stiffness reduction agrees quite well with the reduction in steel content, which for comparison is 11%. To confirm the loss in stiffness of the corroded beam due to loss of reinforcing steel, the moment of inertia is calculated, according to equation (7.2), for the corroded and the intact beam.

$$I_2 = I_c + \alpha_s I_s = \frac{bx^3}{12} + bx \left(\frac{x}{2} \right)^2 + (\alpha_s - 1) A'_s (x - d'_s)^2 + \alpha_s A_s (d_s - x)^2 \quad (7.2)$$

The cross section is considered as cracked, which corresponds to stage II in the analytic calculation. The compressed zone is calculated in stage II by equalizing right and left hand side of the equation

$$\frac{bx^2}{2} + (\alpha_s - 1) A'_s (x - d'_s) = \alpha_s A_s (d_s - x) \quad (7.3)$$

By inserting values for the intact beam in the equation gives

$$\frac{200 \cdot x^2}{2} + (20 - 1) \cdot 402 \cdot (x - 58_s) = 20 \cdot 402 \cdot (257 - x) \quad (7.4)$$

The equation is fulfilled by choosing x to 98,5 mm. The same calculation for the corroded beam specimen gives an x value equal to 94,5 mm from equation (7.5) below.

$$\frac{200 \cdot x^2}{2} + (20 - 1) \cdot 402 \cdot (x - 58) = 20 \cdot 358 \cdot (257 - x) \quad (7.5)$$

Table 7-1. Calculated loss in stiffness due to loss of steel due to corrosion compared to recorded loss of stiffness.

	Theoretical moment of inertia [m ⁴]	Theoretical ratio compared to intact beam [%]	Stiffness ratio from test [%]
Intact beam	2,79·10 ⁻⁴	100	100
Corroded beam	2,57·10 ⁻⁴	91	85

The calculation indicates a 9% loss of stiffness of the corroded beam specimen, if considering the modulus of elasticity, E , as constant. The remaining loss of stiffness recorded during the corrosion phase may be related to creep.

Further, stiffness was also calculated from the resulting curvature measured with FOS. The right part of Figure 7-2 shows the average stiffness from the LVDT setup and the average stiffness calculated by the fibre optical strain measurement during the corrosion phase of the beams referred to as $B1$ and $B2$.

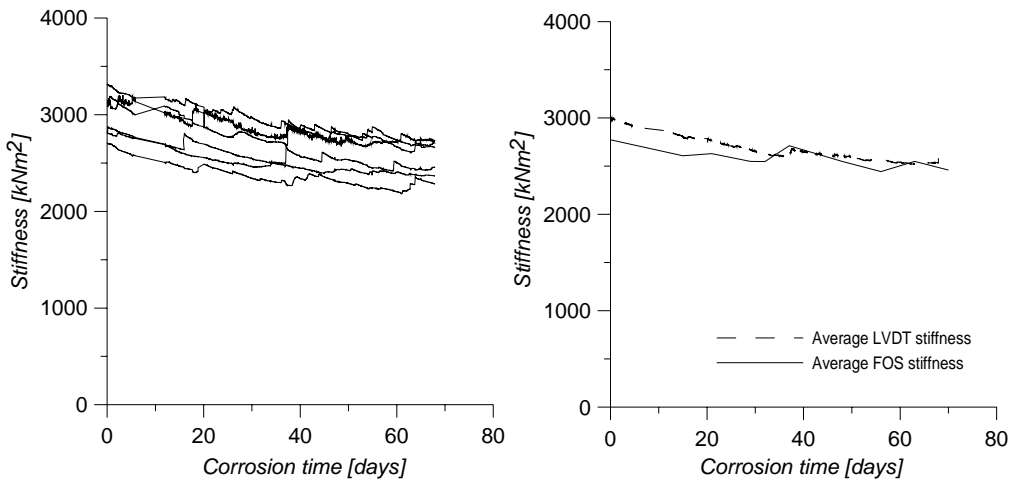


Figure 7-2. Left: Beam stiffness during corrosion stage given by LVDT setup. Bold line gives mean stiffness. Right: The average stiffness from the LVDT setup is compared to the stiffness measured with FOS on beam specimens $B1$ and $B2$ during the corrosion phase.

The result given by Figure 7-2 tells that it is possible to measure stiffness both globally, by the LVDT setup and locally, by the strain gauges located in the beam cross section. The global setup is reliable in the sense that it measures the average curvature over the measured region, and that the test setup fits this method as the bending moment is kept constant. The benefit of using the local strain gauge method is in the case where the bending moment is non-constant in the studied section. The curvature in the specific point could then be coupled with the bending moment in the same point to evaluate stiffness. It should however be mentioned that there is a possible problem when measuring strain along a steel bar in a cracked section, as the strain in the steel bar is heavily dependant on the surrounding cracks (Noghabai, 1998).

The result indicates that there is a strong relation between the deterioration process and the change in curvature and stiffness, suggesting that this is a method to measure the status of the structure. For instance, a performance factor could be defined as 1 for the intact structure and then decrease to represent the relation between the stiffness of the deteriorated and the intact structure.

If the structure is strengthened, the performance factor could be larger than 1. In comparison to this method, evaluation of frequency shift due to a changed stiffness of the structural member is possible. This method could however give very small indications of deterioration, even though the structure is suffering from a large damage (Hejll, 2004).

7.3 Failure load test

7.3.1 Load vs. deflection relations

The relation between load and deflection for each beam in the test series was established during the failure load test. The result is presented in Figure 7-3 and Table 7-2. Notice that the initial deflection is not zero for the beams loaded over long time. The reason for this is that those beams have been affected by creep. The load carrying capacity for beam specimens *B* and *E* were 13 % and 19 % lower than for beam *A* respectively. Beam specimen *D* showed the lowest failure load of only 75 % of the load carrying capacity of beam *A*. This is the weakest beam in the test series. The tensile reinforcement will cut into the curvature of the beam and move towards the centre of gravity when the cracked concrete is removed. The effective height reduction is dependant on how much of the cracked concrete has to be removed, and how much load is acting on the beam when the repair mortar is applied. Beam specimen *F* gave 4 % higher capacity than beam *A*. Table 7-2 summarizes the failure load compared to reinforcement steel mass content together with failure mode. Note that the relative failure load for beam specimen *B* corresponds to the reinforcement steel mass content.

Starting off with beam specimen *A*, which reached yielding of steel reinforcement at 79,8 kN and a crack load of 6 kN. When comparing beam *B* with the intact beam specimen, *A*, it is concluded that the corroded beam, *B*, reaches yielding at the lower load of 69 kN, precisely 10 kN less than beam, *A*. The initial deflection is due to creep during the corrosion stage, and the initial stiffness increase is also connected to the creep effect. (Horrigmoe & Sæter, 2006) noticed the same initial stiffness increase when performing pull-out tests where corroded steel reinforcing bars were pulled out of concrete blocks.

Further on into the life cycle brings beam specimen *D* in focus. This beam is the weakest in the series with a yield load at 60 kN. This is because the steel is corroded, but also because the reduced effective height, leading to a weaker behaviour of this beam compared to both the reference beam, *A*, and the corroded beam, *B*.

The repaired beam, *E*, shows the same initial stiffness increase. This beam reaches yielding of steel reinforcement at 64,8 kN and does not reach the load carrying capacity of the corroded beam.

The load carrying capacity of the repaired & strengthened beam, *F*, at 82,7 kN was just above the load carrying capacity of the intact beam, *A*. It is also seen that the behaviour in the post-debonding area in the load vs. deflection graph follows the behaviour of the corroded beam, *B*.

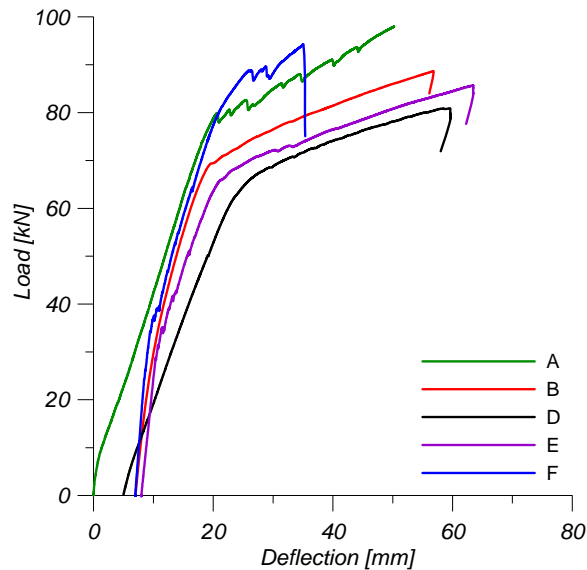


Figure 7-3. Load vs. deflection for all tested beams.

Sand (2001) discovered that the load carrying capacity of a repaired beam with 10 % mass loss of tensile steel reinforcement due to corrosion and an attacked length of 55 % of the free span, was 86 % compared to the intact beam in its series. That calculation is the most suitable for comparing with the result from this study, as the mass loss and length of the attacked area is about the same. Again, this study shows that the load carrying capacity of the repaired beam is 81 % compared to the intact beam. The corresponding relation given in (Sand 2001) was discovered to be 86 %.

Table 7-2. Summarized failure load and failure mode for all tested beams.

Beam notation	Average reinforcing steel mass content [%]	Failure load [kN]	Calculated relative failure load [%]	Failure mode*
A	100	79,8	100	Y
B1	88	69,3	87	Y
D	88	60	75	Y
E	88	64,8	81	Y
F	88	82,7	104	D

* Y: Failure by yielding of tensile reinforcement. D: Debonding of CFRP plate.

7.3.2 Life cycle behaviour

The life cycle behaviour is created by using the failure load test results presented above. The *intact* beam curve is plotted up to the service load giving the behaviour of the undamaged structure. The reduction in stiffness caused by corrosion leads to an increased deflection at the same load. This deflection is determined by plotting the curve for the *corroded* beam up to the service load. The load reduction from service load down to dead load follows the curve for the *corroded* beam. The deflection is increased even more at dead load when the cover concrete is removed. This deflection is determined at dead load for the beam where the cover concrete is removed. From this point in the diagram the final stages could be plotted. If the structure is not strengthened it follows the curve for the *repaired* beam. If the structure instead is strengthened, the behaviour follows the curve for the *repaired and strengthened* beam. The full view of the life cycle is given by the bold line in Figure 7-4.

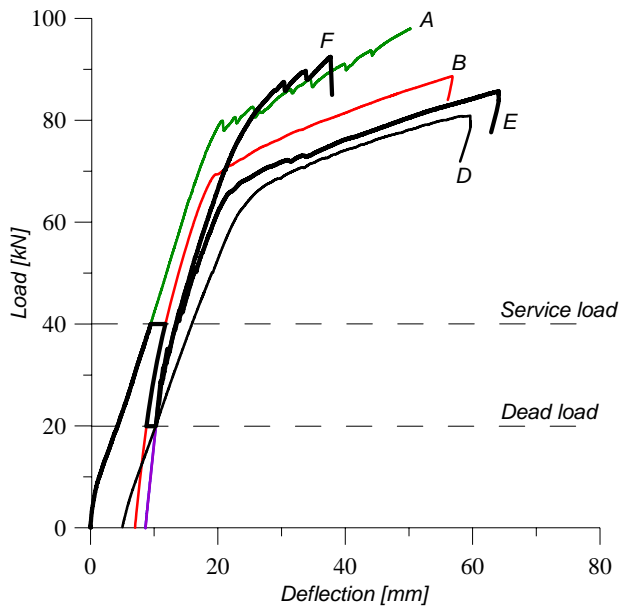


Figure 7-4. Life cycle behaviour is indicated by the bold black line.

7.3.3 Existing strain field

As discussed earlier in chapter 3, a strain field will be created over the cross section of the beam during the repair procure, since the beam was curved due to the dead load. When the repair mortar was cast and had hardened, it forced the beam to keep the shape which it had during the repair procedure. This creates an initial strain field in the beam which will follow the beam throughout the rest of the life cycle.

In this study, the initial strain field is measured after hardening of repair mortar and is taken into consideration by adding it to the measured strain during the failure test for the repaired beams. The principle is given in Figure 7-5 and the initial strain distribution is measured with FOS to be as presented in Figure 7-6. This initial strain field is hence added to the results recorded during the failure test to give the actual strains. Note that the repair mortar is strain-free at the load level when it was applied, 20 kN. This consideration is only proper for the repaired beams, E and F, in the test series, and the results are given in Figure 7-7.

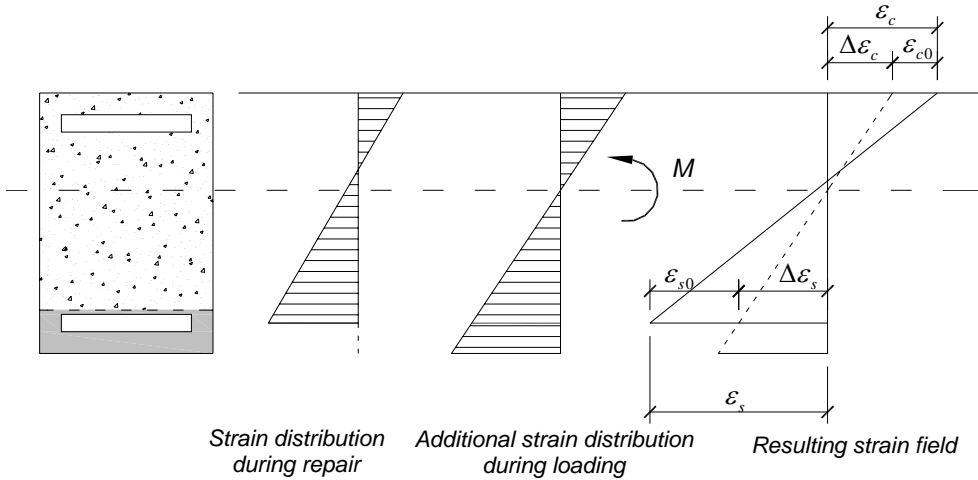


Figure 7-5. Schematic of how to take consideration of strain field created during the repair procedure.

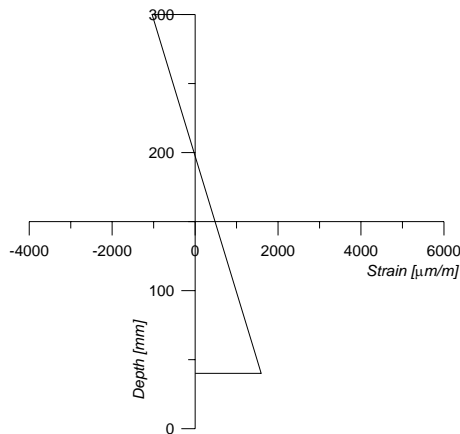


Figure 7-6. The initial strain distribution caused by the repair procedure.

The actual strain distribution where the initial strains are taken into consideration is presented in Figure 7-7.

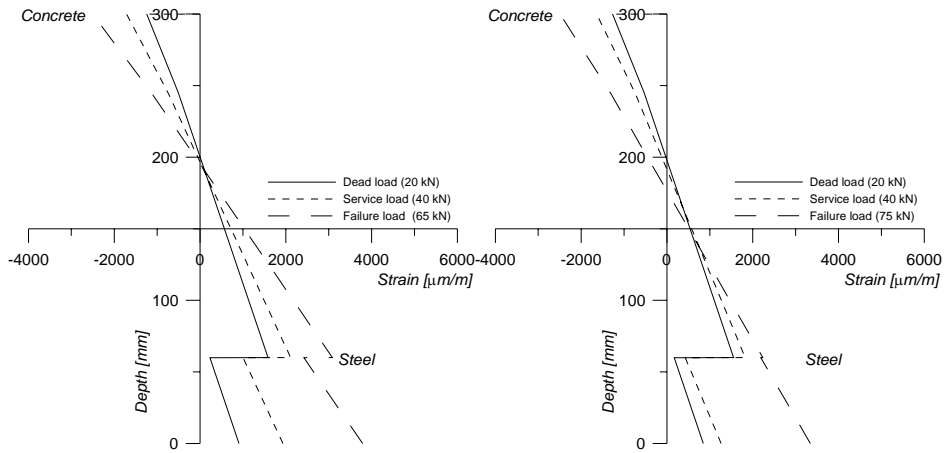


Figure 7-7. Actual strain field at different load levels for the repaired beam specimen, E, (left) and the repaired & strengthened (right) beams, F.

The result is believed to be correct as the strain in the steel reinforcement for the repaired beam at failure, which is defined as yielding of the steel reinforcement, is very close to the yielding strain of steel. The strain at yielding is close to 3000 microstrain and is calculated through the result from material testing presented in Appendix A to

$$\varepsilon_{yield} = \frac{f_{st}}{E_s} = \frac{514}{186,7 \cdot 10^3} \approx 3000 \mu\text{m/m} \quad (7.6)$$

The large cracks which formed in the repair mortar during the failure test may be an effect of the discussed initial strain distribution. The steel yielded soon after uploading at the failure test, as the initial strain in the steel is almost 50% of the yield strain due to the initial strain field. At yielding, the stress in the repair mortar could locally grow very high and cracks are possibly initialized. It is also been shown earlier in the thesis, that pitting corrosion will affect the behaviour of the steel bars, and produce very high local stresses which decreases the ductility. Pitting corrosion could hence also bring more stress to the repair mortar as the load is gradually increased.

7.3.4 Stiffness

Stiffness was measured during the failure test both by using the LVDT setup as well as traditional strain gauges. A comparison in between the two different techniques is presented for the intact beam in the left part of Figure 7-8, and for the beam where cover concrete was removed in the right part. The stiffness measured through the traditional strain sensors shows higher beam stiffness than what the LVDT setup does for the intact beam. There results in between the techniques are small for the beam where cover concrete was removed.

No consideration to the initial strain field is taken for the reference beam and the beam where cover concrete was removed, since it is only coupled to the beams where repair mortar is cast.

It is interesting to see that the stiffness of the reference beam is constant until a deflection of 20 mm, where the concrete crack load is reached and the stiffness decreases. There is a noticeable trend that the stiffness decreases down towards a particular level. Further, in considering the LVDT setup another interesting result is that the value of the initial stiffness, at 10 mm of deflection, and final stiffness, at 50 mm deflection, are in descending order in agreement to what the load carrying capacity according to the failure test showed.

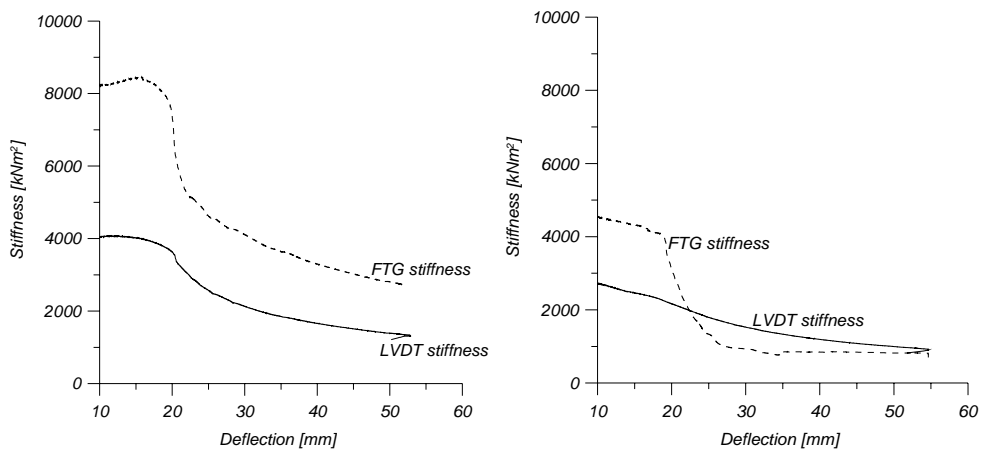


Figure 7-8. Left: Stiffness of reference beam during failure test. Right: Stiffness of beam where cover concrete was removed during failure test.

The initial strain, given in section 7.3.3, is taken into consideration for the repaired beams. If this was not considered, the beam stiffness would have been over estimated as the actual strain is considered as lower than it really was. The two stiffness measurement techniques show very similar results for the repaired and repaired and strengthened beams, which is seen for the repaired beam in the left part of Figure 7-9, and for the repaired and strengthened beam in the right part.

This result shows that both these techniques could be used to measure bending stiffness of a structural member. Measuring stiffness is interesting as stiffness is highly connected to the serviceability limit state in terms of crack width and deflection. Stiffness is also used in resonance and in the evaluation of eigen frequencies, as well as a check to verify the agreement of FE-models.

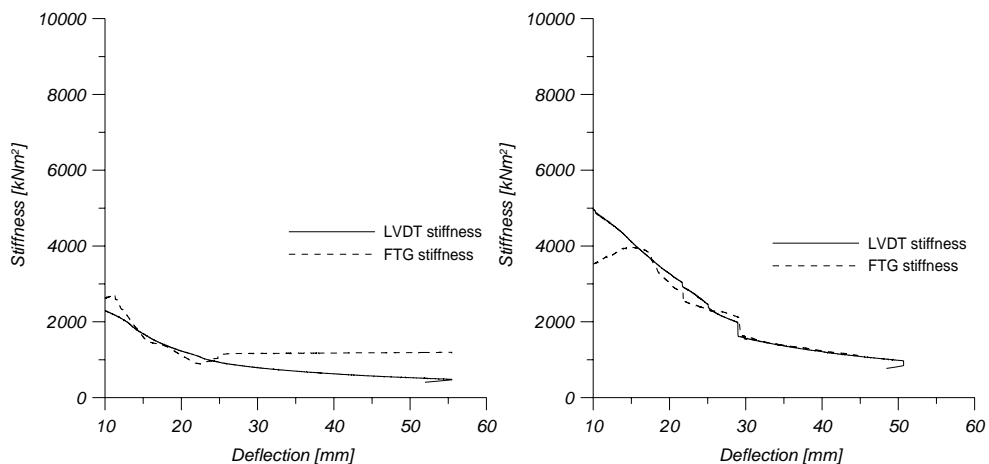


Figure 7-9. Left: Stiffness of repaired beam during failure test. Right: Stiffness of repaired and strengthened beam during failure test.

The stiffness during the failure test is plotted in Figure 7-10 for the repaired and the strengthened beam to see the effect of strengthening in terms of bending stiffness. Debonding occurred just below 30 mm of deflection as can be read earlier in the report. Before debonding just below 30 mm of deflection as can be read earlier in the report. Before debonding the bending stiffness of the strengthened beam is about 30 % higher than for the repaired beam. After debonding of the CFRP plate, the beams are identical and the behaviour should be likewise. This is confirmed by the result presented in the graph.

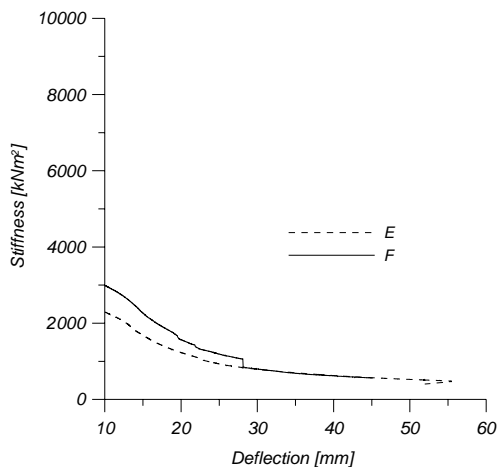


Figure 7-10. Comparison between stiffness measured using the LVDT setup for the repaired beam, E, and strengthened beam, F,

8 Probabilistic evaluation

This chapter presents a calculation example directed to analyze how the probability of failure changes at different stages in the life cycle for a structural member. The load required for an annual probability of failure for an intact beam of $1 \cdot 10^{-6}$ is defined to be the comparing load effect, S . The safety will then be calculated for this load effect for

- corroded beam
- repaired beam
- repaired and strengthened beam

8.1 Analytical models

When analyzing the moment capacity for the reinforced concrete beams and strengthened concrete beams, in this example, the Swedish design code is used.

8.1.1 Reinforced concrete beam

A concrete member loaded in flexure normally undergoes three stages up to failure; stage I, stage II and stage III. The stages are illustrated in Figure 8-1.

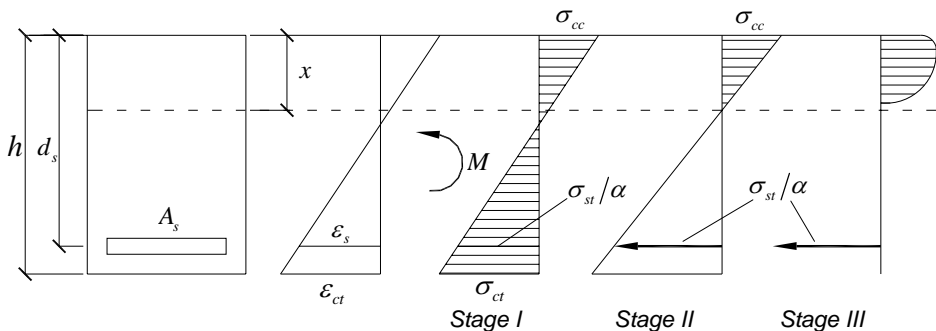


Figure 8-1. Different stages for a beam subjected to bending.

The strains in the serviceability limit states in stage I and stage II are calculated normally according to the elasticity theory with constant modulus of elasticity for concrete and steel, see The Swedish handbook for concrete structures; Betonghandboken Konstruktion 1990. The effect of creep in concrete as a result of long-term loading can be taken into account through a reduced modulus of elasticity

$$E_{ce} = \frac{E_c}{1 + \varphi} \quad (8.1)$$

The section can be assumed un-cracked and the entire cross-section effective if the concrete's design tensile strength for the serviceability limit state is not exceeded according to the Swedish concrete design codes; BBK 94

$$f_{cbt} = k \frac{f_{ct}}{\zeta} = \left(0.6 + \frac{0.4}{\sqrt[4]{h}} \right) \frac{f_{ct}}{\zeta} \quad (8.2)$$

In stage II the concrete's tensile strength is exceeded, and the entire tensile zone of the concrete cross-section, the so-called tension zone, is assumed cracked. Stage III represents the condition at ultimate limit state.

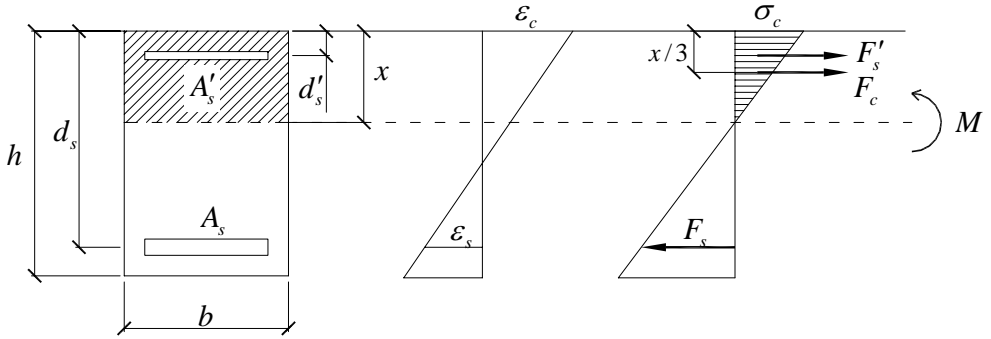


Figure 8-2. Rectangular concrete cross-section in service limit state (SLS) and stage II.

The beams used in this research project are under reinforced, which means that the tensile steel reinforcement reaches its yield stress before crushing of concrete occurs. The stress in the steel reinforcement of the concrete beam in stage II is calculated as

$$\sigma_s = \alpha_s \frac{M}{I_c + \alpha_s I_s} (d_s - x) = \alpha_s \frac{M}{I_2} (d_s - x) \quad (8.3)$$

This gives the moment capacity for beam in stage II as the steel reinforcement reaches its yield stress to

$$M_{intact} = \frac{f_{st} \cdot I_2}{\alpha_s \cdot (d_s - x)} \quad (8.4)$$

α_s is the ratio between the modulus of elasticity of steel, E_s , and the effective modulus of elasticity of concrete, E_{ce} .

$$\alpha_s = \frac{E_s}{E_{ce}} = \frac{E_s (1 + \varphi_e)}{E_c} \quad (8.5)$$

I_2 is the moment of inertia of the cross-section in stage II, and is for a rectangular beam calculated as

$$I_2 = I_c + \alpha_s I_s = \frac{bx^3}{12} + bx \left(\frac{x}{2} \right)^2 + (\alpha_s - 1) A'_s (x - d'_s)^2 + \alpha_s A_s (d_s - x)^2 \quad (8.6)$$

The height of the compressed zone of the concrete, x , is determined by equalizing right and left hand side of the equation

$$\frac{bx^2}{2} + (\alpha_s - 1) A'_s (x - d'_s) = \alpha_s A_s (d_s - x) \quad (8.7)$$

x is calculated in each stage using the mean value of required parameters.

8.1.2 Strengthened beam

The failure of the strengthened beams has by the test shown to be debonding of CFRP without yielding of compressed steel reinforcement. The ultimate strain in the CFRP material is in this particular case defined as the strain just before debonding. This reduces the load carrying capacity, but at the same time will give more relevant capacity compared to the performed test. The moment capacity for this failure mode, according to Täljsten (2004) and Figure 8-3, could be calculated as

$$M = \frac{x - d'_s}{h - x} (\varepsilon_f + \varepsilon_{u0}) A'_s E_s (\beta x - d'_s) + A_s f_y (d_s - \beta x) + \varepsilon_f E_f A_f (h - \beta x) \quad (8.8)$$

where

$$C_1 x^2 + C_2 x + C_3 = 0 \quad (8.9)$$

and

$$\begin{aligned} C_1 &= \alpha f_{cc} b \\ C_2 &= -\alpha f_{cc} b h - (\varepsilon_f + \varepsilon_{u0}) A'_s E_s - A_s f_y - \varepsilon_f E_f A_f \\ C_3 &= (\varepsilon_f + \varepsilon_{u0}) A'_s E_s d'_s + (A_s f_y + \varepsilon_f E_f A_f) h \end{aligned} \quad (8.10)$$

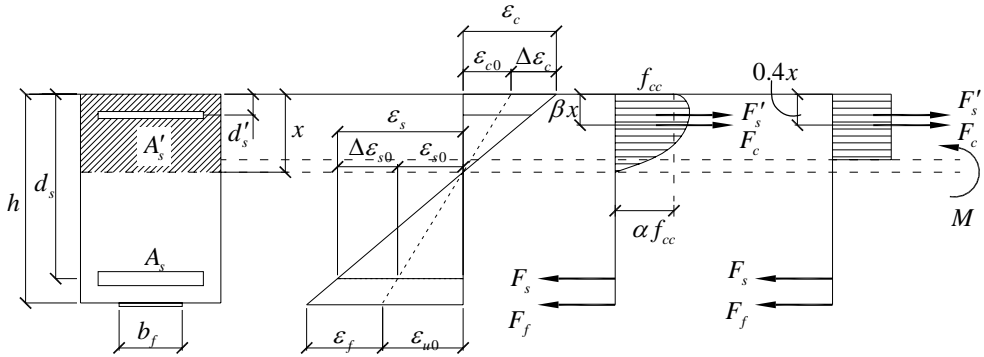


Figure 8-3. Stress and strain diagram for a strengthened concrete beam.

8.2 Statistical and deterministic variables

The parameters discussed in the following section are identified as the most important ones affecting the load capacity of the tested concrete beams.

The fibre area, A_f , as well as the steel reinforcement area, A_s , is assumed according to JCSS PMC (2001) to be normal distributed with a coefficient of variance $V = s/m = 0,02$. The yield stress, f_{yd} , of the reinforcing steel is assumed according to JCSS PMC (2001) to be normal distributed with mean value equal the nominal value plus 2 times the standard deviation where the standard deviation is said to be 30.

The fibre stiffness, E_f , is assumed according to Carolin et al. (2004) to have mean value 150 GPa with a standard deviation of 2,6 GPa.

The compressive strength of concrete, f_{cc} , is determined from six cube tests. Mean value 63,8 MPa and standard deviation 3 MPa. The tensile strength of concrete is established from six split tests to mean value 4,3 MPa and standard deviation 1 MPa.

The load effect parameter, S , is adjusted to give a probability of failure for the intact beam of 10^{-6} , which is safety class 3. Another requirement is that the coefficient of variance is set to 0,15. Simiu et. al (2001) suggests that the extreme load effect parameter, S , could be based on the Gumbel distribution or the inverted Weibull distribution, since those have proven to represent the yearly maximum of an extreme load effect. The Gumbel distribution is chosen in this calculation.

The compressed zone of the concrete is calculated to be very near 100 mm for the intact, corroded and repaired beams. The compressed zone for the strengthened and repaired beam is calculated to 107 mm. The values for the compressed zone are considered deterministic in this example.

Above discussed parameters in addition to a few more are summarized in Table 8-1. The denotation of the stochastic variable for the general parameter, P , is X_p in the failure functions defined later on in this chapter.

Table 8-1. Parameters used to calculate bearing capacity of concrete beams in different stages of the life cycle.

Variable	Description	Unit	Distribution	m	s	$V=s/m$
A_f	Fibre area	mm ²	Normal	70	2	0,03
A_s	Steel reinforcement area	mm ²	Deterministic	402	-	-
$A_{s,c}$	Corroded steel reinforcement diameter	mm ²	Normal	358	10	0,03
d'_s	Distance to compressed reinforcement	mm	Normal	58	5	0,09
d_s	Effective height	mm	Normal	257	5	0,02
$d_{s,cor}$	Effective height for repaired beam	mm	Normal	240	5	0,02
E_f	Fibre stiffness	GPa	Deterministic	150	2,6	0,02
E_s	Steel stiffness	GPa	Normal	210	3,6	0,02
f_{cc}	Compressive strength of concrete	MPa	Ln	63.8	3	0,05
f_{ct}	Tensile strength of concrete	MPa	Ln	4.2	1	0,24
f_{st}	Steel yield strength	MPa	Ln	500	30	0,06
h	Height	mm	Normal	300	2	0,007
S	Load effect variable	kNm	Gumbel	*	*	
w	Width	mm	Deterministic	200	-	-
x	Concrete compressed zone for unstrengthened beam	mm	Deterministic	100	-	-
$x_{upgraded}$	Concrete compressed zone for strengthened beam	mm	Deterministic	107	-	-
ϵ_f	Ultimate fibre strain (measured value at debonding of plate at failure test)	‰	Deterministic	4	-	-

* The load effect is adapted to give the safety class 3 ($p_f=1\cdot 10^{-6}$) for the intact beam. This calculation is shown later on in this chapter.

8.3 Calculations

Analyses were done using computer software named VaP (Variable Processor), version 2.2. This software gives the possibility of defining failure functions and also to define distribution type, mean value and a dispersion measure for each variable. A variable could be defined as deterministic in the program as well.

The analysis is performed using the First Order second moment Reliability Method (FORM), numeric integration or Monte Carlo simulation (<http://www.petschacher.at/>).

The calculation procedure in this study starts by first establishing a relevant load effect, S . The correct load effect is found when the probability of failure is $1 \cdot 10^{-6}$ for the intact beam at the same time as the coefficient of variance is 0,15. This will give realistic properties of the stochastic parameter describing the load situation. This load effect is then used to calculate the safety in all other stages in the life cycle. One interesting aspect is to see how much the safety is affected by different mechanisms during the life cycle.

In this study, no consideration has been taken to the glass fibre rods inserted into the beams. This will give a slightly higher load carrying capacity for the tested beams compared to what will be the result of these calculations. Given the results from the failure load test, it should be noticed that failure is defined as yielding of tensile steel reinforcement for unstrengthened beams and by debonding of CFRP plate for strengthened beam.

8.3.1 Principle for FORM calculation

To get a more clear view of the FORM calculation, a probabilistic calculation example is presented where two stochastic variables are treated in the failure function. Note that this example is just an example on how to calculate such problem by hand.

After the short example, computer software is used to perform the calculations later on in this chapter. This is presented in the section following this one.

Introduction

When analyzing the load carrying capacity of the intact beam, the analytical expression from equation (8.4) is utilized. In the failure function for the intact beam, only two parameters are considered as stochastic, and that is the yield stress of the tensile steel reinforcement, f_{st} , and the load effect, S .

The calculation starts by normalizing all primary variables, f_{st} and S . The stochastic variable, $X_{f_{st}}$, which describes the yield stress, f_{st} , is normalized resulting in a mean value equal to zero and a standard deviation equal to one. This is done as

$$Z_{f_{st}} = \frac{X_i - m_i}{\sigma_i} \quad (8.11)$$

$X_{f_{st}}$ then becomes

$$X_{f_{st}} = Z_{f_{st}} \cdot \sigma_{f_{st}} + m_{f_{st}} \quad (8.12)$$

The same operation for the load effect, S , results in

$$X_S = Z_S \cdot \sigma_S + m_S \quad (8.13)$$

When introducing $X_{f_{st}}$ and X_S the failure function becomes

$$g = \frac{X_{f_{st}} \cdot I_2}{\alpha_s \cdot (d_s - x)} - X_S = \frac{(Z_{f_{st}} \cdot \sigma_{f_{st}} + m_{f_{st}}) \cdot I_2}{\alpha_s \cdot (d_s - x)} - (Z_S \cdot \sigma_S + m_S) \quad (8.14)$$

Where I_2 is the moment of inertia in stage II in equation (8.6). The following equations are approved along the failure surface

$$g = \frac{(\alpha_{f_{st}} \beta \cdot \sigma_{f_{st}} + m_{f_{st}}) \cdot I_2}{\alpha_s \cdot (d_s - x)} - (\alpha_S \beta \cdot \sigma_S + m_S) \quad (8.15)$$

$$\frac{g}{dZ_{f_{st}}} = \frac{\sigma_{f_{st}} \cdot I_2}{\alpha_s \cdot (d_s - x)} \quad (8.16)$$

$$\frac{dg}{dZ_S} = -\sigma_S \quad (8.17)$$

$$\frac{dg}{d\beta} = \frac{\sigma_{f_{st}} \cdot I_2}{\alpha_s \cdot (d_s - x)} \cdot \alpha_{f_{st}} - \alpha_S \cdot \sigma_S \quad (8.18)$$

Solving the problem

The failure function given in equation (8.14) is linear, which means that there are no products of primary variables. If the failure function is non-linear, it is very useful to use an iterative method to find α -values and β -index since it is hard to find an analytic solution. However, the iterative method could be used also in the linear case, as this particular one. The Newton-Raphson iterative method says that

$$\beta^{i+1} = \beta^i - \frac{g(\beta)}{\left(\frac{dg}{d\beta}\right)} \quad (8.19)$$

The calculation starts off by giving a starting value for the α -values and then repeating the iteration procedure until $g(\beta)$ reaches zero, which is the point where the iteration has come to a halt and the final result is provided. In the following calculations computer software, VaP 2.2, is used.

8.3.2 Intact beam

Considering equation (8.4) and inserting stochastic variables, the failure function for the intact beam specimen, A , becomes

$$G_A = \frac{X_{f_{st}} \cdot I_2}{\alpha_s \cdot (X_{d_s} - x)} - X_S \quad (8.20)$$

Note that, for example, $X_{f_{st}}$ is the stochastic variable for the yield stress, f_{st} . The failure function holds three non-deterministic variables. Those are f_{st} , d_s and the so far unknown load effect, S . When choosing a mean value for S of 16,7 kNm and a standard deviation of 2,51 kNm the probability of failure for the intact beam equals 10^{-6} at the same time as the coefficient of variance is 0,15 when performing a FORM calculation in VaP 2.2.

8.3.3 Corroded beam

The failure function for the corroded beam specimen, B , is almost identical to the intact beam, with the difference that the tensile steel reinforcement area is now also stochastic. The failure function for the corroded beam becomes

$$G_B = \frac{X_{f_{st}} \cdot \left\{ \frac{bx^3}{12} + bx \left(\frac{x}{2} \right)^2 + (\alpha_s - 1) A'_s (x - d'_s)^2 + \alpha_s X_{A_{s,c}} (X_{d_s} - x)^2 \right\}}{\alpha_s \cdot (X_{d_s} - x)} - X_S \quad (8.21)$$

The probability of failure for the corroded beam is $2,1 \cdot 10^{-6}$ when applying the Gumbel distributed load effect, S , on the corroded beam. The probability of failure has increased about two times.

8.3.4 Repaired beam

As the concrete is removed the effective height is reduced. No consideration has been taken to a complete loss of bond between steel and concrete in this stage of the calculation. The failure function for the repaired beam specimen, E , becomes

$$G_E = \frac{X_{f_{st}} \cdot \left\{ \frac{bx^3}{12} + bx \left(\frac{x}{2} \right)^2 + (\alpha_s - 1) A'_s (x - d'_s)^2 + \alpha_s X_{A_{s,c}} (X_{d_{s,c}} - x)^2 \right\}}{\alpha_s \cdot (X_{d_{s,c}} - x)} - X_S \quad (8.22)$$

The probability of failure has increased even more compare to the intact beam and for the repaired beam is equal to $7,2 \cdot 10^{-6}$. This probability is close to what safety class 2 requires. However, during the repair operation the load is likely reduced which would cause that the safety during the repair procedure to be increased.

8.3.5 Strengthened beam

By considering equation (8.8) and inserting the stochastic variables, the failure function for the repaired and strengthened beam specimen, F , is

$$G_F = \frac{x - d'_s}{X_h - x} (\varepsilon_f + \varepsilon_{u0}) A'_s X_{E_s} (\beta x - X_{d_s}) + X_{A_s} X_{f_y} (X_{d_s} - \beta x) + \dots \quad (8.23)$$

$$\dots + \varepsilon_f X_{E_f} X_{A_f} (X_h - \beta x) - X_S$$

The probability of failure for the strengthened beam is dramatically increased in relation to the repaired beam to $7,9 \cdot 10^{-7}$. The strengthening procedure has upgraded the repaired beam from safety class 2 back to safety class 3. The strain in the CFRP plate was set to the deterministic value 4‰, since this was the measured strain in the failure test at debonding. However, since debonding occurred prematurely the failure probability should be even lower. One optimization of the last calculation would be to introduce the fibre strain as a stochastic variable.

8.4 Concluding results

8.4.1 Distributions

Distribution characteristics for the load carrying capacity of *intact, corroded, repaired and repaired & strengthened* beams together with the *load effect* are summarized in Table 8-2. The standard deviation for the load carrying capacity distributions gets larger and larger further within the life cycle, as more and more stochastic variables affect the load carrying capacity. The resistance parameter, *R*, for all stages are assumed to be normally distributed. The load effect parameter, *S*, is however purely Gumble distributed.

There is a trend that the actual failure load given from failure test is higher than the average value of the resistance distributions for the respective beam, see Table 8-2. One explanation for this is that the glass fibre rods inserted in the beams are not considered in the calculation.

Table 8-2. Resistance and load effect distribution characteristics.

	<i>R/S</i>	<i>Describing distribution type</i>	<i>Actual moment at failure [kNm]</i>	<i>Mean value [kNm]</i>	<i>Standard deviation [kNm]</i>
<i>Load effect</i>	<i>S</i>	<i>Gumble</i>	-	16,7	2,51
<i>Intact beam</i>	<i>R</i>	<i>Normal</i>	51	44,2	2,17
<i>Corroded beam</i>	<i>R</i>	<i>Normal</i>	44	42,9	2,29
<i>Repaired beam</i>	<i>R</i>	<i>Normal</i>	42	40,5	3,03
<i>Repaired and strengthened beam</i>	<i>R</i>	<i>Normal</i>	53	45,30	4,10

The estimated increase in load carrying capacity from the glass fibre rod, at yielding of steel reinforcement, is calculated for the intact beam. The tensile strain in the glass fibre rod, at yielding of steel reinforcement, is approximately 3000 microstrain in the tensile glass fibre rod. The compressive strain in the compressed glass fibre rod, at yielding of tensile steel reinforcement, is approximately 160 microstrain. The contribution in load carrying capacity in form of bending moment is calculated by a bending moment equilibrium around the top surface of the beam as suggested in Figure 8-5.

The force in the tensile glass fibre rod, $F_{t, gf}$ becomes

$$F_{t, gf} = A_{gf} \cdot E_{gf} \cdot \varepsilon_{t, gf} = 55 \cdot 10^3 \cdot 3000 \cdot 10^{-6} = 12,96 \text{ kN} \quad (8.24)$$

The force in the compressed glass fibre rod, $F_{c, gf}$, becomes

$$F_{c, gf} = A_{gf} \cdot E_{gf} \cdot \varepsilon_{c, gf} = 55 \cdot 10^3 \cdot 160 \cdot 10^{-6} = 0,69 \text{ kN} \quad (8.25)$$

Figure 8-4 gives the condition to determine the contribution to the moment carrying capacity of the glass fibre rods. The contribution is calculated to

$$M_{gf} = F_{t, gf} \cdot 0,235 - F_{c, gf} \cdot 0,055 = 3,0 \text{ kNm} \quad (8.26)$$

M_{gf} is used to reduce the load carrying capacity of the actual failure load of the beams, to create a fair comparison between the actual and calculated result.

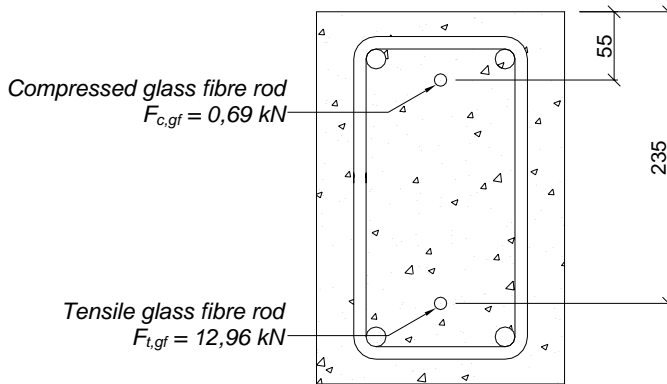


Figure 8-4. Beam cross section with glass fibre rod location and forces at yielding of tensile steel reinforcement.

The visual result is a wider and wider appearance of the load carrying capacity distributions further on in the life cycle, as can be seen in Figure 8-5. Failure loads obtained from failure load tests, which are adjusted with the increase in load carrying capacity of the glass fibre rods, are plotted in the graph as small circles. Each circle giving the failure load for beam at the certain stage of the life cycle. The average value for the intact beam, A , is calculated to 44,2 kNm.

After reduction of the contribution from the glass fibre rod, the actual beam failed at 48 kNm only 3,8 kNm higher than what the calculation suggested. The actual load carrying capacity for the repaired and strengthened beam, *F*, was 4,7 kNm higher than the calculated result. The corroded beam, *B*, and the repaired beam, *E*, had very good correspondence in between actual and calculated failure load.

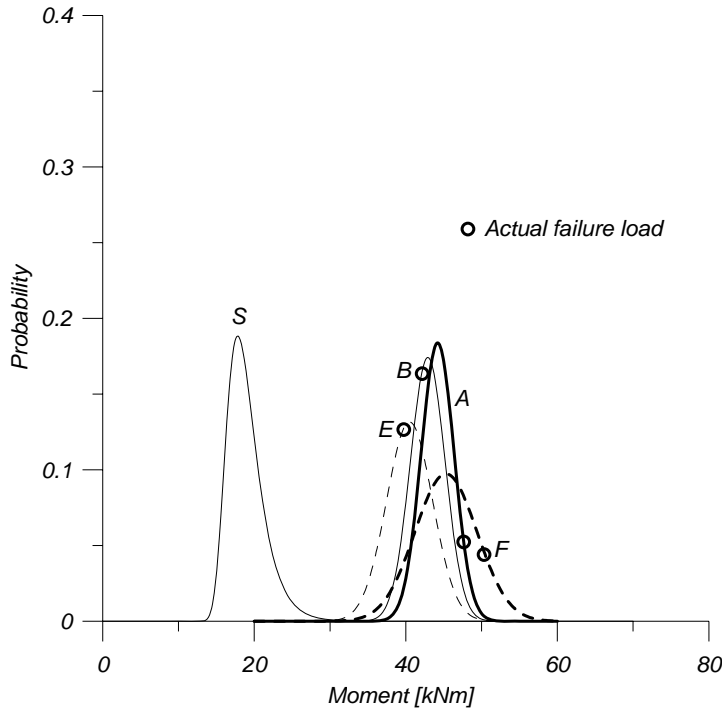


Figure 8-5. Load carrying capacity probability distribution plots for intact, corroded, repaired and repaired & strengthened beams, together with the load effect distribution.

Given the life cycle behaviour from section 7.3.2 and the distributions in Table 8-2, a 95% confidence interval is created and marked by the dotted lines in Figure 8-6. This gives an idea of the width of a 95% interval and presents an idea of the extent of the dispersion when testing the beams. When testing a great amount of beams, 95 % of them fall into this area of the load vs. deflection diagram, if the tested beams are considered as average beams. This consideration is however not fully true, since there is a difference between average value of the load carrying capacity distributions and tested results. The standard deviation is however not affected by this difference. Statistical verification was not possible since that requires a large number of beams.

The probability of failure is analysed using both FORM calculation as well as Monte Carlo simulation. In the software there are two methods when performing the Monte Carlo simulation, Crude or Importance Monte Carlo.

If the expected probability, p_f , is very small, less than 10^{-5} , the Crude Monte Carlo will not give reliable results. Therefore, simulation will be focused on regions where failure can be expected or the most contribution of the probability integral can be gained, as done in the Importance Monte Carlo (IMC). The IMC simulation is used in this example, since the expected probability at 10^{-6} for the intact and strengthened beam should be considered as very small.

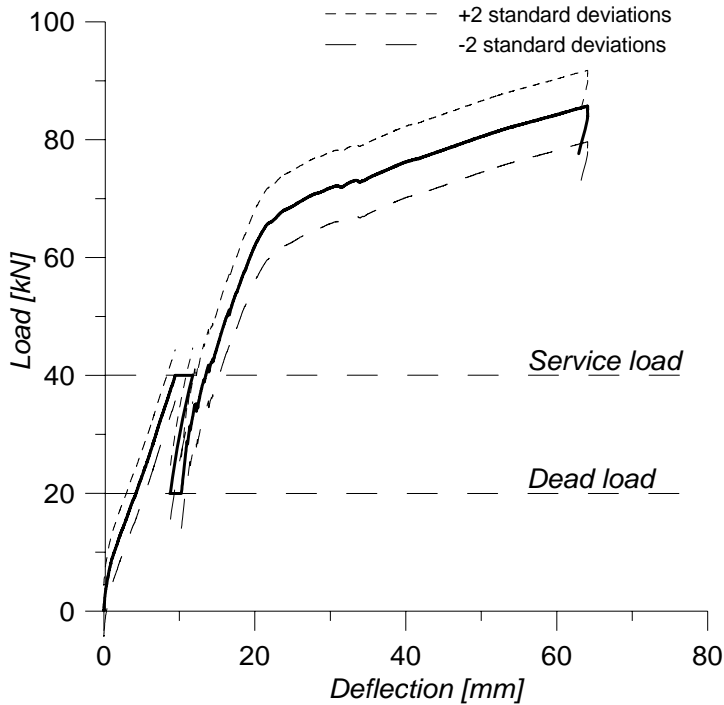


Figure 8-6. Dotted lines give the 95% confidence interval from the actual load vs. deflection behaviour during the life cycle.

This calculation example has shown that the probability of failure does actually change dramatically during the life cycle. Steel bar cross section reduction decreases the safety about 10 times. The decreased effective height, caused by removal of damaged concrete while the beam was loaded adds another decrease in safety by 10 times. By upgrading the beam by bonding of CFRP plate it is shown that the probability of failure is brought back up to the level of safety class 3 for this particular design of strengthening, see Table 8-3 for summarized results from the FORM calculations and the Monte Carlo simulation.

Table 8-3. Results from calculation of safety during the life cycle.

Beam	Cause of safety shift	β -index	FORM probability of failure, $\Phi(-\beta)$	MC probability of failure	Safety class
Intact	-	4,75	$1,0 \cdot 10^{-6}$	$0,6 \cdot 10^{-6}$	3
Corroded	Steel bar diameter reduction	4,60	$2,1 \cdot 10^{-6}$	$1,0 \cdot 10^{-6}$	~3
Repaired	Decreased effective height	4,34	$7,3 \cdot 10^{-6}$	$4 \cdot 10^{-6}$	~2
Strengthened	FRP plate bonding	4,80	$0,8 \cdot 10^{-6}$	$0,6 \cdot 10^{-6}$	3

8.4.2 Sensitivity factors α

Sensitivity factors, α , were investigated to verify the influence of the variations of different parameters. Deterministic parameters are not taken into consideration as the α -value equals zero for those. Table 8-4 shows that the variance for modulus of elasticity for steel and CFRP do not affect the results significantly, since the corresponding α -values are small. This could be claimed for the distance to compressed reinforcement, d'_s , as well. Yield stress of steel, f_{st} , and effective height, d_s , have α values separated from zero, indicating that the most likely value at failure for those parameters lies beneath the average value of the stochastic variable. The theory for this was presented in section 4.2.2.

Table 8-4. α -values for stochastic parameters for all stages in the life cycle.

Parameter	Beam	Intact	Corroded	Repaired	Repaired & strengthened
Load effect, S		0,96	0,96	0,96	0,96
Yield stress of steel, f_{st}		-0,25	-0,25	-0,25	-0,20
Effective height, d_s		-0,06	-0,05	-0,07	-0,18
Distance to compressed reinforcement, d'_s		0,05	0,05	0,06	0,04
Corroded steel cross section, $A_{s,c}$			-0,08	-0,7	-0,09
Stiffness of steel, E_s					0,003
Stiffness of CFRP, E_f					-0,02

9 Discussion and conclusions

9.1 Discussion

Both the experimental work as well as the probabilistic study shows the same intriguing result that the safety is clearly modified during the structural life. Corrosion damage reduces steel content and bond strength between steel and concrete. In addition, if the effective height is reduced during removal of damaged concrete under loading this might lead to a further decreased capacity.

The calculated life cycle behaviour estimated by the FE-analysis (Sand, 2001), is generally also obtained for the tested beam series. The intact beam was applied the service load, 40 kN. When corrosion occurred the bending stiffness of the concrete beam was decreased by 15% from 2980 kNm² down to 2530 kNm², due to a decreased steel mass content of 12%. Another reason for the decrease could be that the cover concrete became severely cracked due to the corrosion, which could result in a decreased stiffness. Consequently, the deflection during the corrosion stage increased, although the load was kept constant, giving the additional deflection which was also suggested by the FE-analysis. The load was reduced to dead load only, which was defined as 20 kN. The concrete beam bending stiffness decreased furthermore as cover concrete was removed. Effective height reduction and loss of bond between the concrete and the tensile reinforcing steel is coupled to this. The repaired beam did not reach up to the load carrying capacity of the intact beam. The load carrying capacity of the repaired and strengthened beam was slightly higher than the intact beam.

The repaired concrete beam specimen was weaker than the corroded beam when analysing the results from the failure test. This could mean that rehabilitation should be considered as a package consisting of a repair procedure together with strengthening. The primary goal of the repair procedure is to replace the deteriorated materials and minimize the deterioration rate. To increase the load carrying capacity strengthening is applied.

Another interesting aspect when repairing a structural member under loading is that an initial strain field exists. The initial strain field is not easy to monitor in any point in time, as it is already acting on the structure. This study has shown that it is possible to measure the existing strain field in laboratory conditions. Furthermore, the study verifies the hypothesis that it is important to estimate the existing strain field when the load carrying capacity is going to be calculated. Consider that material testing of steel reinforcing bar specimens resulted in a yield stress just above 3000 microstrains. The repaired beam failed by yielding of steel reinforcement at 65 kN when the strain readings from the failure test showed 1643 microstrains.

This is not even near the yield stress of the steel, but if taking the initial strain field into consideration another 1594 microstrains is added, which then results in a strain level that corresponds to the steel yielding strain.

Large cracks were formed in the repair mortar for all repaired beams. If considering the initial strain field and how the steel reinforcement will act during further loading, a possible explanation is given. The initial strain field produced a stress in the tensile steel reinforcement corresponding to 50% of the yield stress. The steel reached yielding much sooner after uploading than if the steel would have been unloaded. When yielding occurred and the steel started to behave non-linear, large forces arose in the surrounding repair mortar forming wide cracks.

An interesting finding from the stiffness measurement is that the LVDT setup and the FOS setup provided similar results. The general difference between these two methods is that the LVDT measures global stiffness, through global curvature, and the FOS measures local stiffness by studying strains in a specific cross section. It could be possible to use such monitoring technique to estimate the performance of an existing structure. This could perhaps be done by studying the change of the stiffness when loading the structure at moderate load levels. One possible way to utilize these techniques could also be to estimate the strain situation in the structure. Consider that the global curvature setup is mounted onto a real bridge. The measured curvature could, after some recorded results during a defined load, be translated into the slope of the strain distribution through the cross section of the structure. To determine the strain level a single strain gauge is required, suggestively on the compressed concrete or steel reinforcement, where reliable strain readings are obtained. When looking at the load vs. deflection graph for all tested beams there is no indication up to the service load that the corroded and repaired beam is deficient. In fact, these beams seem stiffer and sounder than the reference beam. This stiff behaviour is probably caused by the load history of the beam. The beam acts stiffer up to the service load level which it was subjected to during the corrosion phase.

The probabilistic evaluation shows that the safety is altered during the structure's life. The decrease in steel bar diameter increases the failure probability two times. The following repair procedure with a decreased effective height as a result decreases the safety down to safety class 2 in this example, with a failure probability seven times larger than the intact beam. The strengthening procedure is shown to improve safety back to safety class 3.

The performance during the life cycle is proposed to be described as presented in Figure 9-1. The performance of the degrading structure is described by an stochastic variable, $L1$, and the deterioration rate is described by slope, $dP1/dt$, of the performance graph. The repair procedure is performed at some point in time and the deterioration rate for the repaired structure, $dP2/dt$, is hopefully decreased and the ingoing materials upgraded. The performance of the repaired structure, $L2$, has probably a larger standard deviation compared to the degrading structure. Upgrading is performed when the probability of failure for the repaired beam, p_{f2} , exceeds a preset requirement.

The degrading rate of the repaired and strengthened structure is given by dP_3/dt . The performance is described by the stochastic variable L_3 and has a furthermore higher standard deviation than the degrading and the repaired structure. The structure is taken out of service when the probability failure for the repaired and strengthened structure, p_{f_3} , exceeds the requirement.

The deterioration rate could be estimated by taking material samples, using suitable monitoring techniques and carrying out visual inspections at two or more occasions. An approximation of the remaining time until upgrading should now be possible to calculate. Another interesting aspect would be to estimate where on the existing life cycle the structure is located.

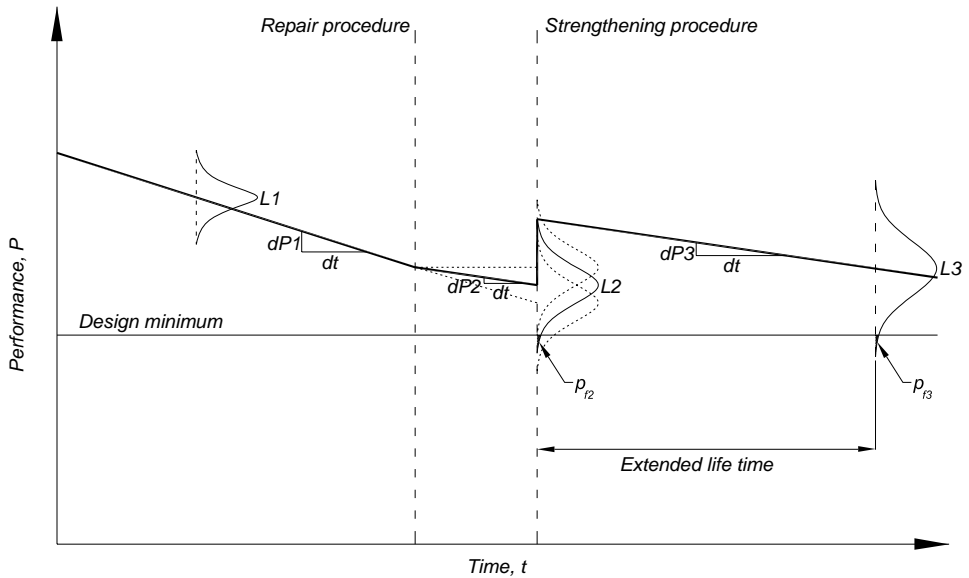


Figure 9-1. Diagram over the structural life described by performance, P .

Monitoring of stiffness during loading has shown to be a suitable measurement in the failure load test of this study. The results has illustrated that the stiffness graph could be divided into three regions principally presented in Figure 9-2. Those are the initial region where the concrete is uncracked, the intermediate region where cracks are formed and the critical region where the steel reinforcement yields. The stiffness is constant in the initial region. After that, the stiffness decreases during the intermediate region down to the new level of the final region.

The slope of the graph could be determined during load tests on the existing structure, and there is a possible relation between this measurement and the status of the structure. For example, if the stiffness gradient, dEI/dL , is linear in the load interval it is assumed that the performance of the structure is in the intermediate region. Another

case would be if the gradient of the stiffness is decreasing and the performance of the structure is assumed to be in the critical region.

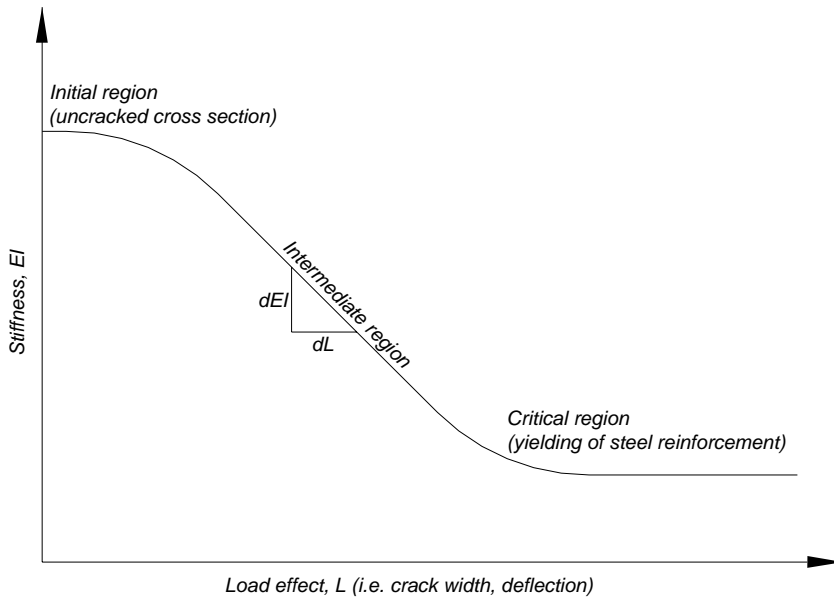


Figure 9-2. General stiffness development of reinforced concrete member loaded in bending based on test results from this study.

9.2 Conclusions

The research questions given in section 1.1 are answered one by one below.

- How do existing loads during repair and strengthening affect the structure?

The research carried out and presented in this thesis clearly shows that the repaired structural concrete member is affected by an existing strain field, and this could severely decrease the load carrying capacity.

- Does the stiffness of the structural member decrease due to deterioration issues?

The test shows that the stiffness of the structural member is heavily affected by steel corrosion. The test has shown that strengthening increased the bending stiffness. This conclusion is based on both local and global stiffness measurements.

- How can the load carrying capacity be determined by a probabilistic approach?

A probabilistic evaluation is a very strong tool in estimating the load carrying capacity of deteriorated, repaired and strengthened concrete structures. This has also been shown in this study.

10 Suggestions for future work

The concept of estimating the load carrying capacity with a probabilistic approach is a powerful tool. Further study of the statistical properties of strengthening in terms of material and anchorage is necessary. Further investigation regarding ductility of steel in combination with corrosion is interesting, especially since the repair procedure of the steel reinforcement generally only reaches blasting or brushing to get rid of corrosion products. FE-analysis of the life cycle behaviour is needed to extrapolate measurement data.

It is necessary to establish understanding and techniques to get information about the existing strain field in the structure at a particular load level. This is of outmost important when considering that it is impossible to draw any conclusions regarding the strain or stress situation if attaching a strain sensor onto a structure, without knowing the condition before it was attached. This is especially important and hard for large structures where large scale effects, such as temperature load, are acting.

The current study was finished in the stage where the structure was strengthened. Further study of the strengthened structure as it meets the remaining service life is left to explore, i.e. deterioration mechanisms, long-term effects of strengthening in combination to deterioration etc.

Further study is required into what happens when steel yields soon after the CFRP plate is applied, in the case where the existing strain field is significant. One aspect could be to study if stress concentrations around large cracks are formed in the strengthening material.

The concept of evaluating stiffness gradient during uploading could become a tool to estimate the current status of an existing structure. This technique could in combination with long term monitoring, probabilistic evaluation, material testing and visual inspection serve as a toolbox to assess the structural performance. Interesting questions which are to be asked and answered through the toolbox could be:

- What is the current status of the structure?
- How fast does the performance decrease?
- Which are the mechanisms that produce the performance loss, and how could they be reduced?
- How much time remains until repair and/or strengthening has to be performed?

References

Cited references

Addis, B.J., 1986; *“Fulton’s concrete technology. 6th edition”*. Halfway House, South Africa: Portland Cement Institute, 1986.

Andersson, B. & Spett, M., 2002; *“Betongbalkar förstärkta med kolfiberkomposit, en studie av förankringslängder”*. Examensarbete 2002:217 CIV, Avdelningen för konstruktionsteknik, Luleå tekniska universitet, Luleå. ISRN: LTU-EX--02/217--SE

Andrade, C.; Alonso, C. & Molina, F.J., 1993; *“Cover cracking as function of bar corrosion”*. Part 1: experimental tests. *Materials and structures*, 26: 453-464.

Anoop, M.B.; Balaji Rao K. & Appa Rao T.V.S.R, 2003; *“A methodology for durability-based service life design of reinforced concrete flexural members”*, Structural Engineering Research Centre, CSIR Campus, Magazine of Concrete Research, 2003, 55, No. 3, June, 289-303.

Arntsen, B., 2004; *“Akselererte korrosjonsforsøk, forslag til gjennomføring”*. Norut Teknologi AS, Narvik, Norway.

Austin, S.A.; Lyons, R. & Ing M.J.; *“Electromechanical behaviour of steel-reinforced concrete during accelerated corrosion testing”*. *Corrosion*; Feb 2004; 60; 2; ProQuest Science Journals, pg. 203.

Ball, C, 2000; *“Corrosion mitigation strategies for FRP composite strengthening systems”*. Vector corrosion Technologies, Inc. Presented at ACI Fall convention, Toronto 2000.

Ballim, Y. & Reid, J.C., 2003; *“Reinforcement corrosion and the deflection of RC beams – an experimental critique of current test methods”*. *Cement & Concrete Composites* 25; 2003; Elsevier; p. 625-632.

Beeby, A.W., 1983; *“Cracking, cover and corrosion of reinforcement”*, *concrete international*, 5(2): 35-40

Belleville, C. & Duplain, G., 1993; "*White light interferometric multimode fiber-optic strain sensor*". Optics Letters, 18(1): 78-80. Canadian Civil Engineer. 1999 16(2): 9-20

Bergström, S-G., 1955; "*Frys försök med cementbruk*". CBI meddelande nr 32, Stockholm, 1955.

Cadei, J. & Holloway, L C., 2002, "*Progress in the technique of upgrading metallic structures with advanced polymer composites*". Prog. Struct. Engng. Mater. 2002; 4; s. 131-148.

Camitz, G. & Pettersson, K., 1989; "*Korrosionsskydd av stål ingjutet i betong – etapp 1. Katodiskt korrosionsskydd av stålarmering i betongkonstruktioner – litteraturundersökning*". Cement och Betonginstitutet, CBI särtryck 3:90, ISSN 1101-1297.

Carolin, A., 2003; "*Carbon fibre reinforced polymers for strengthening of structural elements*". Division of structural engineering, Luleå University of Technology, Doctoral Thesis 2003:18, ISBN: 91-89580-04-4.

Carolin, A., Täljsten, B., Nilsson, M., Enochsson, O., Fahleson, C., 2004; "*Tillförlitlighetsanalys för reparerade eller förstärkta byggnadskonstruktioner*". Technical report 2004:09, Luleå University of Technology, Division of Structural Engineering, Department of Civil and Mining Engineering. ISSN: 1402-1536, p. 66

Castellani, A. and Coronelli, D., 1999; "*Beams with corroded reinforcement: Evaluation of the effects of cross-section losses and bond deterioration by finite element analysis*". Structural Faults and Repair, 8th International Conference on Extending the Life of Bridges, Civil and Building structures, London, 1999.

Chaallal, O.; Nollet, M-J & Perraton, D, 1998; "*Strengthening of reinforced concrete beams with externally bonded fibre-reinforced-plastic plates: design guidelines for shear and flexur*", Canadian Journal of Civil Engineering; Aug 1998; 25, 4; ProQuest Science Journals

Choquet, P. & Leroux, R.; Juneau, F., 1997; "*New Fabry-Perot fibre-optic sensors for structural and geotechnical monitoring applications*". Proceedings of the 75th annual meeting of the NRC transportation research board, Structural and Geotechnical applications for fibre-optic sensors, Washington, D.C., paper 97-0645.

Comite Euro-International du Beton: "*CEB-FIP Model Code 1990*", Thomas Telford, London, 1993.

DeMerchant, M.; Brown, A.; Smith, J.; Bao, X. & Bremner, T., 2000; "*Distributed strain sensing for structural monitoring applications*", Canadian Journal of Civil Engineering; Oct 2000; 27, 5; ProQuest Science Journals, pg. 873

- Djordjevich, A.; Fung, M. & Fung, Richard Y K., 2001: "*Principles of deflection-curvature measurement*". City university of Hong Kong, Measurement Science and Technology, 12 (2001) 1983-1989.
- Fagerlund, G., 1986: "'Tåta' betonger är ingen garanti för frostbeständighet". Cementa CM rapport T 96093, 1986.
- Fagerlund, G., 1992; "*Betongkonstruktioners beständighet – en översikt*". ISBN 91-87334-00-3. AW Grafiska, Uppsala 1992. Tredje upplagan.
- Hansson, C.M.; Frolund Th. & Markussen, J.B., 1985; Cem. Concr. Res. 15; p. 65
- Hearn, N. & Aiello J., 1998; "*Effect of mechanical restraint on the rate of corrosion in concrete*", Canadian Journal of Civil Engineering; Feb 1998; 25, 1; ProQuest Science Journals pg. 81
- Hearn, N., 1996; "*On the corrosion of steel reinforcement in concrete*", proceedings of the 1st Structural Speciality Conference, Canadian Society for Civil Engineering, Edmonton, Alta., Vol. 1, pp. 763-774
- Hejll, A., Huth, O., Feltrin, G. & Motavalli, M., 2004; "*Damage detection of a large-scale 38-years-old prestressed RC bridge girder*". EMPA, Structural Engineering Research Laboratory, Dübendorf, Switzerland. Luleå University of Technology, Division of Structural Engineering, Luleå, Sweden.
- Hejll, A. & Norling, O., 2001; "*Betongbalkar förstärkta med kolfiberkomposit – dynamisk belastning under limmets härdningsförlopp*". Master thesis, Luleå University of Technology, Division of Structural Engineering, Department of Civil and Mining Engineering.
- Hollaway, L.C. & Leeming, M.B., 1999; "*Strengthening of Reinforced Concrete Structures*". Woodhead Publishing Limited. ISBN: 1-85573-378-1.
- Horiguchi, T.; Kurashima, T. & Tateda, M., 1989; "*Tensile strain dependence of Brillouin frequency shift in silica optical fibers*". Photonics Technology Letters, 1: 107-108
- Horrigmoe, G. and Sæter, I., 2006; "*Sustainable bridges – Specifications for Finite Element Modelling of Reinforced Concrete Structures Attacked by Corrosion, D3.10-S: Laboratory investigations of steel bar corrosion in concrete*". Norut Teknologi AS, Norway.
- Horrigmoe, G., 1998; "*Future needs in concrete repair technology*". NORUT Teknologi A.S., Narvik, Norway. International workshop on "Concrete Technology for a Sustainable Development in the 21 Century", Svolvær, Norway, June 24-27, 1998.

JCSS PMC, 1999; *"Probabilistic Model Code, Issued by the Joint Committee on Structural Safety, JCSS"*. 12th draft, March 2001. 1. Basis of Design, 62 pp; 2. Load Models, 73 pp; 3. Material properties, 43 pp. Available in full text on

Johansson, T., 2005; *"Strengthening of concrete structures by Mineral Based Composites"*. Technical report 2005:10, Division of Structural Engineering, Department of Civil and Mining Engineering, Luleå University of Technology, Sweden. ISSN: 1402-1528.

Kalamkarov, A.L. & Georgiades, A.V.; MacDonald, D.O.; Fitzgerald, S.B., 2000; *"Pultruded fibre reinforced polymer reinforcements with embedded fibre optic sensors"*, Canadian Journal of Civil Engineering; Oct 2000; 27, 5; ProQuest Science Journals

Karbhari, V. M., 1996; *"Civil infrastructure and composite materials: issues in material and manufacturing"*. 41st International SAMPE Symposium and Exhibition, March 24-28, 1996. V 41, pp 656-666.

Larsson, T., 2006; *"Material and fatigue properties of old metal bridges"*. Licentiate thesis 2006:26, Luleå University of Technology, Luleå, Sweden. ISSN: 1402-1757.

Lee, C.; Bonacci, J.F.; Thomas, M.D.A.; Maalej, M. et al, 2000; *"Accelerated corrosion and repair of reinforced concrete columns using carbon fibre reinforced polymer sheets"*, Canadian Journal of Civil Engineering; Oct 2000; 27, 5; ProQuest Science Journals pg. 941

Lee, H.S.; Tomosawa, F.; Masuda, Y. & Kage, T., 1997; *"Effect of CFRP sheets on flexural strengthening of RC beams damaged by corrosion of tension rebar. Proceeding of the Third International Symposium on Non-Metallic (FRP) Reinforcement for Concrete Structures"*, Sapporo, Japan, 1: 435-442

Li, X; Johnsen, J; Groza, J. & Prinz, F, 2002; *"Processing and microstructures of fibre bragg grating sensors embedded in stainless steel"*. Metallurgical and Materials Transactions; Sep 2002; 33A, 9; ProQuest Science Journals

Maaddawy, T.E. & Soudki, K., 2005; *"Carbon-fiber-reinforced polymer to extend service life of corroded reinforced concrete beams"*. Journal of Composites for Construction, vol. 9, no. 2, p. 187-194.

MacInnes, D.A., 1939; *"The principles of electrochemistry"*. New York: Reinold Publishing Corporation; 1939, p. 39

Mangat, P.S. & Molloy, B.T., 1992; Mater. Struct. 25; pg. 404

"Marina betongkonstruktioners livslängd – sammanfattning av seminarier hösten 1993", s. 24.

Mays, G.C. & Barnes, R.A., 1996; *"The structural effectiveness of large volume patch repairs to concrete structures"*. Proc. Instn Civ. Engrs Structs & Bldgs, 1995, 110, Nov., 351-360.

- Noghabai, K., 1998; “*Effect of Tension Softening on the Performance of Concrete Structures*”. Luleå University of Technology, Department of Civil and Mining Engineering. Doctoral thesis, 1998:21. ISSN: 1402-1544.
- Nordin, H., 2003; “*Fibre reinforced polymers in civil engineering: flexural strengthening of concrete structures with prestressed near surface mounted CFRP rods*”. Luleå University of Technology, Licentiate thesis 2003:25, ISSN: 1402-1757.
- Pourbaix, M., 1996; “*Atlas of electrochemical equilibrium in aqueous solutions*”, translated from French by J.A. Franklin (New York, NY: Pergamon Press. 1996), p. 409-410
- Reid, M., 1998; “*Opt. eng.*”, vol. 37(1), p. 237
- Rodriguez, J., Ortega, L. M., Garcia, A. M., 1994; “*Corrosion of reinforcing bars and service life of reinforced concrete: Corrosion and bond deterioration*”. International Conference Concrete across borders, Odense, Denmark, 1994.
- Rodriguez, J.; Ortega L.M. & Gracia, A.M, 1994; “*Assessment of structural elements with corroded reinforcement*”. In: Swami RN, editor. Corrosion and corrosion protection of steel in concrete. Sheffield: Sheffield Academic Press; 1994. p. 171-185.
- Sand, B., 2001; “*Nonlinear finite element analysis of deteriorated and repaired RC beams*”. NORUT Teknologi AS, Narvik, Norway.
- Sherwood, E.G. & Soudki, K.A., 1999a; “*Rehabilitation of corrosion damaged concrete beams with CFRP laminates – A pilot study*”, composites part B: Engineering (in press)
- Sherwood, T. & Soudki, K.A., 1999b; “*Confinement of corrosion cracking in reinforced concrete beams with carbon fibre reinforced polymers laminates*”, ACI-SP-188 on Non-Metallic (FRP) Reinforcement for Concrete, pp. 591-603
- Soudki, K.A. & Sherwood, T., 2000; “*Behaviour of reinforced concrete beams strengthened with carbon fibre reinforced polymer laminates subjected to corrosion damage*”, Canadian Journal of Civil Engineering; Oct 2000; 27, 5; ProQuest Science Journals, pg. 1005
- Soudki, K.A., 1999; “*Effects on CFRP wrapping on the bond strength of corroded steel reinforcing bars*”, American Concrete Institute Spring Convention, Chicago, Illinois.
- Thoft-Christensen, P., Baker, M.J., 1982; “*Structural Reliability Theory and Its Applications*”. Springer-Verlag Berlin, Heidelberg, New York. ISBN 3-540-11731-8.
- Tuutti, K., 1982; “*Corrosion of steel in concrete*”. Stockholm : Cement- och betonginst., 1982, p. 468

Täljsten, B., 2000, “Förstärkning av befintliga betongkonstruktioner med kolfiberväv eller kolfiberlaminat. Dimensionering, material och utförande”. Technical report 2000-16. Department of structural engineering, Luleå University of Technology, Luleå. ISSN: 1402-1536.

Täljsten, B., 2004; “FRP strengthening of existing structures, design guidelines”. Luleå University of Technology; 2002; ISBN 91-89580-03-6

Tørten, A. and Horrigmoe, G., 1999; “Modelling bond between reinforcement and concrete in deteriorated and repaired beams (in Norway)”. Report NTAS A98034, NORUT Teknologi AS, Narvik, Norway.

Uomoto, T.; Tsuji, K. & Kakizawa T., 1984; “Deterioration mechanism of concrete structures caused by corrosion of reinforcing bars”, transactions of the Jaman Concrete Institute, 6: 163-170

Utsi, S., 2002; “Optical fibre sensors for use in civil engineering structures – a review of literature”. Luleå University of Technology, Department of Civil and Mining Engineering. Technical report, 2002: 11. ISSN: 1402-1536.

Schneider, J., 1997; “Introduction to Safety and Reliability of Structures”. International Association for Bridge and Structural Engineering, IABSE, Zürich.

Simiu, E., Heckert, N.A., Filliben, J.J., Johnson, S.K., 2001; “Extreme wind load estimates based on Gumbel distribution of dynamic pressure: an assessment”. National Institute of Standards and Technology, Gaithersburg, MD 20899 USA. Structural Safety, Vol. 23, No. 3, 221-229, 2001.

Internet references

The Swedish Road Administration website, www.vv.se, 2006-06-07

Petschacher Software and Project, Ltd., <http://www.petschacher.at/>, 2006-09-01.

Appendix A – Material properties

Table A1. Steel reinforcement and FRP material properties. μ is mean value and σ standard deviation for each property.

Material Parameter	Steel Ks500 ($\phi 16$ mm)		Corroded steel Ks500 ($\phi 15,1$ mm)		Glass fibre ($\phi 10$ mm)		StoFRP Plate E50C ($50 \times 1,4$ mm)	
	5 specimens		3 specimens		μ	σ	20 specimens	
	μ	σ	μ	σ	μ	σ	μ	σ
Ultimate strength [kN]	122,1	1,2	115,5	6,2	79	12,6	-	-
Yield stress [MPa]	514	6,2	588**	35	1007*	161	1860*	122
Yield strain [%]	0,39	0,008	0,43	0,05	-	-	-	-
Ultimate strain [%]	22,5	2,6	9,3	1,3	1,9	0,06	1,20	0,08
Modulus of elasticity [GPa]	186,7	11,0	138,9	17,4	55,70	1,2	150	2,6

* Fibre materials do not have a defined yield stress. Instead, the given value is stress at failure.

** Stress calculated by using the average steel bar diameter of 15,1 mm.

- No information.

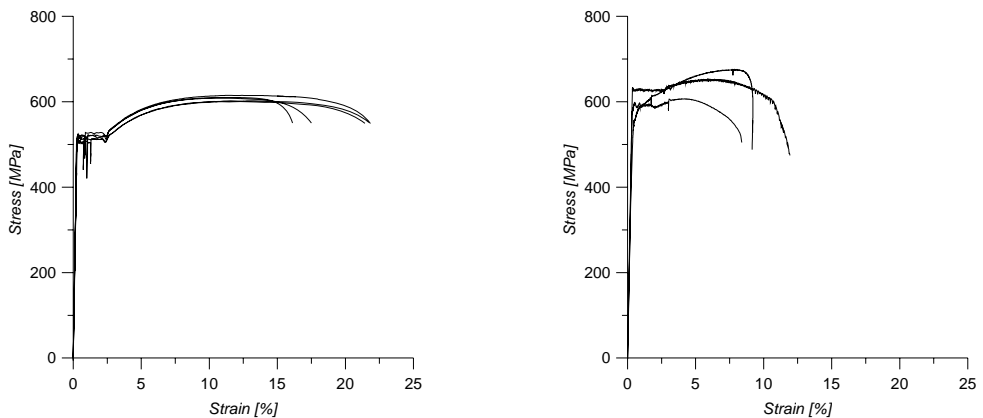


Figure A1. Left: Stress vs. strain diagram for undamaged Ks500 $\phi 16$ mm steel reinforcement. Right: Stress vs. strain diagram for corroded Ks500 steel reinforcement.

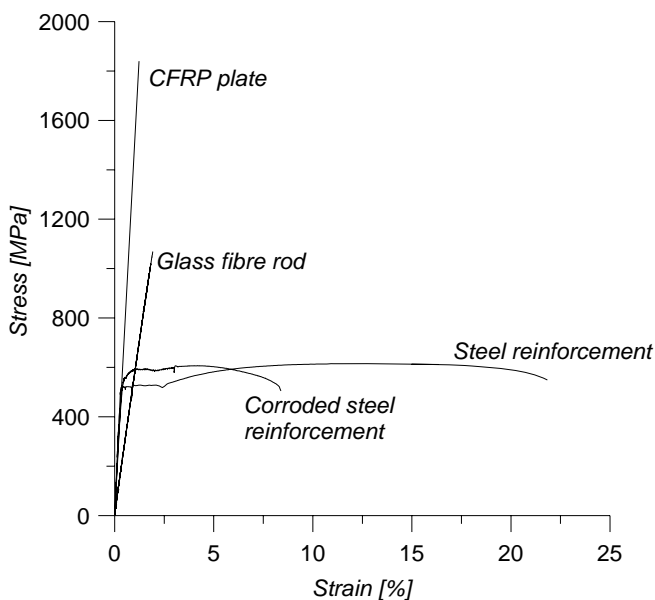


Figure A2. Comparison between stress versus strain curves for non-corroded Ks600 $\phi 16$ mm steel bar specimen used for tensile bending reinforcement, corroded steel reinforcement, glass fibre rod and CFRP plate.

Table A2. Concrete and repair mortar properties. All beams were cast of concrete from the same batch. Repair mortar properties are the same for all repaired beam.

Parameter	Material	Concrete, C28/32 (6 split+6 compress)		Repair mortar, StoCrete GM1 (3 split+3compress)	
		μ	σ	μ	σ
Compressive strength [MPa]		64,9	1,8	65,0	1,3
Tensile strength [MPa]		4,3	0,3	3,9	0,1
Density [kg/m ³]		2370	14,8	2227	6,9
Maximum aggregate size [mm]		16		2	
Date for casting		2005-10-31		2006-03-30	
Date for cube test (during failure test of beam specimens)		2006-06-14		2006-06-14	

Table A3. Material properties for StoBPE Lim 465/464 (A+B) and StoBPE Primer 50 Super, used as the strengthening system to bond CFRP plate onto the repaired beam.

<i>Parameter</i>	<i>Material</i>	<i>StoBPE Lim 465/464 (A+B)</i>	<i>StoBPE Primer 50 Super</i>
<i>Flexural strength [MPa]</i>		42,1	
<i>Flexural modulus of elasticity [Gpa]</i>		4,4	
<i>Shear strength [Mpa]</i>		87,1	
<i>Pot life [min]</i>		58	
<i>Modulus of elasticity [GPa]</i>		7,45	
<i>Glass transition temperature [°C]</i>		47	
<i>Coefficient of thermal expansion[m/mK·10⁶]</i>		53,8±0,6	
<i>Linear shrinkage [%]</i>		0,07	
<i>Adhesiveness to concrete [MPa]</i>			17

Table A4. Material properties for StoBPE Lim 417 (A+B) used to protect stirrups from corrosion.

<i>Parameter</i>	<i>Material</i>	<i>StoBPE Lim 417 (A+B)</i>
<i>Tensile strength [MPa]</i>		50
<i>Tensile shear modulus [MPa]</i>		17,6
<i>Compressive strength [MPa]</i>		80
<i>Ultimate strain [%]</i>		3
<i>Pot life 100 g @ 20 °C [min]</i>		30
<i>Modulus of elasticity [GPa]</i>		2

Appendix B.1 – Intact beam (A)

Beam dimensions

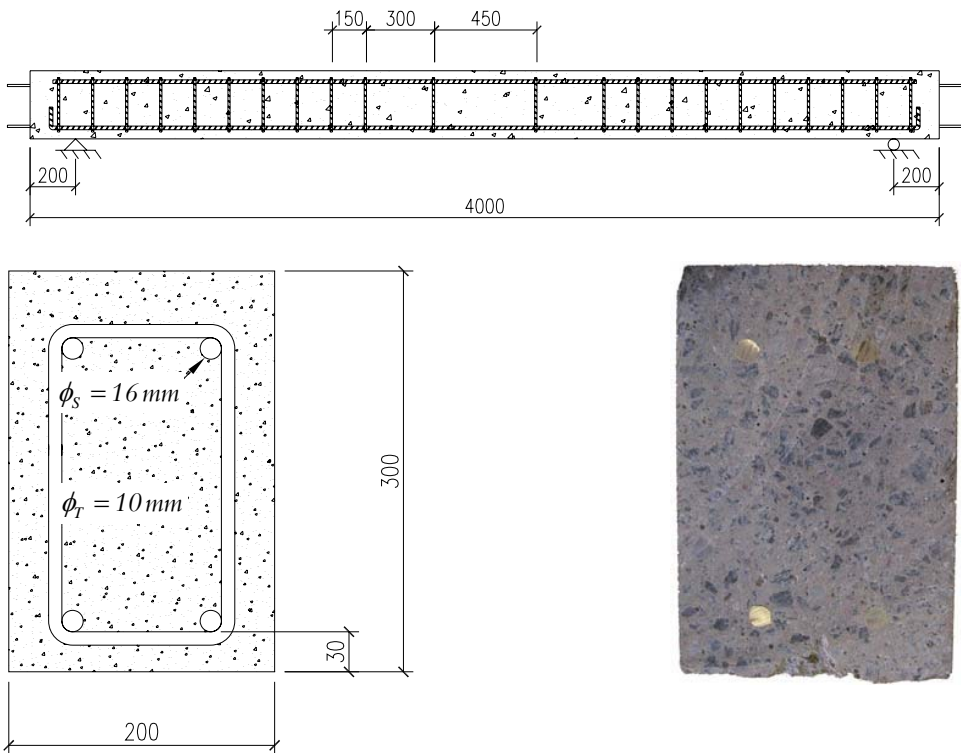


Figure A3. Top: Beam specimen measurements and steel reinforcement layout. Bottom left: Cross sectional view of intact beam. Bottom right: Cross section of real intact beam.

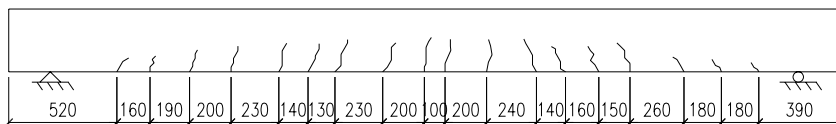


Figure A4. Longitudinal view of intact beam with crack pattern after failure load test.

Monitoring – Corrosion stage

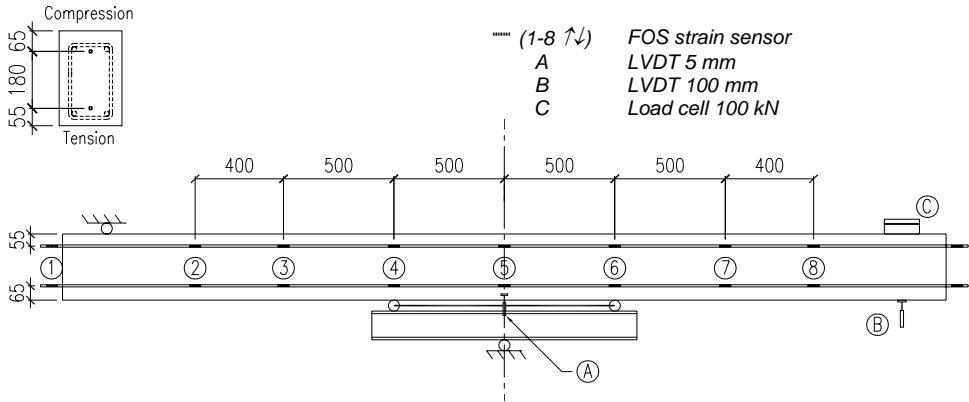


Figure A5. Sensor locations and sensor type on the intact beam specimen during corrosion stage. FOS are located along the glass fibre rods.

Monitoring – Failure test

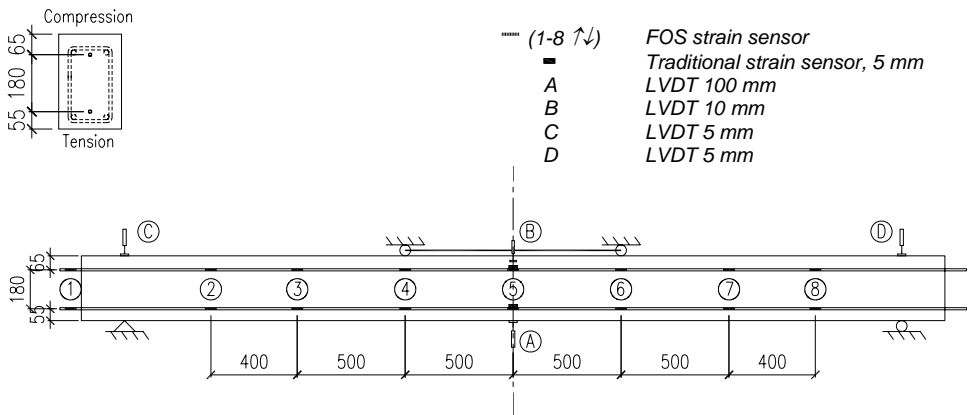


Figure A6. Sensor locations and sensor type on the intact beam specimen. FOS and traditional strain sensors are located along the glass fibre rods.

Results

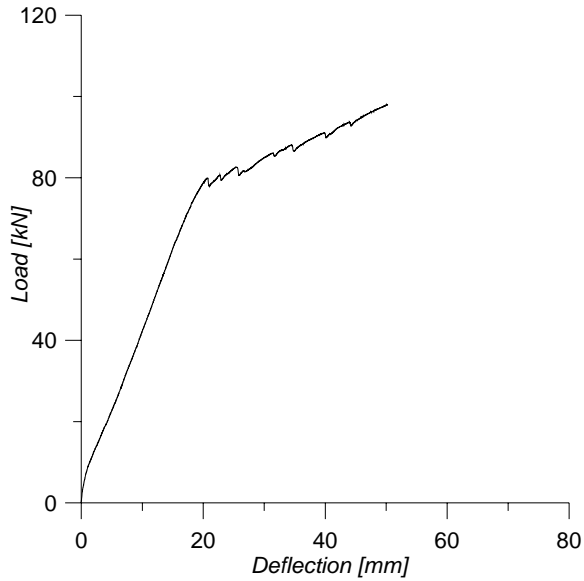


Figure A7. Load vs. deflection relation for intact beam.

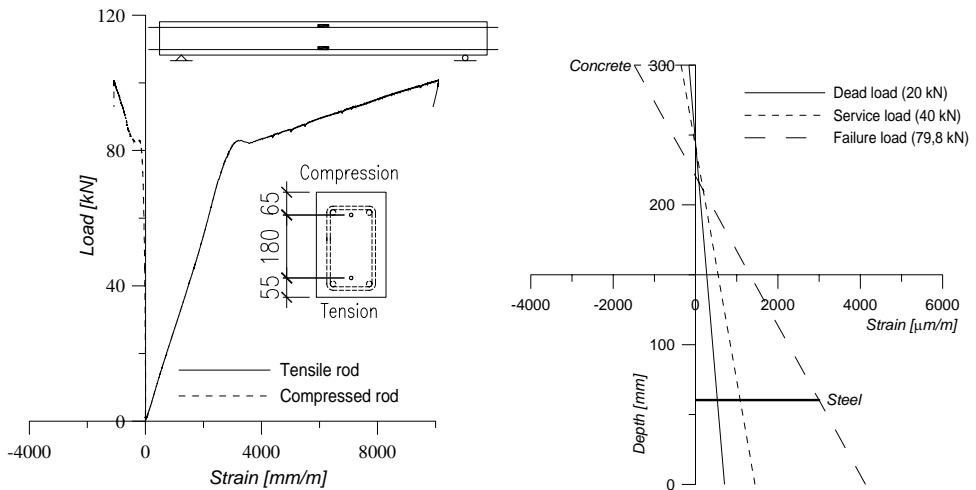


Figure A8. Left: Strain readings on tensile and compressed glass fibre rod. Right: Mid-span strain distribution between tensile steel reinforcement and compressed concrete surface.

Table A5. Crack width measurement during failure load test of intact beam indicates that maximum crack width with respect to serviceability occurs between 40 and 45 kN.

<i>Load</i>	<i>Average crack width</i>	<i>Number of cracks</i>
0		
5		
10		
15	0.05	4
20	0.08	6
25	0.10	13
30	0.15	13
35	0.17	15
<u>40</u>	<u>0.18</u>	<u>17</u>
<u>45</u>	<u>0.21</u>	<u>17</u>
50	0.26	17
55	0.28	18
65	0.34	18

Appendix B.2 – Corroded beam (B)

1. Corrosion was initiated the day after beam casting using electrolyte with high chloride concentration and high corrosion driving current.
2. Beams were left hardening for 28 days.
3. Beams were mounted into the rigs and loaded for 20 days without any further corrosion.
4. Long time accelerated corrosion was applied.
5. Beams were considered corroded after 75 days and the accelerated corrosion process was stopped.

Beam dimensions

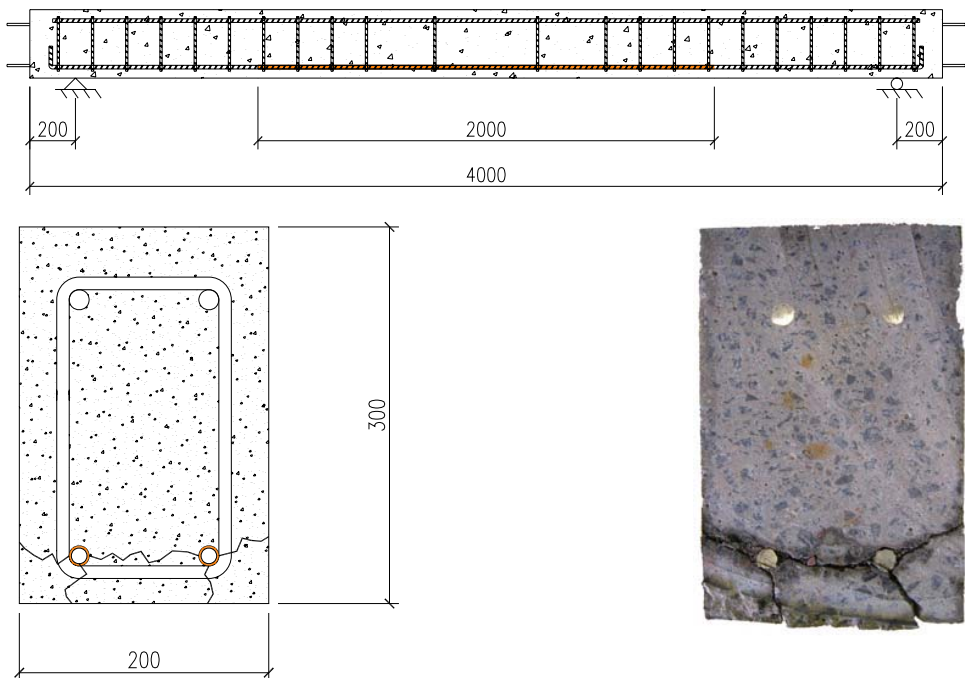


Figure A9. Top: Beam specimen measurements and steel reinforcement layout. Bottom left: Cross sectional view of corroded beam. Bottom right: Cross section of real corroded beam.

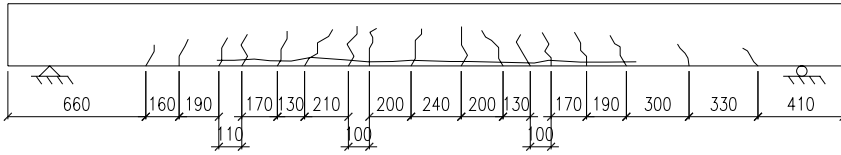


Figure A10. Longitudinal view of corroded beam with crack pattern after failure load test.

Monitoring – Corrosion stage

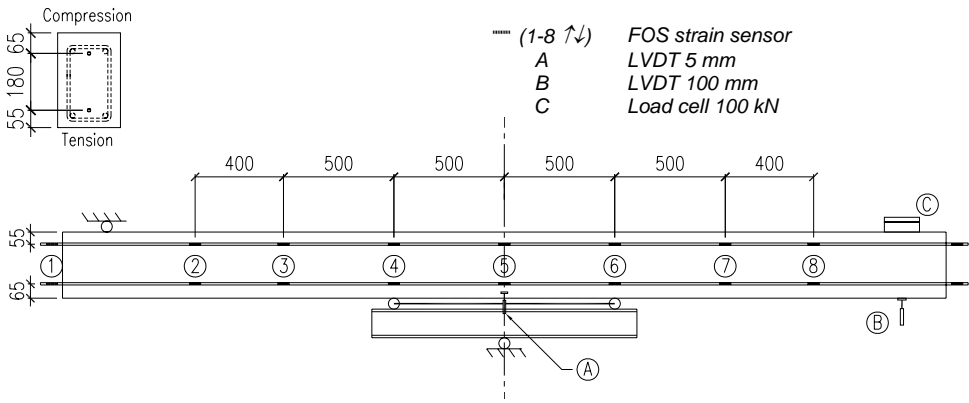


Figure A11. Sensor locations and sensor type on the intact beam specimen during corrosion stage. FOS are located along the glass fibre rods.

Monitoring – Failure load test

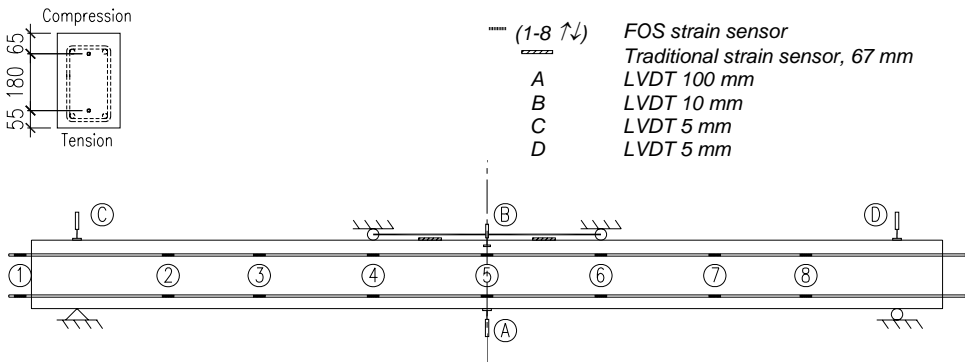


Figure A12. Sensor locations and sensor type on the corroded beam specimen. FOS and traditional strain sensors are located along the glass fibre rods.

Results

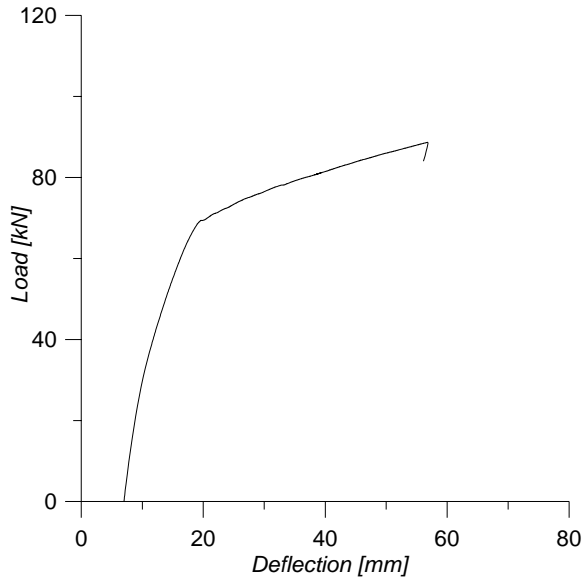


Figure A13. Load vs. deflection relation for corroded beam.

Table A6. Data regarding corrosion initiation.

	Value	Comment
Chloride concentration in electrolyte	10%	Very high concentration (chloride/water) to be sure that this would not interfere with the initiation.
Applied current	1-1,3 A	This current was applied until a negative potential between the concrete surface and steel reinforcement turned negative when the applied current was switched off. As soon as the potential was found negative the initiation process was quickly aborted, since the deterioration process was heavily accelerated in this stage.
Initiation duration	9 days	The potential between the concrete surface and each of the reinforcing bars were negative after 9 days, and the reinforcing bars were considered as de-passivated. Further corrosion was created under loading in test rig.

Table A7. Information regarding the corrosion stage.

<i>Chloride concentration in electrolyte</i>	3%	<i>Pure sodium chloride was used with concentration given in weight percentage.</i>
<i>Applied current density</i>	0.10 mA/cm ²	<i>The absolute value of the applied current is given by multiplying the surface area of the steel bars attacked by corrosion.</i>
<i>Corrosion duration</i>	75 days	<i>Concrete kept wet using construction isolation material.</i>
<i>Degree of corrosion (% mass loss)</i>	B1: 9,8 B2: 8,6	

Table A8. Applied load during corrosion and rehabilitation phase for beam B1 and B2.

	<i>Service load during corrosion</i>		<i>Dead load during rehabilitation</i>	
	<i>Mean value</i>	<i>Standard deviation</i>	<i>Mean value</i>	<i>Standard deviation</i>
<i>B1</i>	40,2	1,0	22,0	2,3
<i>B2</i>	41,7	0,6	25,4	1,4

Appendix B.3 – Beam where cover concrete was removed (D)

1. Cover concrete was removed to a depth of 50 mm, using a jack hammer, along the full length of the corroded steel reinforcement region.
2. Corroded steel reinforcement was brushed by steel brush before casting of repair mortar. Pressurized air was used to get rid of concrete left over on the beams.

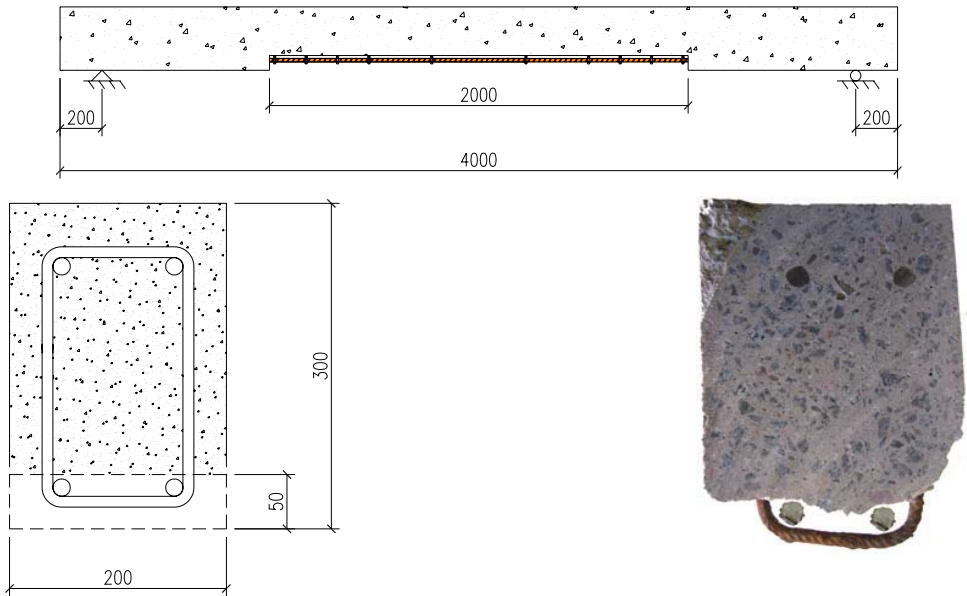


Figure A14. Top: Beam specimen measurements and steel reinforcement layout. Bottom left: Cross sectional view of beam where cover concrete was removed. Bottom right: Cross section of real beam where cover concrete was removed.

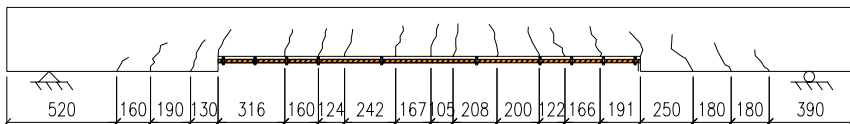


Figure A15. Crack pattern of beam where cover concrete was removed after failure load test.

Monitoring – Corrosion stage

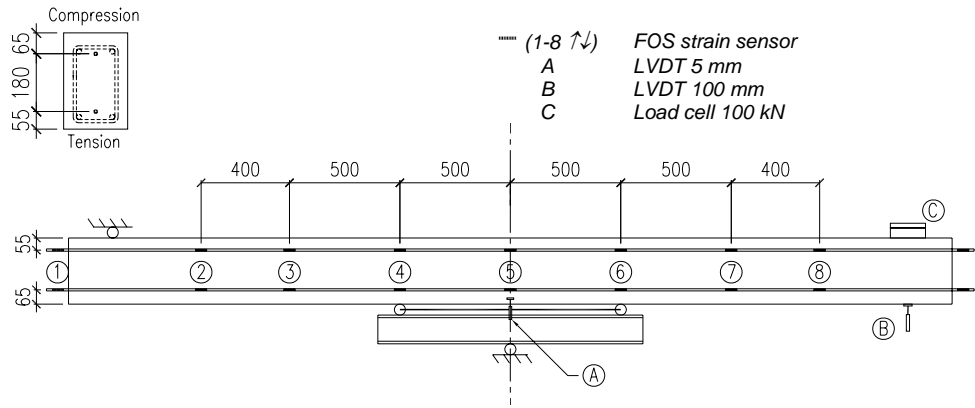


Figure A16. Sensor locations and sensor type on the intact beam specimen during corrosion stage. FOS are located along the glass fibre rods.

Monitoring – Failure load test

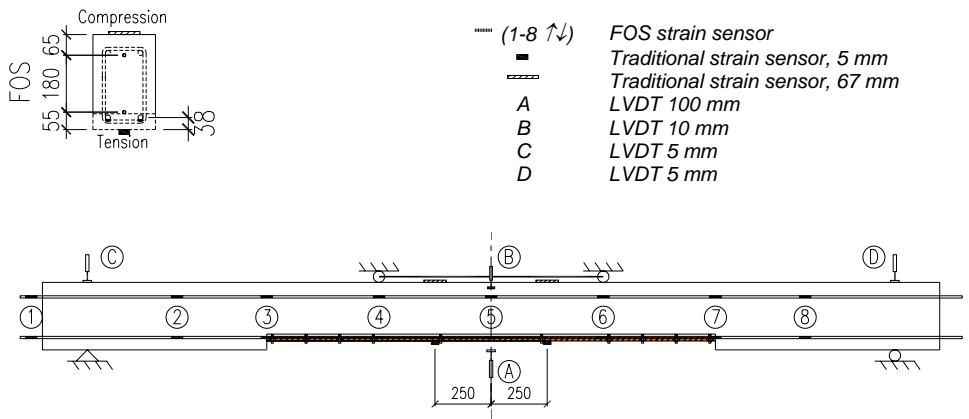


Figure A17. Sensor locations and sensor type on the beam where cover concrete was removed. FOS are located along the glass fibre rods. Traditional strain gauges are located on the concrete surface and onto tensile steel reinforcement.

Results

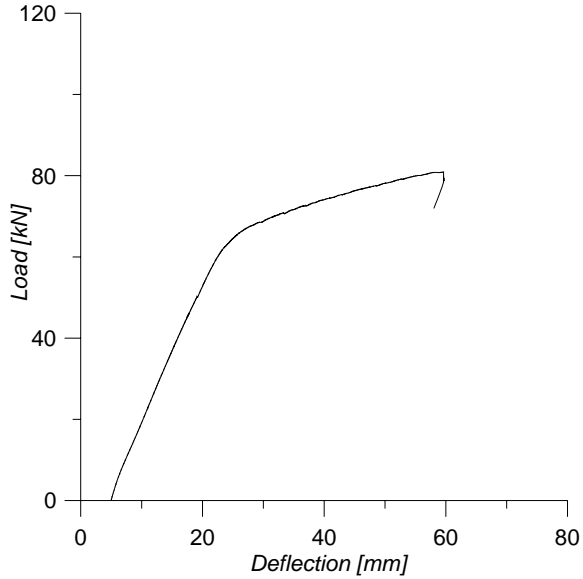


Figure A18. Load vs. deflection relation for beam where cover concrete is removed.

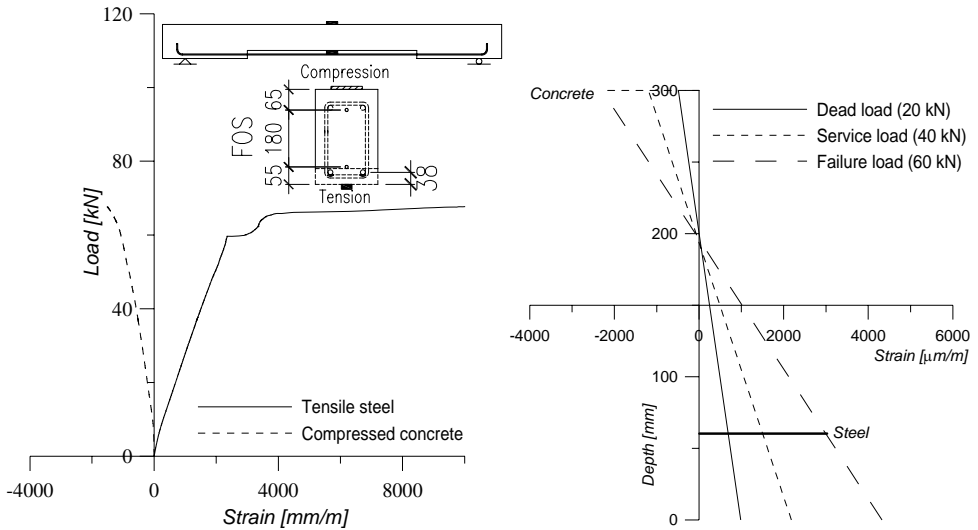


Figure A19. Left: Strain readings on tensile steel reinforcement and compressed concrete on beam where cover concrete is removed. Right: Strain distribution between tensile steel reinforcement and compressed concrete surface.

Table A9. Applied load during corrosion and rehabilitation phase for beam D.

	<i>Service load during corrosion</i>		<i>Dead load during rehabilitation</i>	
	<i>Mean value</i>	<i>Standard deviation</i>	<i>Mean value</i>	<i>Standard deviation</i>
<i>D</i>	<i>40,2</i>	<i>0,7</i>	<i>27,8</i>	<i>0,7</i>

Degree of corrosion (% mass loss): 10,9.

Appendix B.4 – Repaired beam (E)

- 1. Primer, StoCrete TH, was applied on the concrete surface. The purpose with priming was to bind dust and also to wet the dry concrete surface for improved bonding between the repair mortar and the existing concrete.
- 2. A casting frame was mounted on the concrete beam over the cavity intended to be refilled with mortar.
- 3. The cavity was refilled with repair mortar, StoCrete TG3, using a trowel up to the level of the previous concrete.
- 4. A plastic sheet was placed around the wet mortar, reducing the risk of plastic shrinkage and dry cracking.

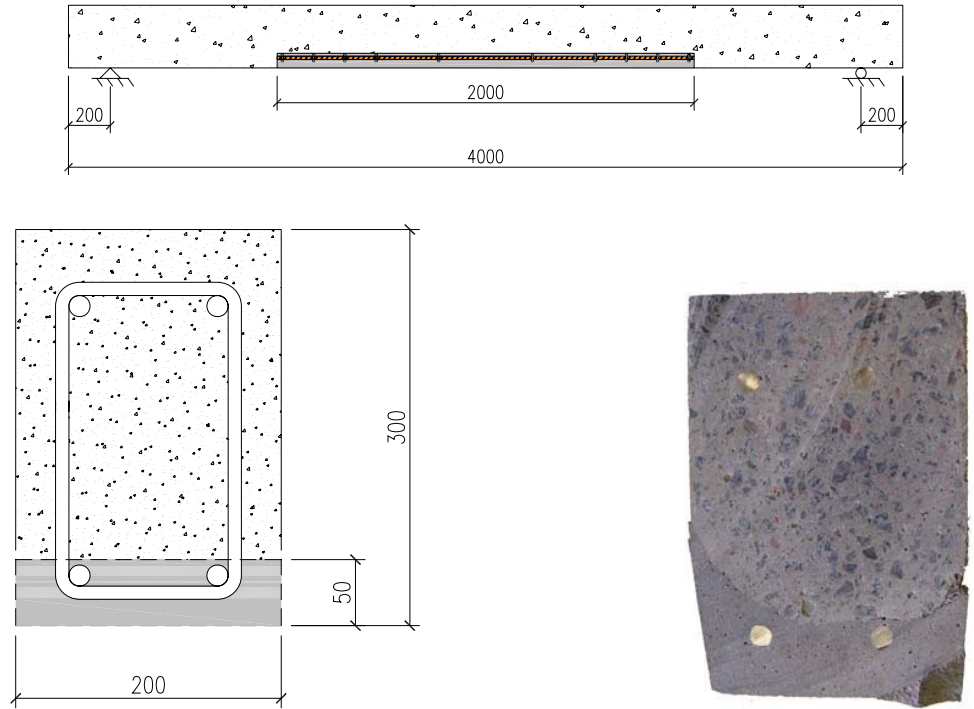


Figure A20. Top: Beam specimen measurements and steel reinforcement layout. Bottom left: Cross sectional view of repaired beam. Bottom right: Cross section of real repaired beam.

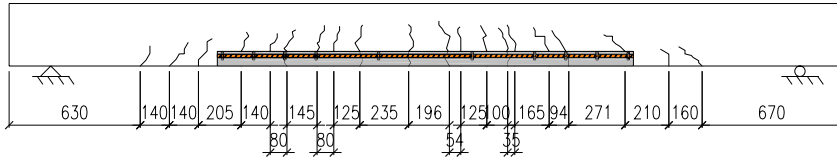


Figure A21. Longitudinal view of repaired beam with crack pattern after failure load test.

Monitoring – Corrosion stage

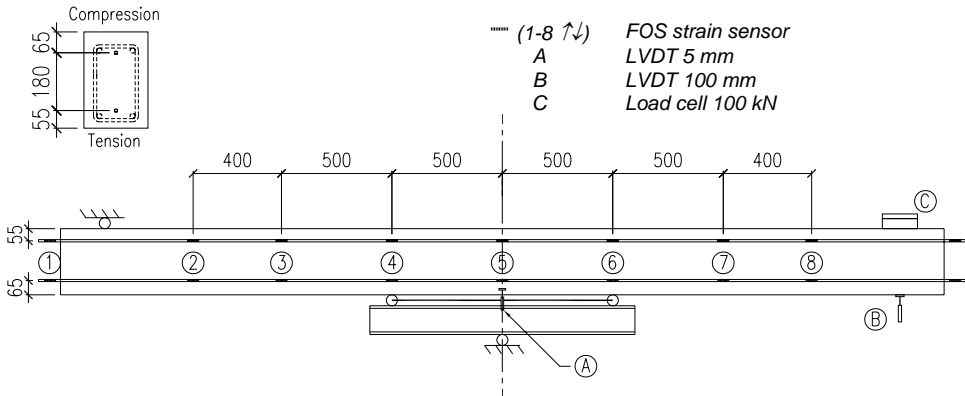


Figure A22. Sensor locations and sensor type on the intact beam specimen during corrosion stage. FOS are located along the glass fibre rods.

Monitoring – Failure test

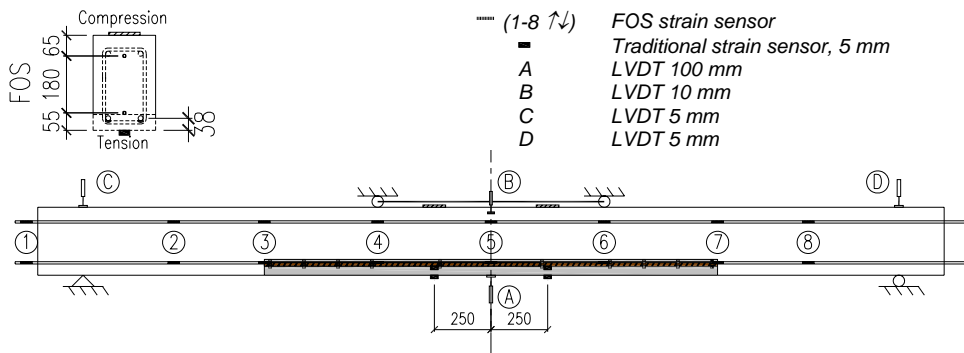


Figure A23. Sensor locations and sensor type on the repaired beam specimen. Fibre optical sensors are located along the glass fibre rods. The traditional strain sensors are located on the tensile steel reinforcement and on the surface of the compressed concrete.

Results

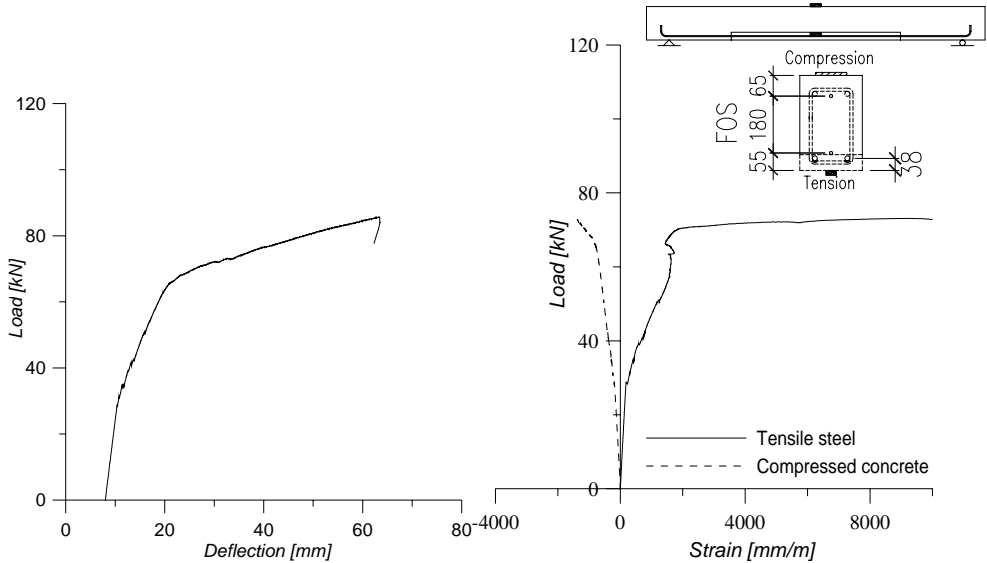


Figure A24. Left: Load vs. deflection relation for repaired beam. Right: Strain readings on tensile reinforcement and compressed concrete on repaired beam.

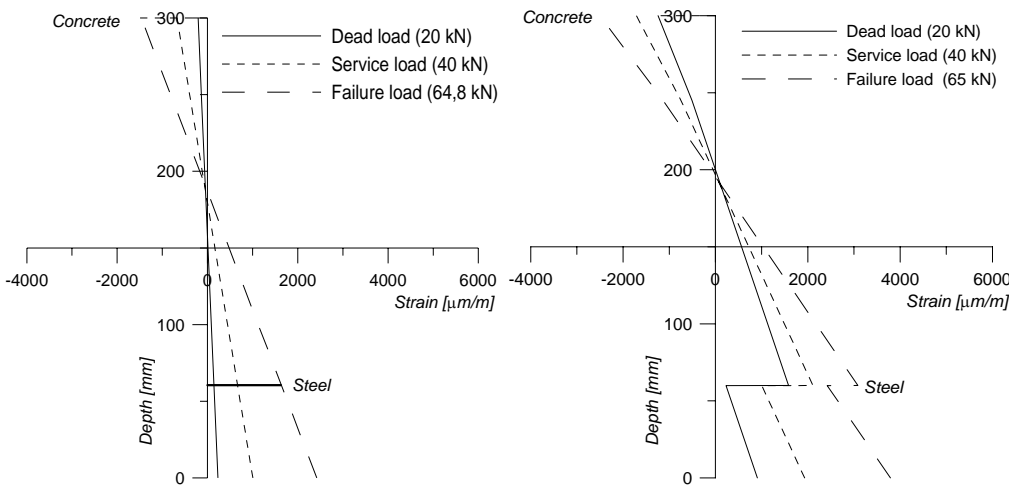


Figure A25. Left: Strain distribution for repaired beam at dead load, service load and failure load without taking the initial strain field into consideration. Right: Strain distribution when taking the initial strain field into consideration.

Table A10. The repair system consisted of a primer and a repair mortar.

		<i>Comment</i>
<i>Primer</i>	<i>StoCrete TH</i>	<i>50-50% mass weight of SroCrete TH and water.</i>
<i>Repair mortar</i>	<i>StoCrete TG3</i>	<i>Single component polymer modified repair mortar based on cement. Grain size 3 mm. Used for bridges, parking decks, industry facilities etc. Blends with water. Fulfils the demands by the Swedish Bridge code "Bro 2002".</i>

Appendix B.5 – Repaired and strengthened beam (F)

1. The cement skin on concrete surface was removed using steel brush.
2. Primer, StoBPE Primer super 50 (A+B), was applied and was left hardening for 24 hours.
3. The peel-ply on the CFRP plate was removed and adhesive, StoBPE Lim 567, was applied.
4. CFRP laminate placed onto beam and was left hardening. The distance from support to plate end was 50 mm.

Beam dimensions

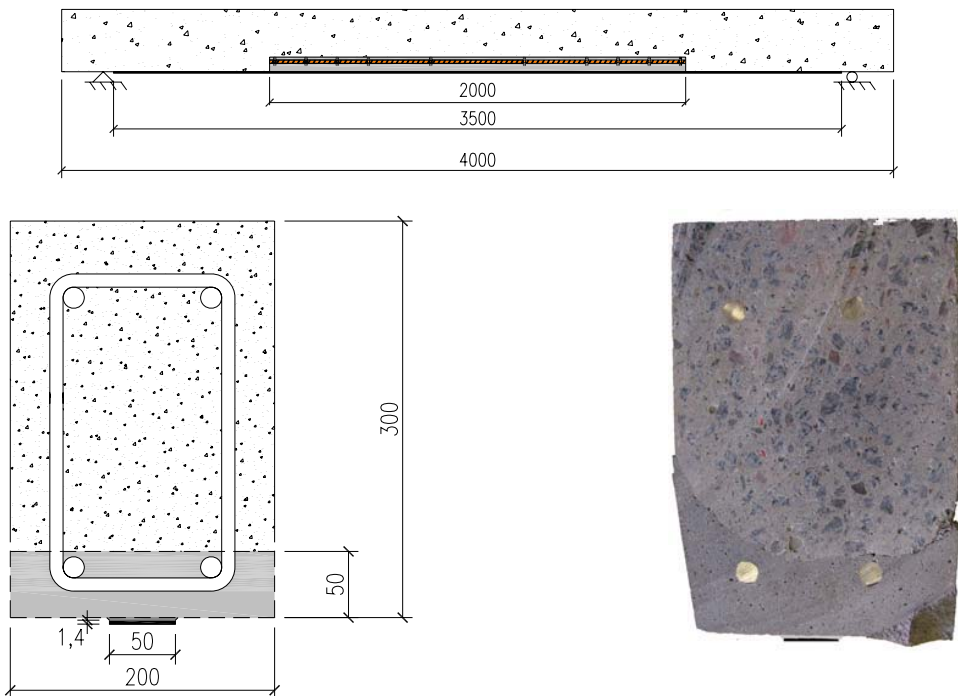


Figure A26. Top: Beam specimen measurements and steel reinforcement layout. Bottom left: Cross sectional view of intact beam. Bottom right: Cross section of real intact beam.

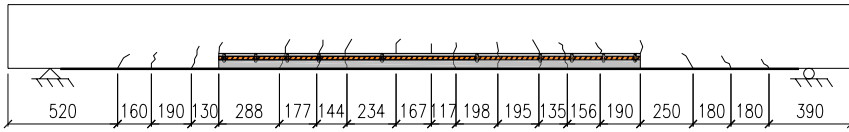


Figure A27. Crack pattern after failure test for repaired and strengthened beam.

Monitoring – Corrosion stage

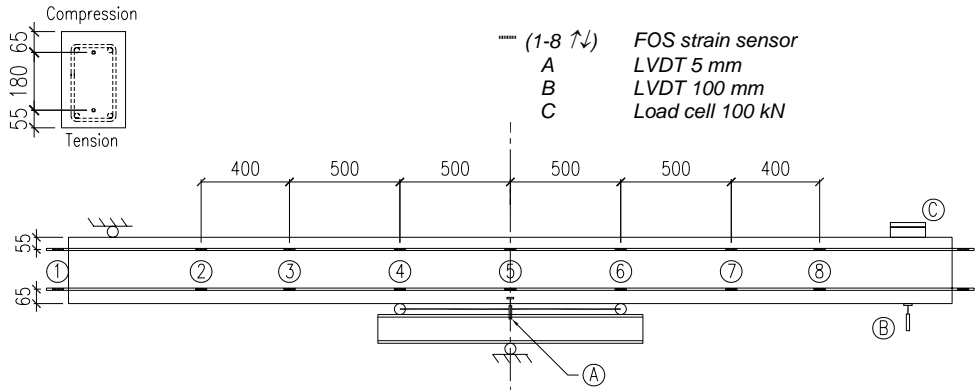


Figure A28. Sensor locations and sensor type on the intact beam specimen during corrosion stage. FOS are located along the glass fibre rods.

Monitoring – Failure load test

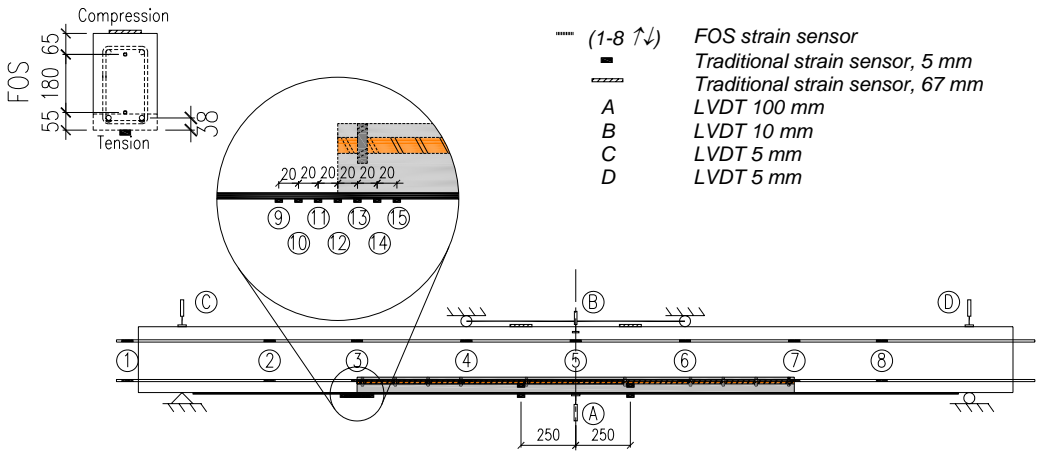


Figure A29. Sensor locations and sensor type on the repaired and strengthened beam specimen. Fibre optical sensors are located along the glass fibre rods. The traditional strain sensors are located on the tensile steel reinforcement and on the surface of the compressed concrete.

Results

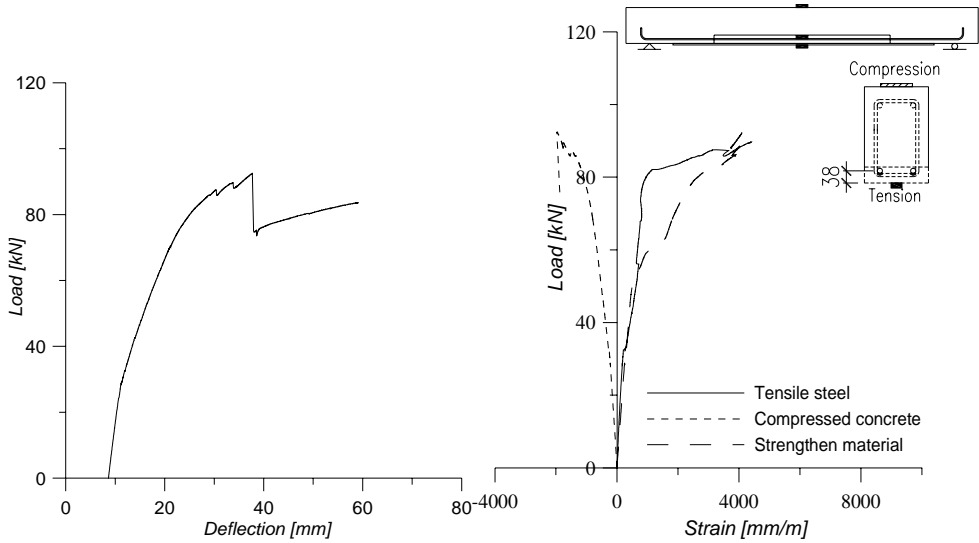


Figure A30. Left: Load vs. deflection relation for repaired & strengthened beam. Right: Strain readings on tensile steel reinforcement, compressed concrete and CFRP plate for repaired & strengthened beam.

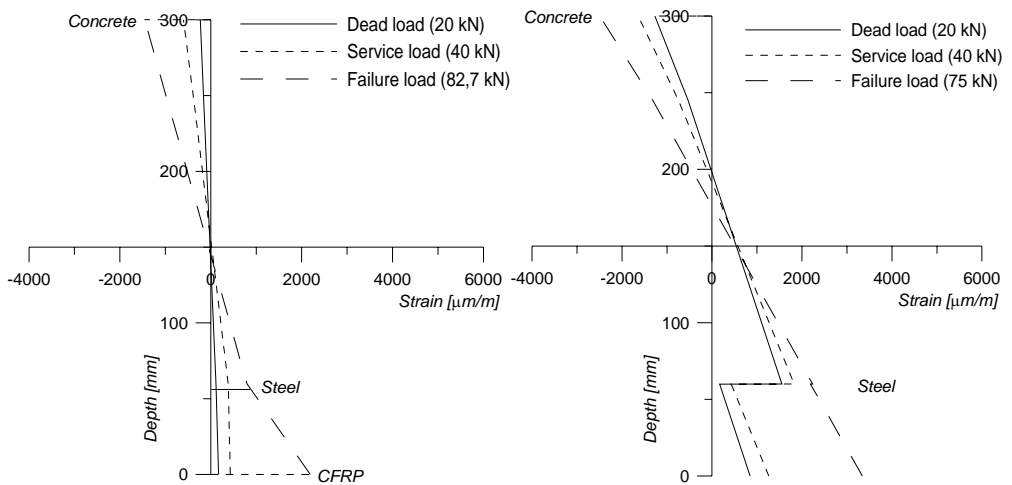


Figure A31. Left: Strain distribution in the repaired and strengthened cross section, without taking the initial strain field into consideration. Right: Strain distribution when taking the initial strain field into consideration.

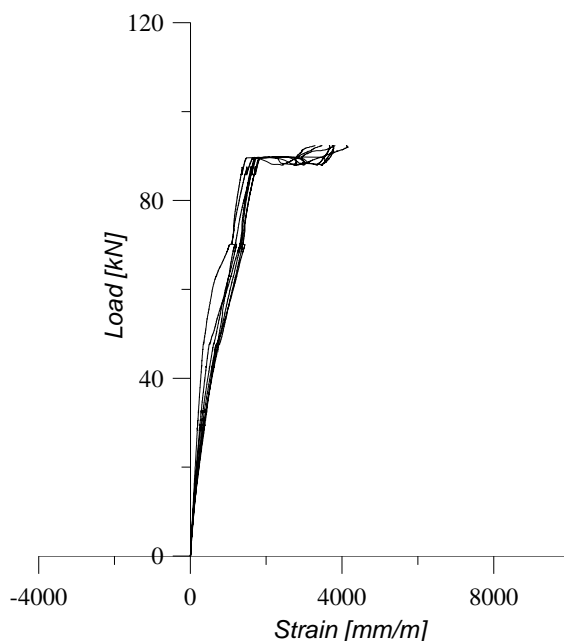


Figure A32. Strain readings from sensors 9 through 14 placed above and near the interface between concrete and repair mortar.

Table A11. Information regarding the strengthening procedure.

		Comment
Epoxy primer	StoBPE Primer 50 Super (A+B)	
Epoxy adhesive	StoBPE Lim 567 (A+B)	
Strengthening material	StoFRP Plate E 50 C	50×1,4 mm dimensions in cross section. CFRP plate with high strength characteristics and unidirectional fibres in the longitudinal direction.
Adhesive layer thickness	2 mm	
Length of plate	3500 mm	The plate was not fixed under the supports.
Degree of corrosion (% mass loss)	9,8	

Table A12. Applied load during corrosion and rehabilitation phase for beam F1 and F2.

	<i>Service load during corrosion</i>		<i>Dead load during rehabilitation</i>	
	<i>Mean value</i>	<i>Standard deviation</i>	<i>Mean value</i>	<i>Standard deviation</i>
<i>F1</i>	33,9	0,9	23,6	1,4
<i>F2</i>	35,8	1,1	19,7	0,7

